UC Riverside
UC Riverside Electronic Theses and Dissertations

Title

Exploring Variation in Late Cambrian Trilobite Dikelocephalus Pygidia Using Landmark-Based Geometric Morphometrics

Permalink

https://escholarship.org/uc/item/0998d8w7

Author

Vargas-Parra, Ernesto Ezequiel

Publication Date

2019

UNIVERSITY OF CALIFORNIA
RIVERSIDE

Exploring Variation in Late Cambrian Trilobite *Dikelocephalus* Pygidia Using
Landmark-Based Geometric Morphometrics

A Thesis submitted in partial satisfaction
of the requirements for the degree of

Master of Science

in

Geological Sciences

by

Ernesto Ezequiel Vargas-Parra

June 2019

Thesis Committee:
     Dr. Nigel C. Hughes, Chairperson
     Dr. Mary L. Droser
     Dr. Peter M. Sadler

The Thesis of Ernesto Ezequiel Vargas-Parra is approved:

_____

_____

_____
Committee Chairperson

University of California, Riverside

ABSTRACT OF THE THESIS

Exploring Variation in Late Cambrian Trilobite *Dikelocephalus* Pygidia Using
Landmark-Based Geometric Morphometrics

by

Ernesto Ezequiel Vargas-Parra

Master of Science, Graduate Program in Geological Sciences
University of California, Riverside, June 2019
Dr. Nigel C. Hughes, Chairperson

Pygidial shape variation of the trilobite morphospecies *Dikelocephalus minnesotensis* (late Cambrian, northern Mississippi Valley) is assessed using landmark-based geometric morphometrics including the use of semilandmarks. Relative warp analyses of pygidial shape show that although pygidial morphospace occupation by *D. minnesotensis* from the St. Lawrence Formation shows some regionalization by collection, variance within collections is notable and overlap in shape occurs among almost all collections. Morphological characters that dominate the structure of pygidial shape variation include the base of the posterolateral spine, proportions of the border, and form of the pleural ribs. Between collections and through time, a continuous gradient of morphotypes suggests a mosaic pattern of variation. Ontogenetic variation plays

little role in shape variance both within individual collections and in the sample as a whole. The designation of St. Lawrence Formation *D. minnesotensis* as a single, highly variable morphospecies stands when analyzed with landmark (and semilandmark) based geometric morphometrics. These results support the view that St. Lawrence Formation *Dikelocephalus* were highly variable in form, and this might relate to environmental variability in this nearshore setting. More generally, results may also exemplify Rosa's rule of elevated morphological variation early in clade history. Further, significant morphological distinctions between *Dikelocephalus* specimens from the underlying Tunnel City Group is consistent with a recent sequence stratigraphic model of the northern Mississippi Valley that suggests both a temporal gap and environmental shift between the deposition of these two units.

Table of Contents

List of Figures

Thin-plate spline deformation grid depicting allometry.

Procrustes superimposition of 14 landmarks for 15 specimens from North

Freedom Bed 8 (NF8).

Partial Procrustes distance versus ln centroid size.

Thin-plate spline deformation grid depicting allometry.

Procrustes superimposition of 21 landmarks and 41 semilandmarks for 6

specimens from Plain (PN).

Partial Procrustes distance versus ln centroid size.

Thin-plate spline deformation grid depicting allometry.

Procrustes superimposition of 14 landmarks for 6 specimens from Plain

(PN).

Partial Procrustes distance versus ln centroid size.

Thin-plate spline deformation grid depicting allometry.

Introduction

By the late Cambrian morphological variation in trilobites was diverse across taxonomic ranks within the clade. At the lowest taxonomic levels, unusually high morphological variation has been posited to occur both among and within species during this time, based both on specific case studies (Hughes, 1994; Hopkins and Webster, 2009; Webster, 2015) and as a general property of Cambrian trilobite species versus later ones (Webster, 2007). The late Cambrian trilobite *Dikelocephalus* from the northern Mississippi Valley provides one such case study and is a large and locally abundant trilobite with a notable range of forms (Hughes, 1994); yet, difficulty arises when delimiting boundaries in morphological variation between morphospecies in contrast to that within species. Discriminating between interspecific variation and intraspecific variation is important in evolutionary study because heritable variation within species is the raw material upon which natural selection operates and thus the magnitude and structure of variation within species influences the rate and direction of evolution at the species level and beyond. It is also relevant to paleontology's role in geochronology and biogeography because species are the natural units of biostratigraphy and community analysis. Thus, quantifying morphological variation is required to assess the continuity and structure of variation within a purported species. This study aims to optimally quantify the shape of *Dikelocephalus* pygidia specimens to explore patterns of variation therein.

Relatively recent work has concluded that all *Dikelocephalus* from the St. Lawrence Formation are conspecific (Hughes, 1994), but, with regard to the pygidia, this was based on a small number of nominal, meristic, and metric characters and employed traditional morphometric methods based on linear measurements only. The aim of this study is to use the power of geometric morphometrics to resolve and partition morphological variation more effectively.

Intraspecific variation within any fossil species can be divided into ontogenetic, taphonomic, and static (non-ontogenetic) components (Webster, 2015). Ontogenetic variation accounts for shape changes with growth, while taphonomic variation describes differences due to preservation; this study is most interested in residual variation within species once ontogenetic and taphonomic components are accounted for. Possible drivers of static variation in *Dikelocephalus* include developmental constraints and environment. High morphological variation within species observed shortly after the Cambrian radiation has by some been attributed to weak developmental regulation but might conceivably also relate to fluctuating environmental conditions. The tendency in the evolutionary history of a clade for variation of a character in primitive members to become fixed in advanced members has been termed Rosa's rule (Jaanusson, 1975; Ramsköld, 1991; Webster, 2018). Novel developmental pathways may have been less strongly canalized during the Cambrian resulting in more phenotypic variation within species (Hughes, 1991; Erwin, 2007). Interactions between *Dikelocephalus* and its physical environment

may also explain observed variation within species. Relatively nearshore environments, where *Dikelocephalus* is interpreted to have lived, are generally higher energy, and more stressful environments subject to marked and rapid changes in ambient conditions. In a time of global highstand and wide, shallow flooded continental shelves, relative sea level change may have resulted in shorelines significantly shifting and such environmental perturbations might be expressed as patterns of elevated or marked intraspecific variation. This study will consider both development and environment as drivers of intraspecific variation, specifically static variation, in *Dikelocephalus*.

The geological setting of *Dikelocephalus* can be used to understand regional environmental conditions during the late Cambrian. Study of lithofacies in which *Dikelocephalus* occurs aids the interpretation of the nearshore depositional setting on a paleocontinent situated equatorially (Hughes and Hesselbo, 1997; Runkel, 1994). Further, recent work on the sequence stratigraphy of the northern Mississippi Valley holds great potential for understanding the distribution and variation of *Dikelocephalus* by providing a temporal-environmental framework (Runkel et al., 2007; Runkel et al., 2008). Sequence stratigraphy conceptualizes the stratigraphic architecture of the northern Mississippi Valley as stacked sedimentary packages bounded by unconformities. Within these sequence packages are parasequences, bounded by flooding surfaces, deposited during cycles of relative sea level and sediment supply change. In this model, the St. Lawrence Formation, where most

Dikelocephalus specimens have been collected, is a series of shingled nearshore parasequences prograding paleoseaward during relative sea level highstand and fall. Despite the overall nearshore setting being stratigraphically condensed (Runkel et al., 2007), the occurrence of *Dikelocephalus* reveals high temporal fidelity through its representation in a highstand systems tract and falling-stage systems tract represented by the St. Lawrence and Jordan Formations. Sequence stratigraphy provides a spatio-temporal framework on which to project the patterns of variation witnessed in *Dikelocephalus* and will enable evaluation of whether any such patterns are artifacts of sediment accumulation, or whether they require specific biological explanation. This study thus seeks associations between patterns of morphological variation and prograding sedimentary packages in order to examine microevolutionary trends through relative time.

Background and previous research

Dikelocephalus is a well-documented trilobite with over a century and a half of reporting in the scientific literature including work on systematics, ontogeny, morphological variation, biometry, biostratinomy, taphonomy, distribution and functional morphology (Owen, 1852; Ulrich and Resser, 1930; Raasch, 1951; Labandeira, 1983; Hesselbo, 1987; Hughes, 1991; Hughes, 1993; Hughes, 1994; Labandeira and Hughes, 1994). Over the years the taxonomy of

Dikelocephalus has been influenced by additional collecting of specimens, advancing analytical methods, and changing species definitions (Hughes and Labandeira, 1995). The history of splitting and grouping of *Dikelocephalus* is indicative of a wider issue in taxonomy especially when morphology is the only data available for classification (Hughes and Labandeira, 1995).

Most recently, Hughes (1994) formally synonymized twenty-six species of *Dikelocephalus* occurring within the St. Lawrence Formation into the single, highly variable morphospecies *Dikelocephalus minnesotensis*. Using well localized collections, morphological variation in *Dikelocephalus* specimens was shown to be continuous. Morphological variation within collections from single beds at particular localities was notably high. Nominal and ordinal characters were shown to vary in a clinal manner, in some cases, while traditional morphometric analyses showed continuity in variation among all collections; bivariate regressions and multivariate analyses based on linear measurements of the cranidia and pygidia showed no discrete clustering that warranted recognition of more than one species of *Dikelocephalus* from the St. Lawrence Formation (Labandeira and Hughes, 1994; Hughes, 1994). Multivariate methods included principal component analyses (PCAs) and canonical variate analyses (CVAs) to assess patterns and groups, respectively, within St. Lawrence Formation *Dikelocephalus*. In the PCAs, the great majority of the variance was accounted for by the first principal component while the remaining principal components explained only a small portion of the variance. Results were consistent in both

cranidial and pygidial analyses revealing no emergent structure in the variation by locality that would permit recognition of multiple species within the sample. Studies emphasized the importance of recognizing intraspecific variation within species and the mosaic pattern of variation observed in *Dikelocephalus minnesotensis*. They detected no obvious temporal variations in *Dikelocephalus* within the St. Lawrence Formation but noted that *Dikelocephalus* from the underlying Tunnel City Group may belong to a separate taxon (Hughes, 1994).

Little work has been published on *Dikelocephalus* since the 1990's but more advanced morphometric methods have been developed since. Accordingly, Hughes (2011) employed landmark-based geometric morphometrics techniques to *Dikelocephalus* cranidia in an exploration of their potential use in species recognition. Landmark-based geometric morphometrics is a powerful tool for summarizing and quantifying shape (Bookstein, 1991; Zelditch et al., 2004; Webster and Sheets, 2010). This method is based on landmarks–homologous anatomical loci recognizable on all specimens in the study. Geometric morphometrics offers improved resolution of shape variation compared to traditional morphometrics because a configuration of landmarks captures more information than a set of linear measurements. With landmark data, multivariate analyses can be conducted using PCA and CVA analysis of the results of a decomposition of a hierarchical series of patterns of shape variation revealed via analysis of shape coordinates. Landmark-based geometric morphometrics has become standard in morphometric studies and trilobites are often used as the

model organism for guides to two-dimensional geometric morphometrics

(Webster and Sheets, 2010). Further, semilandmarks, which are not discrete,

anatomical loci, but which can be used to capture information about outlines and

curves (Bookstein, 2007; Sheets et al., 2004), are particularly relevant in this

case because of evident morphological variation in the form of the pygidial

furrows of *Dikelocephalus*. The number or spacing of semilandmarks along a

curve is not biologically informative, but the variation in curving morphologies is.

Use of semilandmarks helps better summarize shape and has been applied to

geometric morphometric analyses of trilobite cranidia (Sheets et al., 2004;

Webster, 2011). Landmark-based geometric morphometrics, including the use of

semilandmarks, holds great promise in summarizing the shape of *Dikelocephalus*

pygidia because it can capture information on structures not easily quantified with

traditional methods, such as the division of the pleural ribs.

The stratigraphy and sedimentology of the northern Mississippi Valley has

been documented by study of sections outcropping across southwest Wisconsin,

southeast Minnesota, and northeast Iowa (Hughes and Hesselbo, 1997; Runkel,

1994). Most *Dikelocephalus* collected from the northern Mississippi Valley are

from the St. Lawrence Formation but it is also found in the overlying Jordan

Formation and underlying Tunnel City Group. Previous biostratigraphic

subdivisions of the St. Lawrence Formation based on species of *Dikelocephalus*

(Raasch, 1951) were claimed to be invalid once intraspecific variation in

Dikelocephalus was recognized (Hughes, 1994). Member-level subdivisions of

the St. Lawrence Formation, the Lodi Member and Black Earth Member, are not of practical use due to their imprecise definition and because they do not represent contiguous rock units nor distinct environments of deposition (Hughes and Hesselbo, 1997). The main lithofacies of the St. Lawrence Formation include a heterolithic dolomite-sandstone facies, flat-pebble conglomerate and laminated sandstone facies, and a stromatolitic dolomite facies (Hughes and Hesselbo, 1997). The base of the St. Lawrence Formation, mainly composed of glauconitic flat-pebble conglomerates and laminated sandstones, is interpreted to have been deposited during relative sea-level rise. The top of the St. Lawrence Formation, a mixture of heterolithic facies and flat-pebble conglomerate/laminated sandstone facies, is interpreted to have been deposited during relative sea-level highstand and initiation of the subsequent and falling stage systems tract. The depositional setting of the St. Lawrence Formation is interpreted to be nearshore to shallow shelf (Hughes and Hesselbo, 1997).

Recent work on the sequence stratigraphy of the northern Mississippi Valley has contributed to the understanding of the deposition and temporal framework of the St. Lawrence Formation (Runkel et al., 2007; Runkel et al., 2008). The middle Cambrian to early Ordovician strata of the northern Mississippi Valley is composed of four depositional sequences in a shallow epeiric sea. The topmost sequence includes the St. Lawrence Formation and Jordan Sandstone. The St. Lawrence Formation is composed of a highstand systems tract (HST) and a falling-stage systems tract (FSST). The HST forms when relative sea level

rises at a slow rate and then ceases to rise, during which sediment accumulates more rapidly than accommodation space is created (also known as a normal regression) resulting in the basinward progradation of depositional units (Patzkowsky and Holland, 2012). This is followed by a FSST, which forms as relative sea level falls (also known as a forced regression). In both systems tracts, parasequences prograde and build out paleoseaward in a shingled pattern (Patzkowsky and Holland, 2012). Individual parasequences in the St. Lawrence Formation are observed to be a maximum of ~25 m thick in shoreface facies. Traced paleoseaward, they taper to a few meters or less over distances of 5–30 km as they downlap (Runkel et al., 2007). Average parasequence duration is of between 75 and 150 k.y. (Runkel et al., 2007). Due to wave erosion and subaerial exposure, the highstand and falling-stage systems tracts are capped by an unconformity that forms the sequence boundary. The underlying Mazomanie and Lone Rock Formations of the Tunnel City Group represent a highstand systems tract (HST) and a highly condensed transgressive systems tract (TST), respectively, deposited during relative sea level rise and highstand.

Material and methods

An image library of specimens was compiled by Nigel Hughes during and after his doctoral study on *Dikelocephalus* (Hughes, 1990)*.* Specimens are

housed at various museums and institutions including the American Museum of Natural History (AMNH), Cincinnati Museum Center (CMCIP), Field Museum of Natural History (FMNH), Milwaukee Public Museum (MPM), Museum of Comparative Zoology (MCZ), Natural History Museum of Los Angeles County (LACMIP), Science Museum of Minnesota (SMM), United States National Museum of Natural History (USNM), University of Iowa Museum of Natural History (UI), University of Minnesota Paleontology Collection (UMPC), University of Wisconsin Geology Museum, Madison (UW), and Yale Peabody Museum of Natural History (YPM). Original 35 mm negatives were scanned using a Polaroid SprintScan 35 Plus film scanner. Images, which were taken in standard orientation with the base of the pygidium lying flat and lit most strongly from the top-left, were rotated so that the saggital axis lies vertically and image resolution was increased to 180 pixels per inch, as needed, with Adobe Photoshop in order to produce images of broadly comparable resolution. Photography of additional specimens from the University of Wisconsin Geology Museum, Madison (UW) and the Natural History Museum of Los Angeles County (LACMIP) was conducted to supplement the image library.

New collections of *Dikelocephalus* specimens from fieldwork in Wisconsin and Minnesota were amassed by visiting known and new localities including Arcadia (AAa) and Crystal Valley (CV), respectively. Specimens were prepared using a pin vise and needle then photographed. For specimens to be usable in this study, at least half of the specimen must be preserved along with an intact

midline, so as to allow all midline landmarks to be specified and at least one of each pair of off-axial landmarks. A total of 157 pygidia from the St. Lawrence Formation and Reno Member satisfy this condition.

Images were organized by locality and data was collected using the "tps" series of software by F. James Rohlf for use in geometric morphometrics on Windows-based computers (https://life.bio.sunysb.edu/morph/). TpsUtil was used to build initial .tps files from images; .tps files were then input to TpsDig2 where landmark coordinates and semilandmark curves were digitized. Landmark data collected with TpsDig2 was in pixel units, so a scale factor was set for each image. The first seven landmarks represent the midline and the rest represent landmark pairs that were digitized alternating left to right. Individual semilandmark curves were digitized starting from the axis then proceeding laterally outwards. Semilandmark curves were anchored by landmarks on both ends. Paired curves were digitized in alternating left to right sequence (Fig. 1).

After data collection, data manipulation and analysis were done with the Integrated Morphometrics Package (IMP) 8 by H. David Sheets (http://www.filogenetica.org/cursos/Morfometria/IMP_installers/index.php) and the R-package geomorph. Landmark data was scaled to millimeters using geomorph and then the IMP8 program BigFix8 was used to reflect and average paired off-axial landmarks, or to use whichever left or right landmark was available in cases where only one of the pair is available. Partial Procrustes superimposition was done in CoordGen8 which centers each configuration by

making their centroid the origin, rescales configurations so they share a common

centroid size of 1, and minimizes the partial Procrustes distance (root of summed

squared distances between homologous landmarks) by rotating configurations.

This removes differences in location, scale, and orientation between

configurations (Webster and Sheets, 2010). Coordinates of semilandmarks were

calculated from the curve data in SemiLand8 using the minimized Procrustes

distance method to optimize their location along the curve (Webster and Sheets,

2010; Webster, 2011). Both BigFix8 and SemiLand8 are subroutines of the

CoordGen8 program within IMP8. Principal component analyses of warp scores,

referred to as relative warp analyses (RWAs), were completed in PCAGen8.

Partial warp scores are mathematically independent styles of deformation

summarizing shape differences between the mean configuration and all

configurations in a Procrustes superimposition. PCA of partial warp scores

results in relative warps: independent axes ordered so that the first is aligned

with the direction of maximal variance and the second is orthogonal to the first

and aligned with the direction of the next greatest variance and so on (Webster

and Sheets, 2010). Regression analyses were performed in Regress8 to assess

the contribution of ontogenetic variation to overall shape variation. Partial

Procrustes distance was regressed against ln centroid size to examine size

related shape variation. Also, partial warp scores were regressed against ln

centroid size (CS) in a multivariate regression to produce a vector of regression

coefficients; contribution of allometry to total shape variance is then calculated.

Bootstrapping methods determine the significance of the regression (from 1600 bootstraps). Data visualization was done with the R-package ggplot2.

The species concept used in this study follows the phylogenetic species concept where a species is "the smallest aggregation of comparable individuals diagnosable by a unique combination of characters" (Nixon and Wheeler, 1990; Wheeler and Meier, 2000). In this morphometric study, multiple species within *Dikelocephalus* may be distinguished if distributions form more than one statistically distinguishable group.

Abbreviations and names of localities (Hughes, 1993) included in the analysis along with the number of pygidia specimens from each are as follows. AAa: Arcadia Bed 18 (13 pygidia), BHa: Black Hawk (Moseman's Farm) (1 pygidium), BQ: Beans Quarry (1 pygidium), CR: Chippewa River Falls (1 pygidium), CV: Crystal Valley (3 pygidia), FN: Frontenac (2 pygidia), GE: Galesville (1 pygidium), LG: Lodi (1 pygidium), LRc: Button Bluff (2 pygidia), LSa: Lansing (6 pygidia), ME: Marine (3 pygidia), MMa: Mazomanie (3 pygidia), MT: Lucas (1 pygidium), NF2: North Freedom Bed 2 (21 pygidia), NF8: North Freedom Bed 8 (15 pygidia), NN: Newton (1 pygidium), OB: Osceola (1 pygidium), PD: Pierce-Dunn (5 pygidia), PN: Plain (6 pygidia), RCa: Richland Center (5 pygidia), RCe: Richland Center (5 pygidia), Reno: Freeburg (FG) (2 pygidia) and Newton (NNa) (2 pygidia), RV: Rene Valley (2 pygidia), RWa: LaGrange Mountain (5 pygidia), SPb: Prairie du Sac (8 pygidia), SRa: Spring

Green (10 pygidia), SWa: Stillwater (Fairy Glen) (27 pygidia), SWb: Stillwater (4 pygidia).

Description of all landmarks shown in Figure 1 are as follows.

Pygidial saggital landmarks:

1. Intersection of saggital axis and anterior axial furrow of first axial ring.

2. Intersection of saggital axis and axial furrow between first and second axial rings.

3. Intersection of saggital axis and axial furrow between second and third axial rings.

4. Intersection of saggital axis and axial furrow between third and fourth axial rings.

5. Intersection of saggital axis and posterior axial furrow of fourth axial ring.

6. Intersection of saggital axis and posterior edge of terminal axial piece.

7. Intersection of saggital axis and posterior margin.

Pygidial paired landmarks (left, right):

8, 9. Junction of anterior axial furrow of first axial ring with first pleural furrow.

10, 11. Junction of axial furrow between first and second axial rings with second and third pleural furrows.

12, 13. Junction of axial furrow between second and third axial rings with fourth and fifth pleural furrows.

14, 15. Junction of axial furrow between third and fourth axial rings with sixth pleural furrow.

16, 17. Junction of posterior axial furrow of fourth axial ring with seventh pleural furrow.

18, 19. Point of maximum curvature of lateral margin.

20, 21. Base of posterolateral spine.

22, 23. Termination of first pleural furrow.

24, 25. Termination of second pleural furrow.

26, 27. Termination of third pleural furrow.

28, 29. Termination of fourth pleural furrow.

30, 31. Termination of fifth pleural furrow.

32, 33. Termination of sixth pleural furrow.

34, 35. Termination of seventh pleural furrow.

Pygidial paired semilandmarks (left, right):

36-43, 44-51. First pleural furrow. 8 semilandmarks.

52-59, 60-67. Second pleural furrow. 8 semilandmarks.

68-74, 75-81. Third pleural furrow. 7 semilandmarks.

82-87, 88-93. Fourth pleural furrow. 6. semilandmarks.

94-98, 99-103. Fifth pleural furrow. 5 semilandmarks.

104-107, 108-111. Sixth pleural furrow. 4 semilandmarks.

112-114, 115-117. Seventh pleural furrow. 3 semilandmarks.

The structure of pygidial shape variation within *Dikelocephalus:* analytical results

This section presents the results of a series of investigations of the dataset using different combinations and subsets of landmarks and semilandmarks. This approach was employed to explore the extent to which results obtained were robust and indiscriminate to landmark choice. Analyses with semilandmarks seek to explore pygidial shape variation with contribution from pleural rib form. Analyses without semilandmarks (and anchoring landmarks) seek to explore pygidial shape variation more generally and serve as

a reference to compare against analyses with semilandmarks. Results from relative warp analyses (RWAs) and regression analyses are as follows.

21 landmarks, 41 semilandmarks. 157 specimens (Fig. 2).

Five outliers identified from the RWA (Fig. 3-8).

14 landmarks. 157 specimens (Fig. 9).

Five outliers identified from the RWA (Fig. 10-15).

Four outliers cluster together and discretely on RW3 of the analysis with semilandmarks (Figs. 4, 5). The same four outliers cluster together and discretely on RW1 versus RW2 (Fig. 10) and RW2 versus RW3 (Fig. 12) of the landmark only analysis. These four specimens are from the Reno Member underlying the St. Lawrence Formation. Compared to the rest of the specimens, these four are from the preceding systems tract. The remaining outlier is an aberrant form from the St. Lawrence Formation that is distinctive on the same RWs as the Reno outliers but is not allied to them as they lie in opposite areas of morphospace.

21 landmarks, 41 semilandmarks. 152 specimens, no outliers (Fig. 16).

63.7% of the shape variation among the 152 pygidia of *Dikelocephalus* is summarized by the first four relative warps (Fig. 22). RW1 explains 32.4% of the total shape variance in the sample and relates primarily to variation in the area of the posterolateral border: specimens with more positive scores have a narrower (sag., exsag., and tr.) posterolateral border, especially the area between the

base of the posterolateral spine and the distal extent of the pleural furrows. RW2 explains 15.2% of the total shape variance in the sample and relates primarily to variation in the position of the base of the posterolateral spine: specimens with more positive scores have a spine base closer to the saggital axis. RW3 explains 8.3% of the total shape variance in the sample and relates primarily to variation in the area posterior to the pygidial axis: specimens with more positive scores have a shorter (sag., exsag.) and wider (tr.) posterolateral area. RW4 explains 7.8% of the total shape variance in the sample and relates primarily to variation in pleurae division and the area posterior to the pygidial axis: specimens with more positive scores have proportionally more expanded (sag., exsag., and tr.) propleural bands and a shorter (sag., exsag.) posterolateral area. Higher RWs each explain <6% of total variance and relate to trivial components of shape variation.

A significant positive relationship exists between partial Procrustes distance and lnCS (slope=0.0093, p=0.0021, Fig. 23), but only 2.58% of the total shape variance was explained by allometry (p=0.001250 from 1600 bootstraps, Fig. 24).

19 landmarks, 34 semilandmarks. 152 specimens, no outliers (Fig. 25).

65.4% of the shape variation among the 152 pygidia of *Dikelocephalus* is summarized by the first four relative warps (Fig. 31). RW1 explains 35.0% of the total shape variance in the sample and relates primarily to variation in the area of

the posterolateral border: specimens with more positive scores have a narrower (sag., exsag., and tr.) posterolateral border, especially the area between the base of the posterolateral spine and the distal extent of the pleural furrows. RW2 explains 15.5% of the total shape variance in the sample and relates primarily to variation in the position of the base of the posterolateral spine: specimens with more positive scores have a spine base closer to the sagittal axis. RW3 explains 8.4% of the total shape variance in the sample and relates primarily to variation in the area posterior to the pygidial axis: specimens with more positive scores have a longer (sag., exsag.) posterolateral area. RW4 explains 6.5% of the total shape variance in the sample and relates primarily to variation in division of pleurae and in the area posterolateral to the axis: specimens with more positive scores have proportionally more expanded (sag., exsag., and tr.) propleural bands and a shorter (sag., exsag.) posterolateral area. Higher RWs each explain <6% of total variance and relate to trivial components of shape variation.

A significant positive relationship exists between partial Procrustes distance and lnCS (slope=0.0100, p=0.0011, Fig. 32), but only 2.81% of the total shape variance was explained by allometry (p<0.000625 from 1600 bootstraps, Fig. 33).

14 landmarks. 152 specimens, no outliers (Fig. 34).

79.6% of the shape variation among the 152 pygidia of *Dikelocephalus* is summarized by the first four relative warps (Fig. 40). RW1 explains 35.4% of the

total shape variance in the sample and relates primarily to variation in the area posterior to the pygidial axis: specimens with more positive scores have a shorter (sag., exsag.) and wider (tr.) posterolateral area. RW2 explains 22.1% of the total shape variance in the sample and relates primarily to length (sag., exsag.) of the terminal piece of the axis relative to the area posterior to the pygidial axis: specimens with more positive scores have a shorter (sag., exsag.) axis termination relative to a longer (sag., exsag.) posterolateral area. RW3 explains 11.7% of the total shape variance in the sample and relates primarily to variation in the length (sag., exsag.) of the terminal piece of the axis and pygidial width (tr.): specimens with more positive scores have a longer (sag., exsag.) axis termination and narrower (tr.) lateral area. RW4 explains 10.4% of the total shape variance in the sample and relates primarily to variation in relative area of the area posterolateral to the axis: specimens with more positive scores have a proportionally more expansive (sag., exsag., and tr.) posterolateral area. Higher RWs each explain <7% of total variance and relate to trivial components of shape variation.

A significant positive relationship exists between partial Procrustes distance and lnCS (slope=0.0165, p<0.0001, Fig. 41), but only 6.59% of the total shape variance was explained by allometry (p<0.000625 from 1600 bootstraps, Fig. 42).

13 landmarks. 152 specimens, no outliers (Fig. 43).

85.9% of the shape variation among the 152 pygidia of *Dikelocephalus* is summarized by the first four relative warps (Fig. 49). RW1 explains 31.9% of the total shape variance in the sample and relates primarily to variation in the area posterior to the pygidial axis and the length (sag., exsag.) of the terminal piece of the axis: specimens with more positive scores have a shorter (sag., exsag.) posterior area and longer (sag., exsag.) axis termination. RW2 explains 21.9% of the total shape variance in the sample and relates primarily to variation in the area posterolateral to the axis and the length (sag., exsag.) of the terminal piece of the axis: specimens with more positive scores have a wider (tr.) lateral area with a shorter (sag., exsag.) posterior area and shorter (sag., exsag.) axis termination. RW3 explains 17.7% of the total shape variance in the sample and relates primarily to variation in the area posterior to the pygidial axis and the length (sag., exsag.) of the terminal piece of the axis: specimens with more positive scores have a shorter (sag., exsag.) posterior area and longer (sag., exsag.) axis termination. RW4 explains 14.4% of the total shape variance in the sample and relates primarily to variation in the shape of the axial rings: specimens with more positive scores have proportionally larger (sag., exsag., and tr.) axial rings. Higher RWs each explain <7% of total variance and relate to trivial components of shape variation.

A significant positive relationship exists between partial Procrustes distance and lnCS (slope=0.0119, p<0.0001, Fig. 50), but only 5.30% of the total

shape variance was explained by allometry (p<0.000625 from 1600 bootstraps, Fig. 51).

Despite using different combinations and subsets of landmarks and semilandmarks from the dataset, analyses show similar patterns of pygidial shape variation. Variation in the proportions of the border and the position of the posterolateral spine base seem to dominate the structure of pygidial shape variation and despite the marked variation in pleural division this does not appear to be a species diagnostic character. Variation in pleural division has been shown to occur within collections (Hughes, 1994) so it is clearly not a temporally diagnostic characteristic (contra Raasch, 1951). Also, ontogenetic variation contributes little to total pygidial shape variation in the sample as a whole.

Allometry by locality

Now that size related shape variation has been shown for the sample as a whole, this section presents regression analyses examining ontogenetic variation by locality collection. This is done to see whether collections by locality have similar or differing growth parameters.

Arcadia Bed 18 (AAa)

21 landmarks, 41 semilandmarks. 13 specimens (Fig. 52).

In this collection a significant positive relationship exists between partial Procrustes distance and lnCS (slope=0.0537, p=0.0099, Fig. 53), and 21.56% of

the total shape variance was explained by allometry (p=0.0294 from 1600 bootstraps, Fig. 54).

14 landmarks. 13 specimens (Fig. 55).

In this collection a significant positive relationship exists between partial Procrustes distance and lnCS (slope=0.0445, p=0.0293, Fig. 56), and 24.96% of the total shape variance was explained by allometry (p=0.0263 from 1600 bootstraps, Fig. 57).

Lansing (LSa)

21 landmarks, 41 semilandmarks. 6 specimens (Fig. 58).

In this collection a significant positive relationship exists between partial Procrustes distance and lnCS (slope=0.1762, p=0.0056, Fig. 59), but the total shape variance explained by allometry is not significant at a 95% confidence interval (26.06% of total variance explained, p=0.1875 from 1600 bootstraps, Fig. 60).

14 landmarks. 6 specimens (Fig. 61).

In this collection a significant positive relationship exists between partial Procrustes distance and lnCS (slope=0.1735, p=0.0163, Fig. 62), but the total shape variance explained by allometry is not significant at a 95% confidence interval (37.15% of total variance explained, p=0.0963 from 1600 bootstraps, Fig. 63).

North Freedom Bed 2 (NF2)

21 landmarks, 41 semilandmarks. 21 specimens (Fig. 64).

In this collection no significant relationship exists between partial Procrustes distance and lnCS (slope=0.0080, p=0.2066, Fig. 65), and the total shape variance explained by allometry is not significant at a 95% confidence interval (3.94% of total variance explained, p=0.6119 from 1600 bootstraps, Fig. 66).

14 landmarks. 21 specimens (Fig. 67).

In this collection no significant relationship exists between partial Procrustes distance and lnCS (slope=0.0122, p=0.0901, Fig. 68), and the total shape variance explained by allometry is not significant at a 95% confidence interval (8.49% of total variance explained, p=0.1063 from 1600 bootstraps, Fig. 69).

North Freedom Bed 8 (NF8)

21 landmarks, 41 semilandmarks. 15 specimens (Fig. 70).

In this collection no significant relationship exists between partial Procrustes distance and lnCS (slope=0.0027, p=0.4107, Fig. 71), and the total shape variance explained by allometry is not significant at a 95% confidence interval (3.62% of total variance explained, p=0.8950 from 1600 bootstraps, Fig. 72).

14 landmarks. 15 specimens (Fig. 73).

In this collection no significant relationship exists between partial Procrustes distance and lnCS (slope=0.0160, p=0.0500, Fig. 74), and the total shape variance explained by allometry is not significant at a 95% confidence interval (5.57% of total variance explained, p=0.5531 from 1600 bootstraps, Fig. 75).

Plain (PN)

21 landmarks, 41 semilandmarks. 6 specimens (Fig. 76).

In this collection no significant relationship exists between partial Procrustes distance and lnCS (slope=0.0007, p=0.4759, Fig. 77), and the total shape variance explained by allometry is not significant at a 95% confidence interval (13.51% of total variance explained, p=0.8706 from 1600 bootstraps, Fig. 78).

14 landmarks. 6 specimens (Fig. 79).

In this collection no significant relationship exists between partial Procrustes distance and lnCS (slope=-0.0126, p=0.7538, Fig. 80), and the total shape variance explained by allometry is not significant at a 95% confidence interval (11.36% of total variance explained, p=0.7775 from 1600 bootstraps, Fig. 81).

Prairie du Sac (SPb)

21 landmarks, 41 semilandmarks. 8 specimens (Fig. 82).

In this collection no significant relationship exists between partial Procrustes distance and lnCS (slope=0.0282, p=0.1472, Fig. 83), and the total shape variance explained by allometry is not significant at a 95% confidence interval (19.94% of total variance explained, p=0.1594 from 1600 bootstraps, Fig. 84).

14 landmarks. 8 specimens (Fig. 85).

In this collection no significant relationship exists between partial Procrustes distance and lnCS (slope=0.0358, p=0.1437, Fig. 86), and the total shape variance explained by allometry is not significant at a 95% confidence interval (7.50% of total variance explained, p=0.7625 from 1600 bootstraps, Fig. 87).

Spring Green (SRa)

21 landmarks, 41 semilandmarks. 10 specimens (Fig. 88).

In this collection a significant positive relationship exists between partial Procrustes distance and lnCS (slope=0.0922, p=0.0363, Fig. 89), but the total shape variance explained by allometry is not significant at a 95% confidence interval (11.70% of total variance explained, p=0.4031 from 1600 bootstraps, Fig. 90).

14 landmarks. 10 specimens (Fig. 91).

In this collection a significant positive relationship exists between partial Procrustes distance and lnCS (slope=0.1170, p=0.0237, Fig. 92), but the total shape variance explained by allometry is not significant at a 95% confidence interval (13.02% of total variance explained, p=0.3400 from 1600 bootstraps, Fig. 93).

Stillwater, Fairy Glen (SWa)

21 landmarks, 41 semilandmarks. 27 specimens (Fig. 94).

In this collection no significant relationship exists between partial Procrustes distance and lnCS (slope=0.0202, p=0.0501, Fig. 95), and the total shape variance explained by allometry is not significant at a 95% confidence interval (7.13% of total variance explained, p=0.1038 from 1600 bootstraps, Fig. 96).

14 landmarks. 27 specimens (Fig. 97).

In this collection a significant positive relationship exists between partial Procrustes distance and lnCS (slope=0.0329, p=0.0046, Fig. 98), and 10.54% of the total shape variance was explained by allometry (p=0.0256 from 1600 bootstraps, Fig. 99).

As shown, the contribution of ontogenetic variation to total pygidial shape variation differs by locality collection. Collections have varying growth parameters, but most are not significant.

Discussion

Relative warp analysis of 157 *Dikelocephalus* pygidia specimens identified
five outliers in both combined landmark plus semilandmark (Figs. 2-8) and
landmark only (Figs. 9-15) configurations. Four of these specimens are from
relatively older localities including Freeburg (FG), Newton (NNa) (both from the
Reno Member of the Tunnel City Group) and one morphologically anomalous
specimen is from the St. Lawrence Formation at Prairie du Sac (SPb). These five
outliers are distinctive on RW3 of the analysis with semilandmarks (Figs. 4, 5),
and on RW1 versus RW2 (Fig. 10) and RW2 versus RW3 (Fig. 12) of the
landmark only analysis. The Reno outliers cluster discretely and are not allied to
the aberrant SLF outlier as they lie in opposite areas of morphospace. Once
these outliers were removed, relative warp analysis of 152 *Dikelocephalus*
pygidia specimens form a single cloud of morphospace with pygidial shape
variation continuous along all RW axes (Figs. 17-21, 26-30, 35-39, 44-48). It
must be noted that the outliers lie within the sample as a whole on RW1, RW2,
and RW4 of the analysis with semilandmarks (Figs. 3-6), and on RW1 versus
RW3 (Fig. 11) and RW1 versus RW4 (Fig. 13) of the landmark only analysis.
With respect to these RWs, the outliers are within a single cloud of morphospace.

The structure of pygidial shape variation is influenced primarily by variation in the base of the posterolateral spine, pleural furrows, posterior border, lateral border, and tip of the axis. Landmarks corresponding to the four axial rings cluster tightly in partial Procrustes superimposition (Figs. 16, 25, 34, 43) compared to all other landmarks. Relatively little variation in axial ring shape is observed in the first four RWs of all configurations compared to other morphological features. Patchy clustering is notable within scatter of landmarks corresponding to the base of the posterolateral spine in partial Procrustes superimpositions including semilandmarks (Figs. 16, 25). Scatter of landmarks corresponding to the termination of pleural furrows have just as much scatter as those of other landmarks (except the axial rings) (Figs. 16, 25); yet they scatter more than the semilandmarks along the pleural furrows. In both RWAs including semilandmarks, RW4 relates primarily to variation in the pleural semilandmarks while little variation in pleural division is observed in the first three RWs (Figs. 22, 31). The amount of variation in the border extent is striking; this could be partially taphonomic based on where the furrows end, but there does seem to be biological variation in the position of the spine along the margin and the extent of the postaxial border. The most visually obvious variation, that of the division of the pleurae, plays a relatively modest role – perhaps this is because, in terms of (semi)landmark point relative position, the difference between equal and subequal division is small but the visual difference is very noticeable. This character may have had higher latitude to vary without selective consequence

than it would have had in the thorax, where the constraints of articulation would likely have required a more consistent form. So, in the pygidium, whatever the function of the pleural furrow is, its position doesn't seem to have been constrained.

Comparing the relative warp analyses based on landmark and semilandmark data herein to the principal component analysis based on traditional linear measurements by Hughes (1994, Figs. 38, 39), RWAs reveal a collection-related structure in pygidial shape variation of *Dikelocephalus* by locality that was not revealed by traditional methods. PCAs of linear measurements show overlapping locality clusters as a homogenous cloud of variation. Any given pair of locality clusters may be partially overlapping, contiguous, or discrete in the RWAs revealing previously unrecognized structure in shape variation. An exception to this structure in RWAs can be seen in the analysis of the 13 landmark configuration (Fig. 43), the simplest configuration presented herein, in which the landmark related to the base of the pygidial spine has been removed. Bivariate plots of RWs (Figs. 44-47) are similar to those of PCs by Hughes (1994, Figs. 38, 39) in that no structure in pygidial shape variation is observed by locality. Appending a single landmark to the 13 landmark configuration introduces structure to the RWAs as seen in the analysis of the 14 landmark configuration (Figs 34-38); this landmark corresponds to the base of the posterolateral spine. This pattern of shape variation is consistent in the landmark only and landmark plus semilandmark RWAs.

As for locality related shape variation, the position of the base of the posterolateral spine separates most specimens from North Freedom (NF2 and NF8) and Stillwater (SWa and SWb) although overlap is observed in the RWAs. Variation in pleural division is shown to be continuous in a quantitative way (Figs. 20, 22, 29, 31) beyond the use of ordinal character states (Hughes, 1994, Fig. 13) and is apparently neither locality-based nor size-related. Size-related pygidial shape variation is visually assessed in bivariate plots of RW1 versus centroid size (Figs. 21, 30, 39, 48). Pygidial shape variation does not appear to be strongly size related, but localities do vary in their ranges of centroid size.

Statistically assessing allometry within *Dikelocephalus* shows little shape change with growth in 152 pygidia specimens (outliers excluded). The relationship between partial Procrustes distance and ln centroid size is statistically significant at a 95% confidence interval for the sample as a whole but the amount of variation explained by allometry is low for all landmark and semilandmark configurations (Figs. 23, 32, 41, 50). Allometry is statistically significant at a 95% confidence interval but among all configurations only 2.6% to 6.6% of total shape variance is explained by allometry (Figs. 24, 33, 42, 51). Shape change with growth consistently relates to posterior shortening and lateral widening of the pygidial border along with a relative lengthening tip of the axial terminal piece as shown in thin-plate spline deformation grids (Figs. 24, 33, 42, 51). Thus, ontogenetic variation within *Dikelocephalus* pygidia is determined to be modest in the sample as a whole.

Specimens from individual locality collections mostly lack significant

relationship between shape variation against size, and no significant allometry.

The exceptions are specimens from Arcadia Bed 18 (AAa) which do show a

significant relationship between partial Procrustes distance and ln centroid size,

with 25.0% and 21.6% of total shape variance explained by allometry in landmark

only and landmark plus semilandmark analyses, respectively (Figs. 52-57). The

allometric signal in AAa specimens is much larger than that of the sample as a

whole. Allometry among these specimens relates to lateral widening and

posterior shortening of the pygidial border along with expanding propleural bands

as shown in thin-plate spline deformation grids (Figs. 54, 57). This may suggest

that pleural division is allometric but if so only AAa specimens show this.

Previous work on *Dikelocephalus* pygidia showed allometry only in the length of

the posterolateral spine, notably in AAa specimens (Hughes, 1994). The tip of

the posterolateral spine proved difficult to measure in a landmark-based

geometric morphometric analysis due to small sample size and was not included

in this study. Despite this, pygidial allometry has now been demonstrated in the

sample as a whole and in single bed locality collections. Thus, ontogenetic

variation plays a small, but significant, role in pygidial shape variance in

Dikelocephalus pygidia. Noting that the smallest pygidium in this study is 9.8 mm

in saggital length, all specimens analyzed herein are morphologically mature

because this length is well above that of the largest meraspid of any known

trilobite (Fusco et al., 2012). Morphologically immature specimens of

Dikelocephalus are not known and thus the preholaspid ontogenetic variation remains unknown. The absence of small, morphologically immature *Dikelocephalus* specimens may be related to taphonomy, likely due to the fragility of such small sclerites.

Taphonomy impacts the structure of pygidial shape variation due to variation in specimen preservation. Compaction and effacement from preservation in siliciclastic matrix introduces shape variation that is taphonomic in origin (Webster and Hughes, 1999). Pleural furrows are the morphological feature of the pygidium most affected by taphonomy. Both compaction and effacement make pleural furrows appear shorter than they originally were. Thus, in specimens preserved in shale, placement of the landmark at the end of the pleural furrow may be an underestimate of the true termination. Yet, the scatter of landmarks corresponding to the end of pleural furrows is not markedly greater than that of other landmarks (except those of the axial rings) (Figs. 16, 25), though it must be noted these clusters are oblong in shape, suggesting variation in where along the furrow's axis, its expression became obsolete. In RWAs of configurations including semilandmarks, RW1 apparently includes shape variation in pleural furrow length that may be explained by taphonomy because this seems to reflect variation in the extent of all pleural furrows. However, RW2 shows shape variation where the posteriormost pleural furrows elongate as the anteriormost pleural furrows shorten, a pattern not expected to be a taphonomic artifact.

According to Runkel et al.'s (2007) sequence stratigraphic model of the

northern Mississippi Valley, the St. Lawrence Formation is composed of a

highstand systems tract (HST) and a falling stage systems tract (FSST). The top

of the HST and base of the FSST lies between, and might lie within,

Dikelocephalus locality sections. In the figures, *Dikelocephalus* locality

collections are color coded according to the expected temporal sequence of

localities using Runkel et al.'s (2007) sequence stratigraphic model. The color

spectrum, with red localities being the oldest and purple localities being the

youngest, reflects Runkel et al.'s (2007) estimate of temporal order and provides

a temporal framework onto which patterns of variation can be examined. Arcadia

Bed 18 (AAa) occurs just before this boundary just at the end of the HST.

Localities relatively older than AAa are within the HST (includes most localities in

this study). Few localities are within the FSST and only a small number of

Dikelocephalus pygidia have been collected from these. To interpret, relative sea

level is rising in older SLF localities and in AAa but sediment accumulation rates

exceed the rate of relative sea level rise (and increase in accommodation)

resulting in a net regression of the shoreline. Relative sea level fall and lower

sediment accumulation rates in localities younger than AAa result in a forced

regression of the shoreline. Thus, net water depth is decreasing throughout the

SLF in both systems tracts as the shoreline moved paleoseaward.

The structure of pygidial shape variation appears to be locality related but

this pattern is likely an oversimplification; sequence stratigraphy reveals

environmental and geographical changes with significant impacts on the nearshore setting of *Dikelocephalus*. Patterns of variation in *Dikelocephalus* may be dominated by microevolutionary changes or by clines, changes in morphology along environmental or geographic gradients. Shape variation due to decreasing water depth or geographical position along the paleoshoreline may be misinterpreted as unidirectional morphological change when they are in fact clinal and static through time (Patzkowsky and Holland, 2012). When examining the RWAs of all configurations (without outliers), no obvious trend in pygidial shape variation emerges that can be attributed to decreasing water depth through time (as observed in Webber and Hunda (2007)). It can be argued that the same environment is being sampled but its expression passes through time as it shifts in a paleoseaward direction. Geographical variation may explain patterns of variation observed between distant localities such as North Freedom (NF2 and NF8) and Stillwater (SWa and SWb). The sheer amount of shape variation, especially from single bed locality collections, is impressive considering the relatively high sedimentation rates expected in portions of the highstand systems tract of siliciclastic settings (Patzkowsky and Holland, 2012). Lower levels of time-averaging, thus, are expected in an HST compared to other systems tracts (Patzkowsky and Holland, 2012) taking into account Hunt (2004) showed that time-averaging only slightly inflates morphological variation (about 5%) in ancient samples.

Four of the five outliers excluded in the beginning of the analysis were

collected from two localities of the Reno Member of the Tunnel City Group

underlying the St. Lawrence Formation. According to Runkel (2007), the Reno

Member is part of a transgressive systems tract (TST) marked by relative sea-

level rise, shoreline transgression, and a maximum flooding surface bounding the

top of the systems tract. TST deposits of siliciclastic settings are stratigraphically

condensed due to relatively low sedimentation rates thus higher levels of time-

averaging are expected compared to an HST (Patzkowsky and Holland, 2012).

These four Reno Member *Dikelocephalus* specimens separate as a group from

St. Lawrence Formation *Dikelocephalus* specimens in RWAs of landmark only

and landmark plus semilandmark configurations (Figs. 2-15). Reno Member

Dikelocephalus pygidia have a shorter posterior border area compared to St.

Lawrence Formation *Dikelocephalus* pygidia. Hughes (1994) argued that

insufficient evidence was available to evaluate the status of Reno Member

Dikelocephalus specimens (described as *Dikelocephalus freeburgensis* Bell et

al., 1952) but stated they may belong to a taxon distinct from St. Lawrence

Formation *Dikelocephalus.* It can now be shown that Reno Member

Dikelocephalus pygidia are morphologically and stratigraphically distinct from St.

Lawrence Formation *Dikelocephalus* pygidia. The name *Dikelocephalus*

freeburgensis is appropriate for these forms.

The remaining outlier is a St. Lawrence Formation *Dikelocephalus*

pygidium collected from Prairie du Sac (SPb). This specimen has a relatively

small axis and a proportionally large posterior border area. The outlier is considered an aberrant form of St. Lawrence Formation *Dikelocephalus* and is an outlier within its locality collection. Aberrant forms occur in other locality collections but are not outliers within the sample as a whole.

Conclusion

Dikelocephalus pygidia from the St. Lawrence Formation remain best considered as belonging to a single morphospecies: *Dikelocephalus minnesotensis*. Use of landmarks and semilandmarks reveal the structure of pygidial shape variation within *D. minnesotensis* and confirm this species was highly variable in form. The pattern of variation observed may relate to a combination of geographical variation, environmental variability in a nearshore setting, and, more generally, elevated morphological variation early in clade history. Allometry plays little role in total pygidial shape variation both within individual collections and in the sample as a whole. *Dikelocephalus* pygidia from the Reno Member of the Tunnel City Group are likely a separate taxon, *Dikelocephalus freeburgensis*; additional geometric morphometric analysis of cranidia from the Reno Member is needed to support this hypothesis.

References

Bell, W.C., Feniak, O.W., and Kurtz, V.E., 1952, Trilobites from the Franconia Formation, Southeast Minnesota: Journal of Paleontology, v. 26, p. 175–198.

Bookstein, F.L., 1991, Morphometric Tools for Landmark Data: New York, Cambridge University Press, 435 p.

Bookstein, F.L., 1997, Landmark methods for forms without landmarks: morphometrics of group differences in outline shape: Medical Image Analysis, v. 1, p. 97–118.

Erwin, D.H., 2007, Disparity: morphological pattern and developmental context: Palaeontology, v. 50, p. 57–73.

Fusco, G., Garland, T. Jr., Hunt, G., and Hughes, N.C., 2012, Developmental trait evolution in trilobites: Evolution, v. 66, p. 314–329.

Hesselbo, S.P., 1987, The biostratinomy of *Dikelocephalus* sclerites: implications for the use of trilobite attitude data: Palaios, v. 2, p. 605–608.

Hopkins, M.J., and Webster, M., 2009, Ontogeny and geographic variation of a new species of the corynexochine trilobite *Zacanthopsis* (Dyeran, Cambrian): Journal of Paleontology, v. 83, p. 524–547.

Hughes, N.C., 1990, The Upper Cambrian trilobite *Dikelocephalus minnesotensis* and its geological setting [Ph.D. dissertation]: Bristol, University of Bristol, 483 p.

Hughes, N.C., 1991, Morphological plasticity and genetic flexibility in a Cambrian trilobite: Geology, v. 19, p. 913–916.

Hughes, N.C., 1993, Distribution, taphonomy, and functional morphology of the Upper Cambrian trilobite *Dikelocephalus*: Milwaukee Public Museum Contributions in Biology and Geology, v. 84, 49 p.

Hughes, N.C., 1994, Ontogeny, intraspecific variation, and systematics of the Late Cambrian trilobite *Dikelocephalus*: Smithsonian Contributions to Paleobiology, v. 79, 89 p.

Hughes, N.C., 2011, *Dikelocephalus* revisited: species discrimination and methodological progress: Geological Society of America Abstracts with Programs, v. 43, no. 5, p. 333.

Hughes, N.C., and Hesselbo, S.P., 1997, Stratigraphy and sedimentology of the St. Lawrence Formation, Upper Cambrian of the northern Mississippi Valley: Milwaukee Public Museum Contributions in Biology and Geology, v. 91, 50 p.

Hughes, N.C., and Labandeira, C.C., 1995, The stability of species in taxonomy: Paleobiology, v. 21, p. 401–403.

Hunt, G., 2004, Phenotypic variance inflation in fossil samples: an empirical assessment: Paleobiology, v. 30, p. 487–506.

Jaanusson, V., 1975, Evolutionary processes leading to the trilobite suborder Phacopina: Fossils and Strata, v. 4, p. 209–218.

Labandeira, C.C., 1983, The paleobiology of the Dikelocephalidae (Trilobita, Upper Cambrian) and systematic revision of the genus *Dikelocephalus* (Owen) with special reference to changing species concepts in North American paleontological thought [M.S. thesis]: Milwaukee, University of Wisconsin, 328 p.

Labandeira, C.C., and Hughes, N.C., 1994, Biometry of the late Cambrian trilobite genus *Dikelocephalus* and its implications for trilobite systematics: Journal of Paleontology, v. 68, p. 492–517.

Nixon, K.C., and Wheeler, Q.D., 1990, An amplification of the phylogenetic species concept: Cladistics, v. 6, p. 211–223.

Owen, D.D., 1852, Report of the Geological Survey of Wisconsin, Iowa, and Minnesota: Philadelphia, Lippencott, Grambo and Co., 638 p.

Patzkowsky, M.E., and Holland, S.M., 2012, Stratigraphic Paleobiology: Understanding the Distribution of Fossil Taxa in Time and Space: Chicago, University of Chicago Press, 259 p.

Raasch, G.O., 1951, Revision of the Croxian Dikelocephalids: Transactions of the Illinois State Academy of Science, v. 44, p. 137–151.

Ramsköld, L., 1991, Pattern and process in the evolution of the Odontopleuridae (Trilobita). The Selenopeltinae and Ceratocephalinae: Transactions of the Royal Society of Edinburgh: Earth Sciences, v. 82, p. 143–181.

Rohlf, F.J., 2018, tpsDig2. https://life.bio.sunysb.edu/morph/

Rohlf, F.J., 2019, tpsUtil. https://life.bio.sunysb.edu/morph/

Runkel, A.C., 1994, Deposition of the uppermost Cambrian (Croixan) Jordan Sandstone, and the nature of the Cambrian–Ordovician boundary in the Upper Mississippi Valley: Geological Society of America Bulletin, v. 106, p. 427–440.

Runkel, A.C., Miller, J.F., McKay, R.M., Palmer, A.R., and Taylor, J.F., 2007, High-resolution sequence stratigraphy of Lower Paleozoic sheet sandstones in central North America: the role of special conditions of cratonic interiors in development of stratal architecture: Geological Society of America Bulletin, v. 119, p. 860–881.

Runkel, A.C., Miller, J.F., McKay, R.M., Palmer, A.R., and Taylor, J.F., 2008, The record of time in cratonic interior strata: does exceptionally slow subsidence necessarily result in exceptionally poor stratigraphic completeness?, *in* Pratt, B.R. and Homden, C., eds. Geological Association of Canada Special Paper 48, p. 341–362.

Sheets, H.D., 2014, Integrated Morphometrics Package 8. http://www.filogenetica.org/cursos/Morfometria/IMP_installers/index.php

Sheets, H.D., Kim, K., and Mitchell, C.E., 2004, A combined landmark and outline-based approach to ontogenetic shape change in the Ordovician trilobite *Triarthrus becki*, *in* Elewa, A.M.T., ed. Morphometries: Applications in Biology and Paleontology: Berlin, Springer-Verlag, p. 67-82.

Ulrich, E.O., and Resser, C.E., 1930, The Cambrian of the Upper Mississippi Valley, Part 1: Trilobita; Dikelocephalinae and Osceolinae: Bulletin of the Public Museum, Milwaukee, v. 12, p. 1–122.

Webber, A.J., and Hunda, B.R., 2007, Quantitatively comparing morphological trends to environment in the fossil record (Cincinnatian Series, Upper Ordovician): Evolution, v. 61, p. 1455–1465.

Webster, M., 2007, A Cambrian peak in morphological variation within trilobite species: Science, v. 317, p. 499–502.

Webster, M., 2011, The structure of cranidial shape variation in three early ptychoparioid trilobite species from the Dyeran-Delamaran (traditional "Lower-Middle" Cambrian) boundary interval of Nevada, U.S.A.: Journal of Paleontology, v. 85, p. 179–225.

Webster, M., 2015, Ontogeny and intraspecific variation of the early Cambrian trilobite *Olenellus gilberti*, with implications for olenelline phylogeny and macroevolutionary trends in phenotypic canalization: Journal of Systematic Palaeontology, v. 13, p. 1–74.

Webster, M., 2019, Morphological homeostasis in the fossil record: Seminars in Cell & Developmental Biology, v. 88, p. 91–104.

Webster, M., and Hughes, N.C., 1999, Compaction-related deformation in Cambrian olenelloid trilobites and its implications for fossil morphometry: Journal of Paleontology, v. 73, p. 355–371.

Webster, M., and Sheets, H.D., 2010, A practical introduction to landmark-based geometric morphometrics, *in* Alroy, J., and Hunt, G., eds. Quantitative Methods in Paleontology: Paleontological Society Papers Vol. 16., p. 163–188.

Wheeler, Q.D., and Meier, R., 2000, Species Concepts and Phylogenetic Theory: New York, Columbia University Press, 230 p.

Zelditch, M.L., Swiderski, D.L., and Sheets, H.D., 2012, Geometric Morphometrics for Biologists: A Primer: San Diego, Elsevier Academic Press, 478 p.

Figures
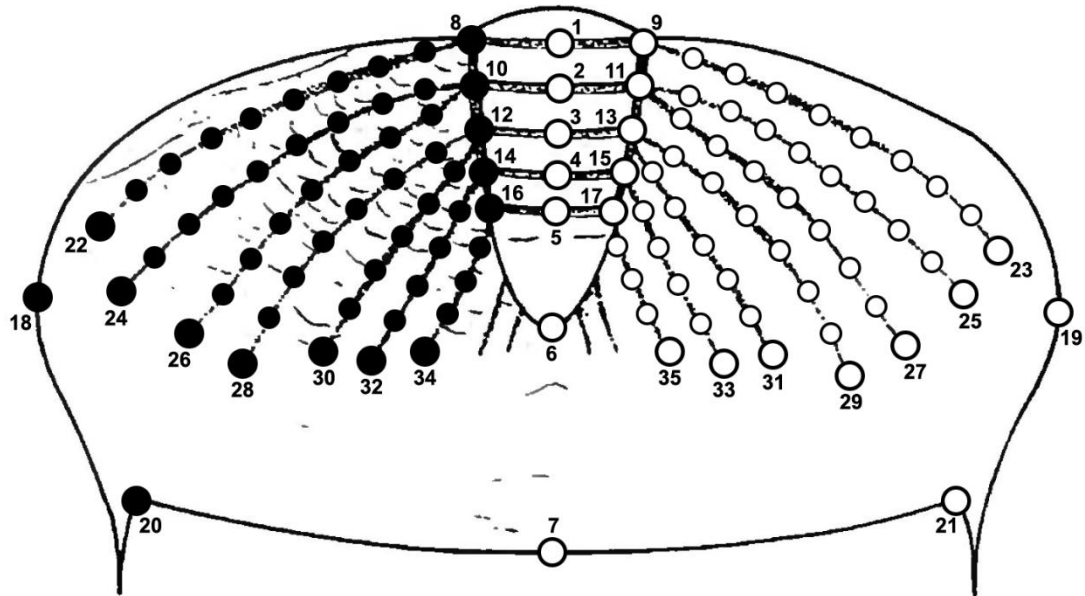
Figure 1. Selection of landmarks and semilandmarks on the pygidium of

Dikelocephalus (modified from Hughes, 1994, Fig. 46). Thirty-five landmarks

(large circles) and eighty-two semilandmarks (small circles) in total. Eight

semilandmarks between landmarks 8 and 22, 9 and 23, 10 and 24, and 11 and

25. Seven semilandmarks between landmarks 10 and 26, and 11 and 27. Six

semilandmarks between landmarks 12 and 28, and 13 and 29. Five

semilandmarks between landmarks 12 and 30, and 13 and 31. Four

semilandmarks between landmarks 14 and 32, and 15 and 33. Three

semilandmarks between landmarks 16 and 34, and 17 and 35. Empty circles

show configuration after reflecting and averaging of paired homologous

landmarks across the saggital axis. The averaged configuration has twenty-one

landmarks and forty-one semilandmarks.
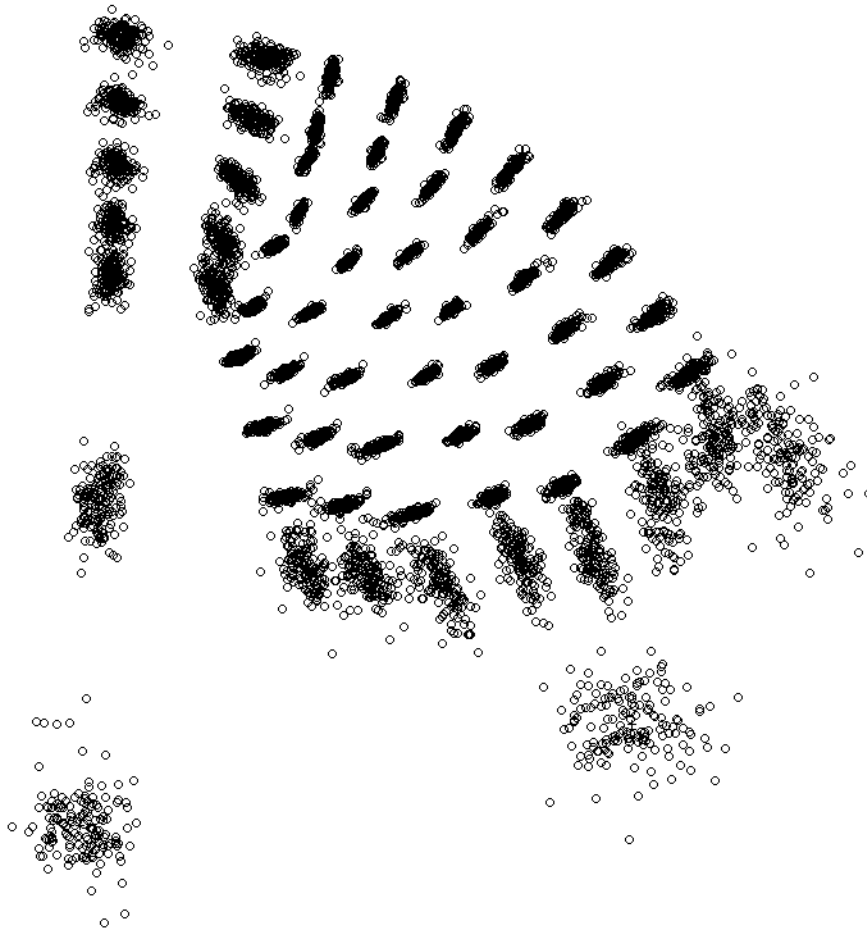
Figure 2. Partial Procrustes superimposition of 21 landmarks and 41 semilandmarks for 157 pygidia specimens of *Dikelocephalus* from multiple localities.
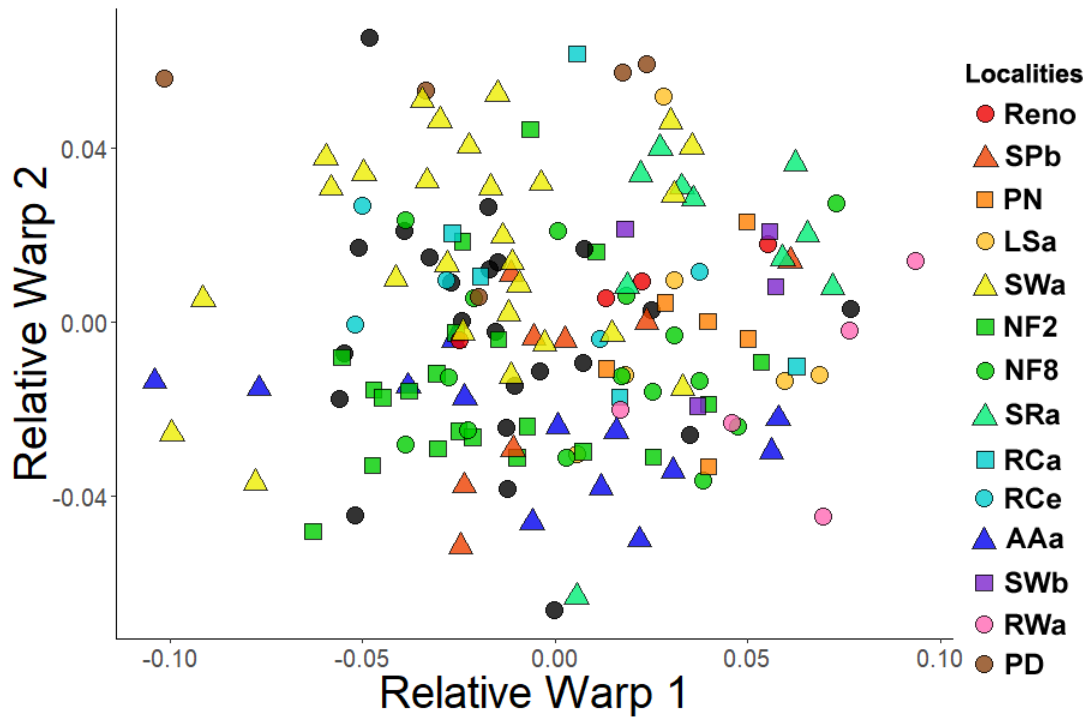
Figure 3. RW1 (30.1% variance explained) versus RW2 (14.1% variance explained). Landmark configuration shown in Fig. 2; reference form is the mean of all 157 configurations in the sample. Color gradient represents relative age with the red locality being the oldest and the purple locality being the youngest. Relative ages of pink and brown localities are unknown. Black circles represent localities with less than four specimens.
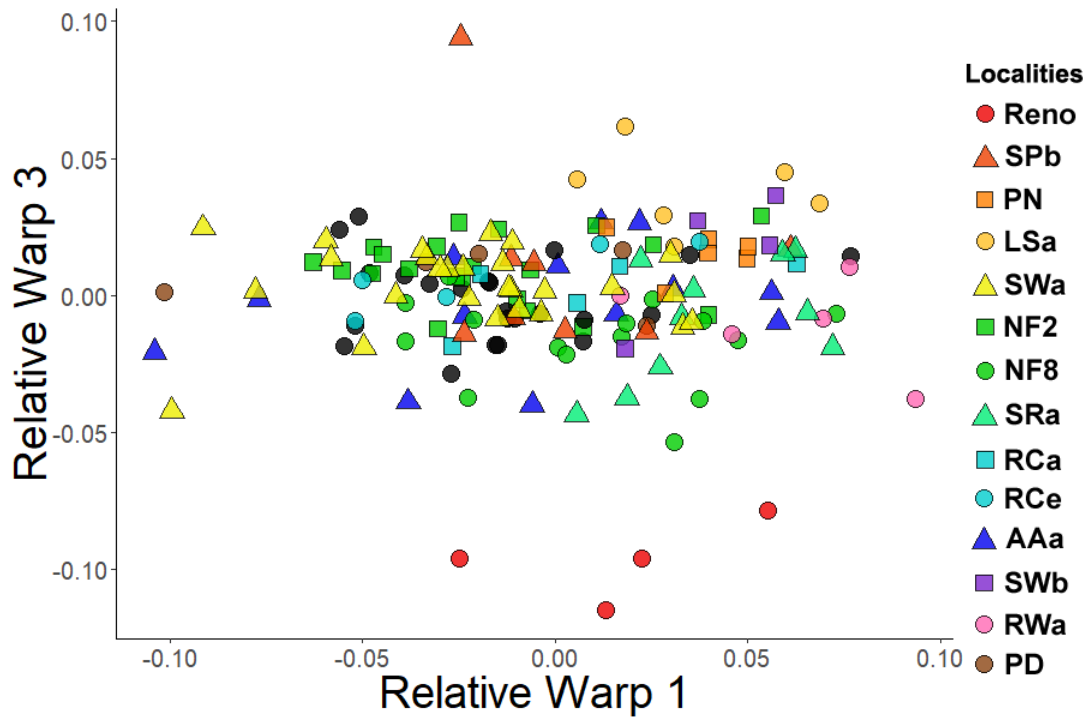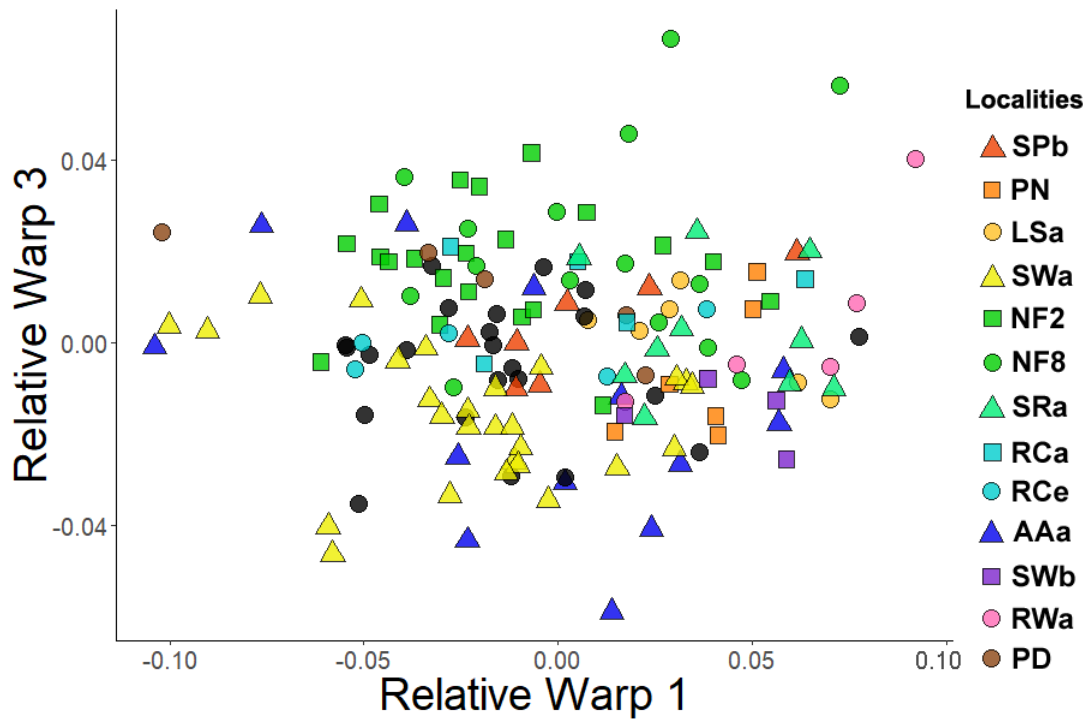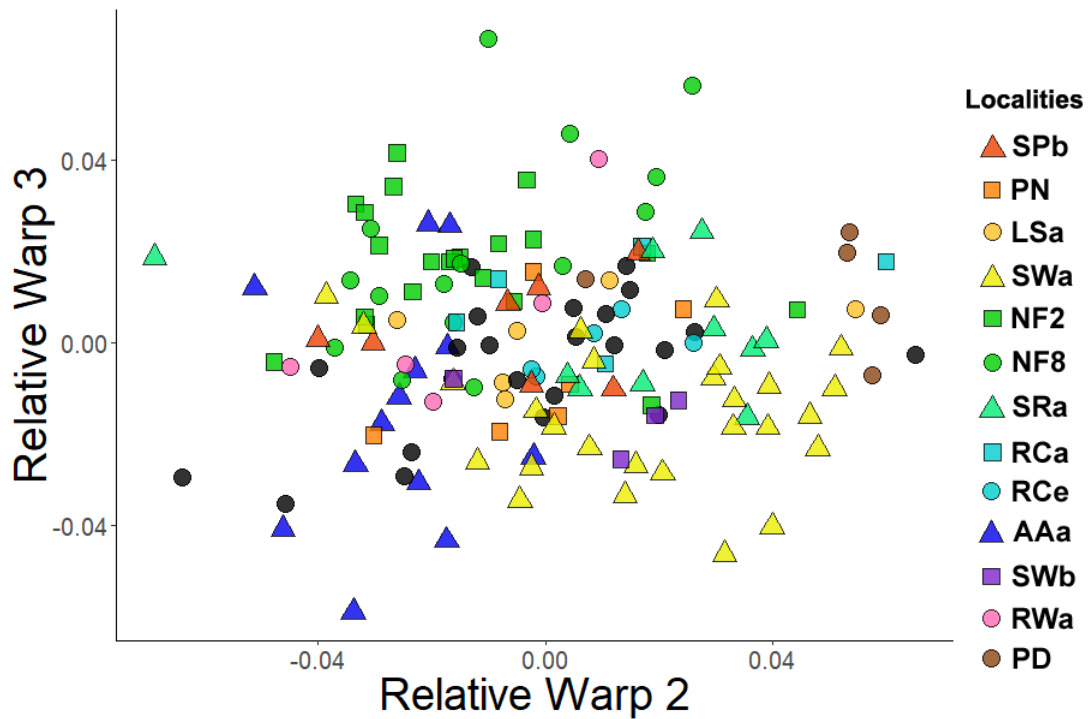
Figure 4. RW1 (30.1% variance explained) versus RW3 (12.2% variance

explained). Landmark configuration shown in Fig. 2; reference form is the mean

of all 157 configurations in the sample. Color gradient represents relative age

with the red locality being the oldest and the purple locality being the youngest.

Relative ages of pink and brown localities are unknown. Black circles represent
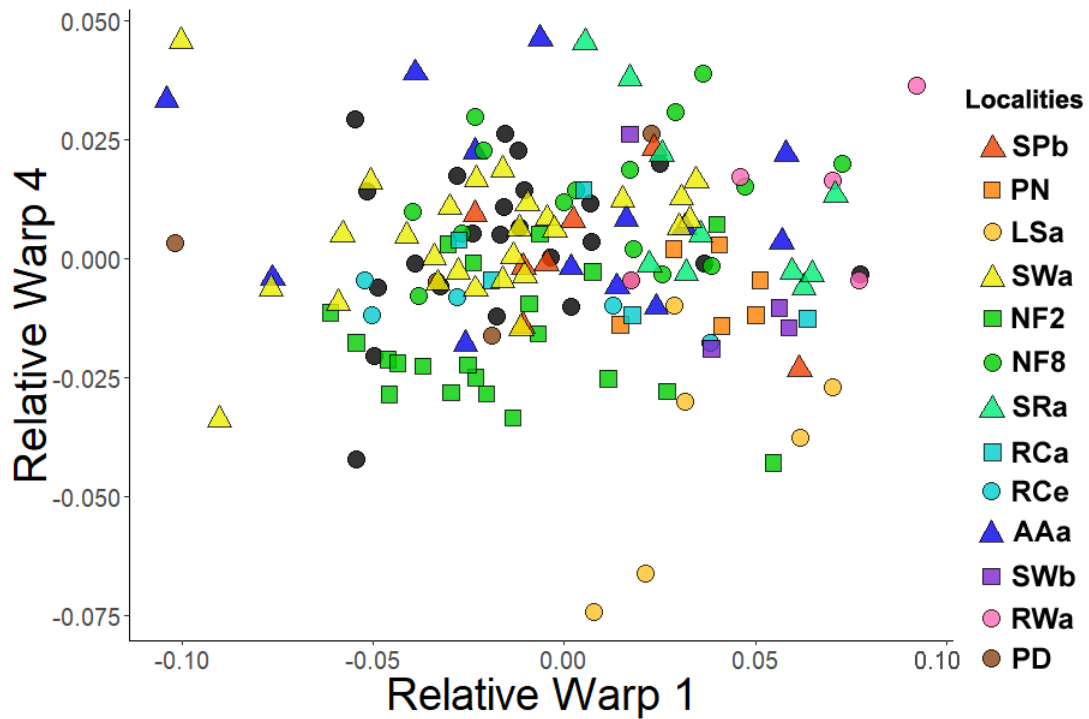
localities with less than four specimens.
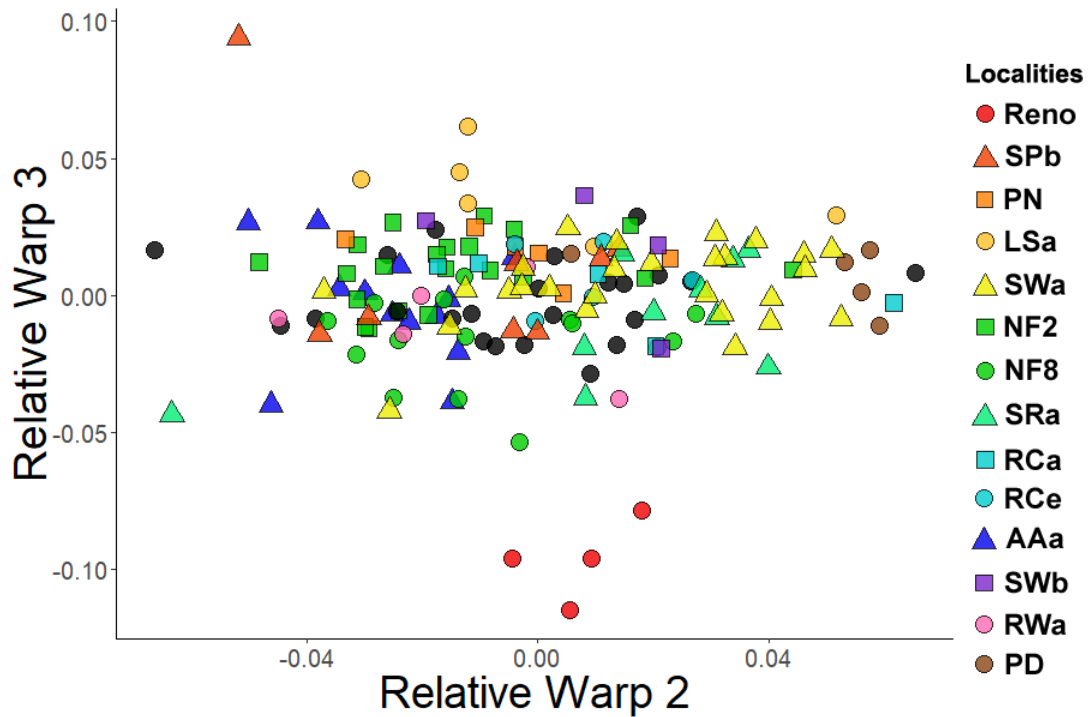
Figure 5. RW2 (14.1% variance explained) versus RW3 (12.2% variance explained). Landmark configuration shown in Fig. 2; reference form is the mean of all 157 configurations in the sample. Color gradient represents relative age with the red locality being the oldest and the purple locality being the youngest. Relative ages of pink and brown localities are unknown. Black circles represent localities with less than four specimens.
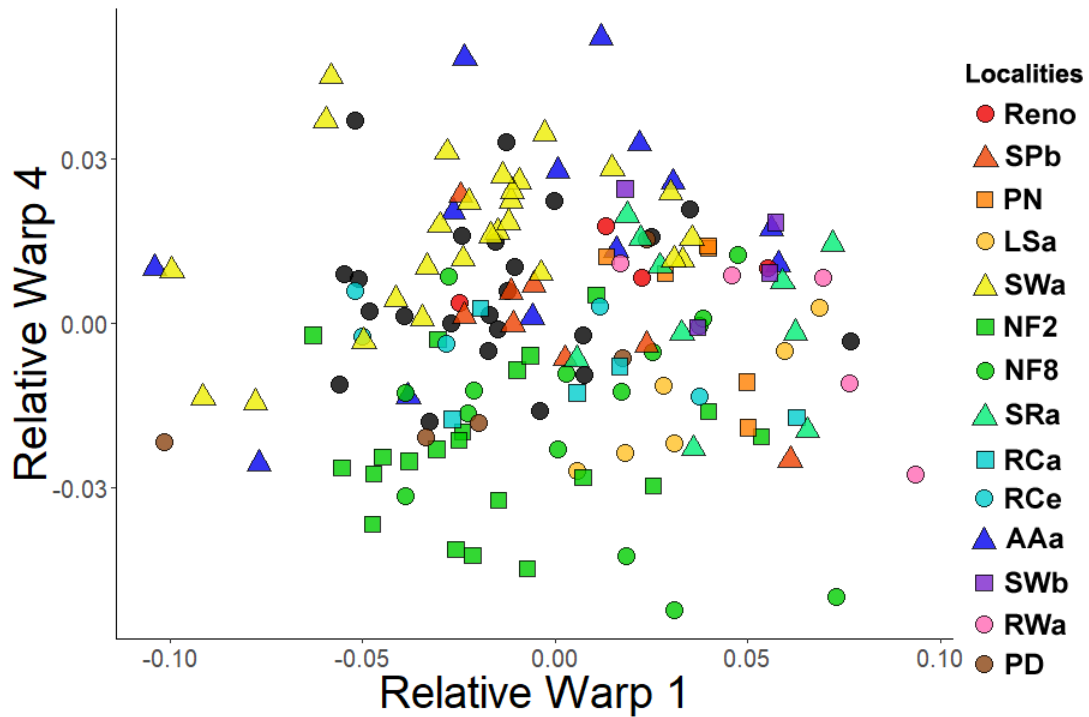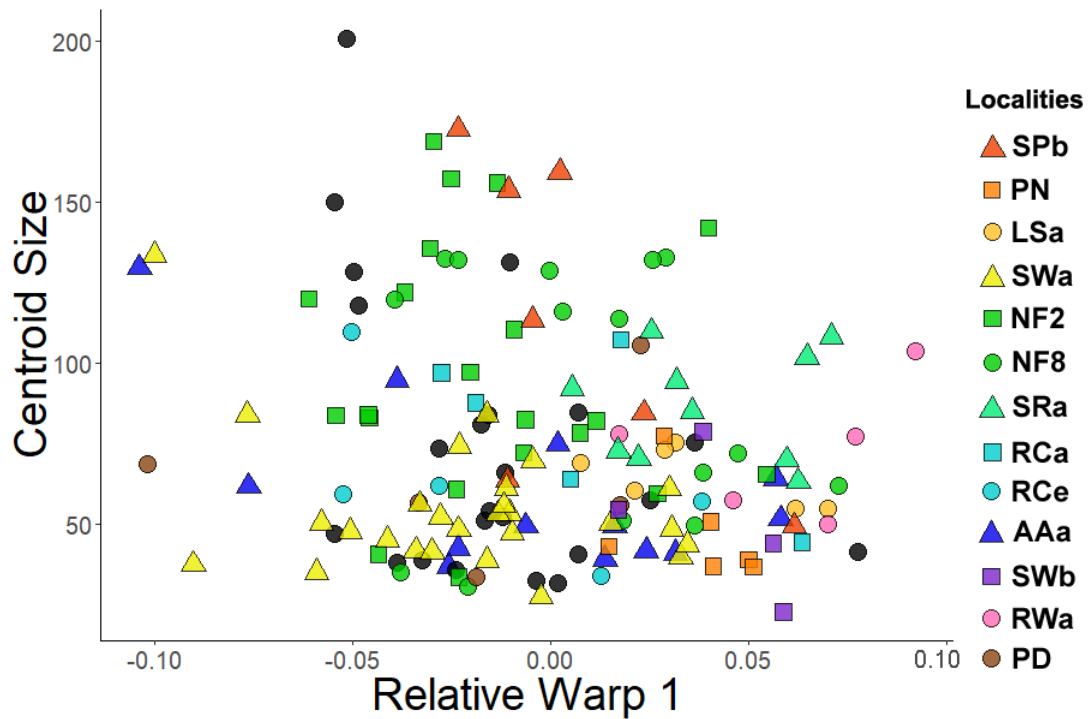
Figure 6. RW1 (30.1% variance explained) versus RW4 (7.6% variance explained). Landmark configuration shown in Fig. 2; reference form is the mean of all 157 configurations in the sample. Color gradient represents relative age with the red locality being the oldest and the purple locality being the youngest. Relative ages of pink and brown localities are unknown. Black circles represent localities with less than four specimens.
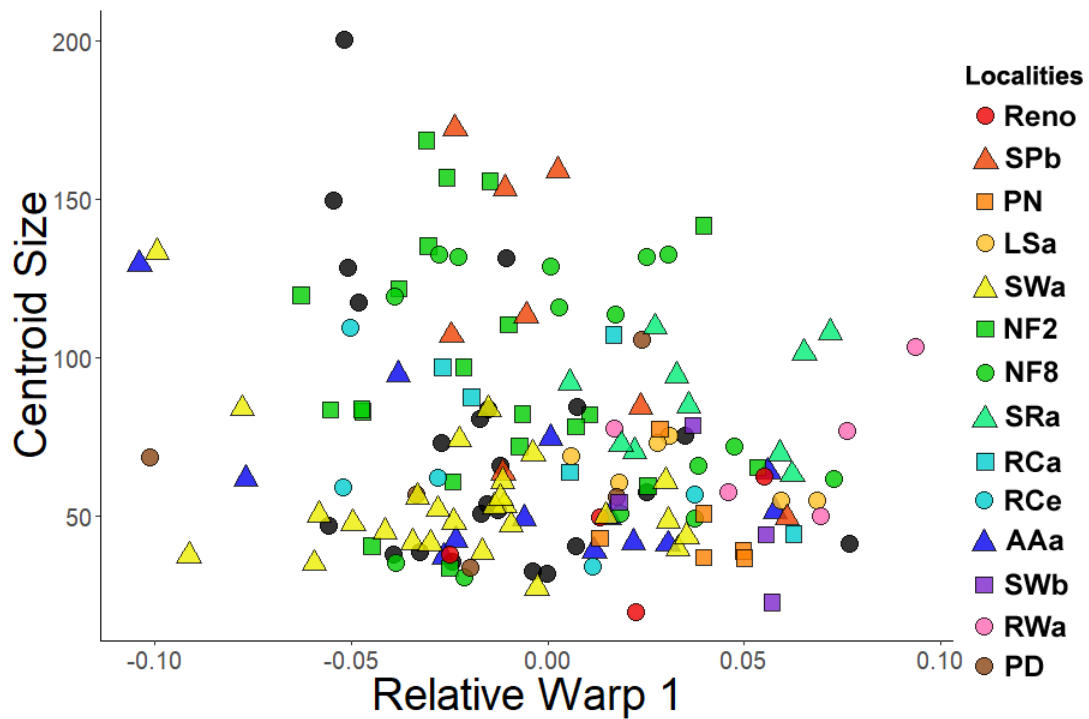
Figure 7. RW1 (30.1% variance explained) versus centroid size. Landmark configuration shown in Fig. 2; reference form is the mean of all 157 configurations in the sample. Color gradient represents relative age with the red locality being the oldest and the purple locality being the youngest. Relative ages of pink and brown localities are unknown. Black circles represent localities with less than four specimens.
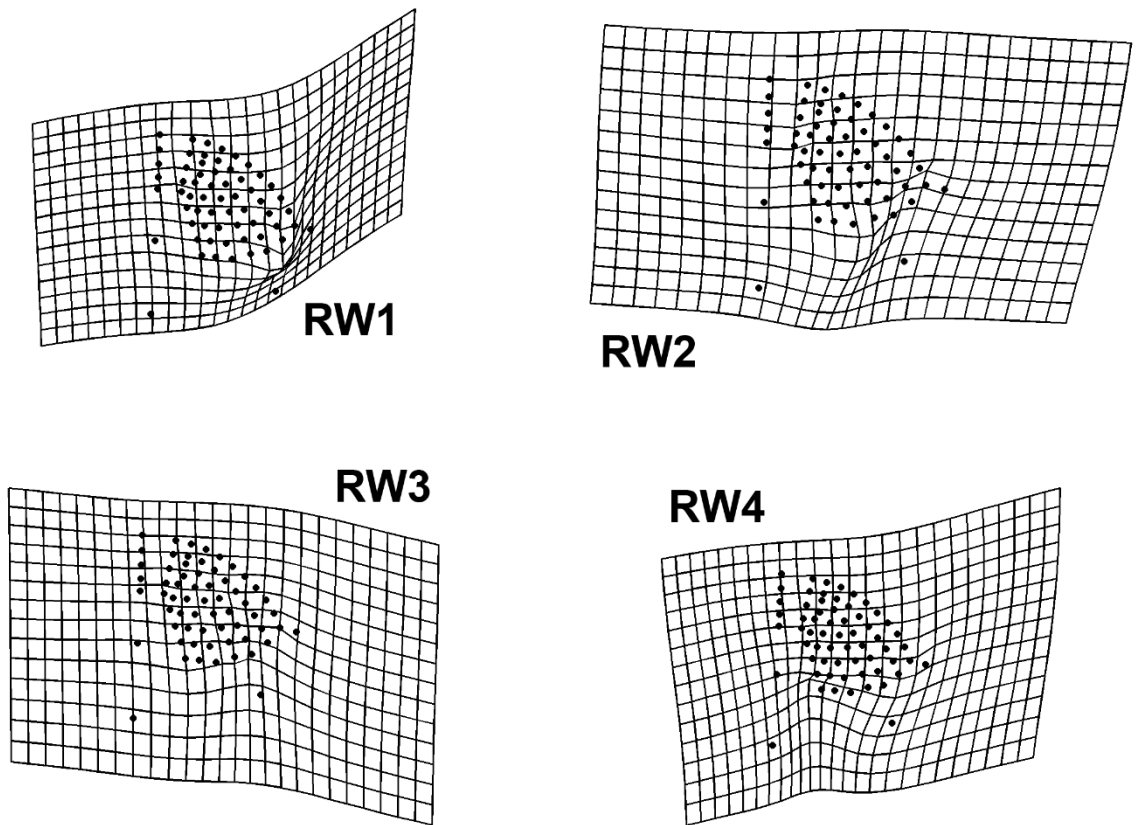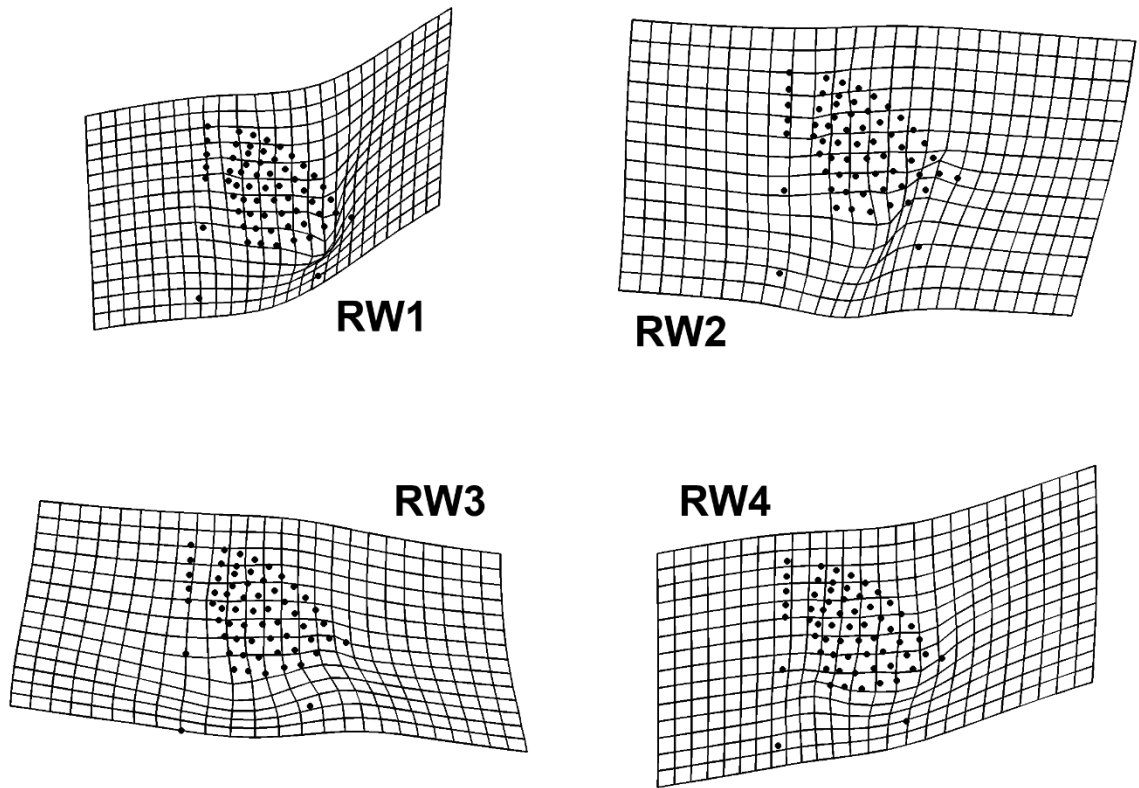
Figure 8. Thin-plate spline deformation grids depicting shape variation along the first four relative warps in a positive direction for 21 landmarks and 41 semilandmarks of 157 *Dikelocephalus* specimens (Fig. 2). RW1 summarizes 30.1% of the variation, RW2 summarizes 14.1% of the variation, RW3 summarizes 12.2% of the variation, and RW4 summarizes 7.6% of the variation.
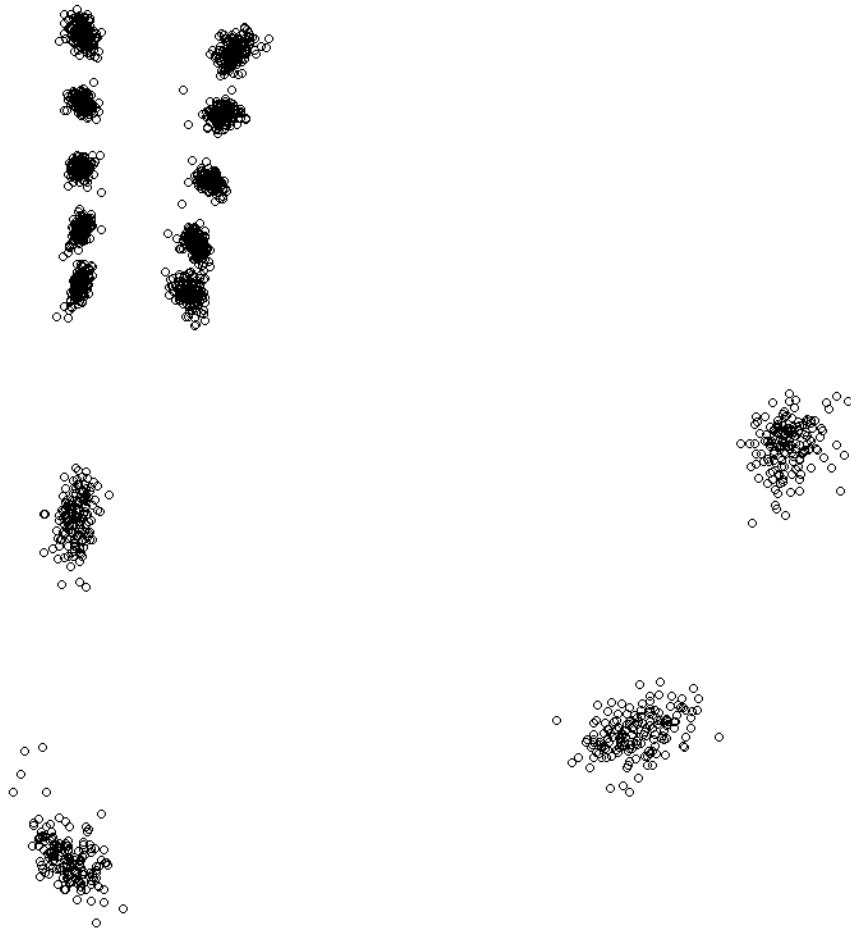
Figure 9. Partial Procrustes superimposition of 14 landmarks for 157 pygidia specimens of *Dikelocephalus* from multiple localities. Landmarks and semilandmarks corresponding to pleural furrows removed (compare to Fig. 2).
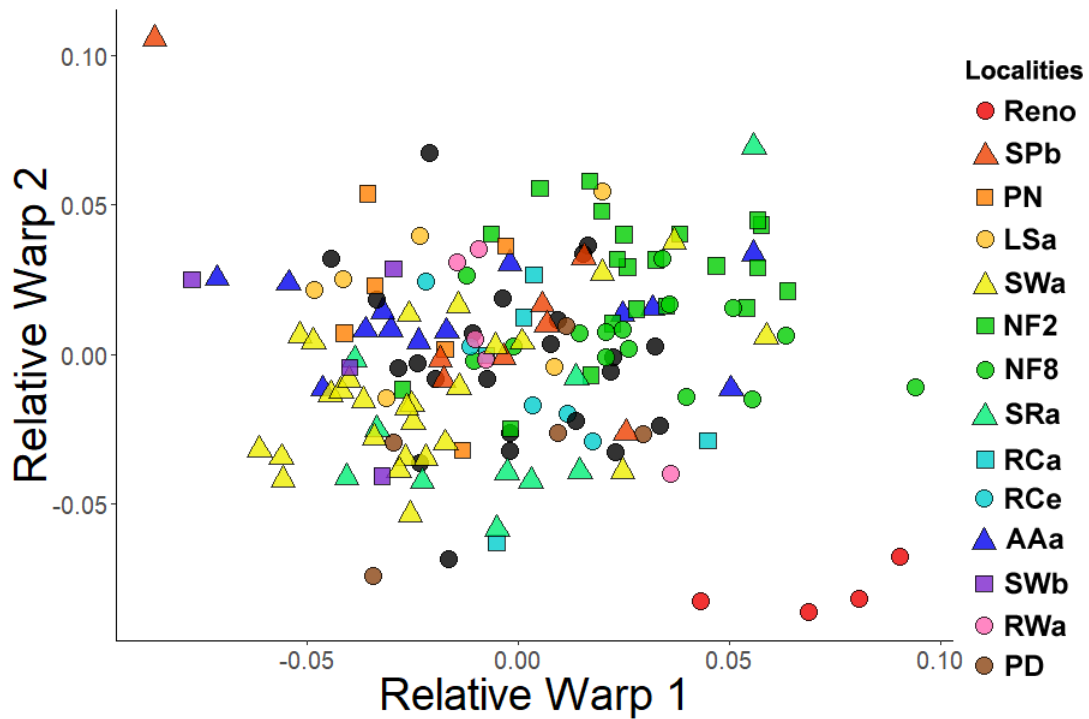
Figure 10. RW1 (32.2% variance explained) versus RW2 (27.5% variance explained). Landmark configuration shown in Fig. 9; reference form is the mean of all 157 configurations in the sample. Color gradient represents relative age with the red locality being the oldest and the purple locality being the youngest. Relative ages of pink and brown localities are unknown. Black circles represent localities with less than four specimens.
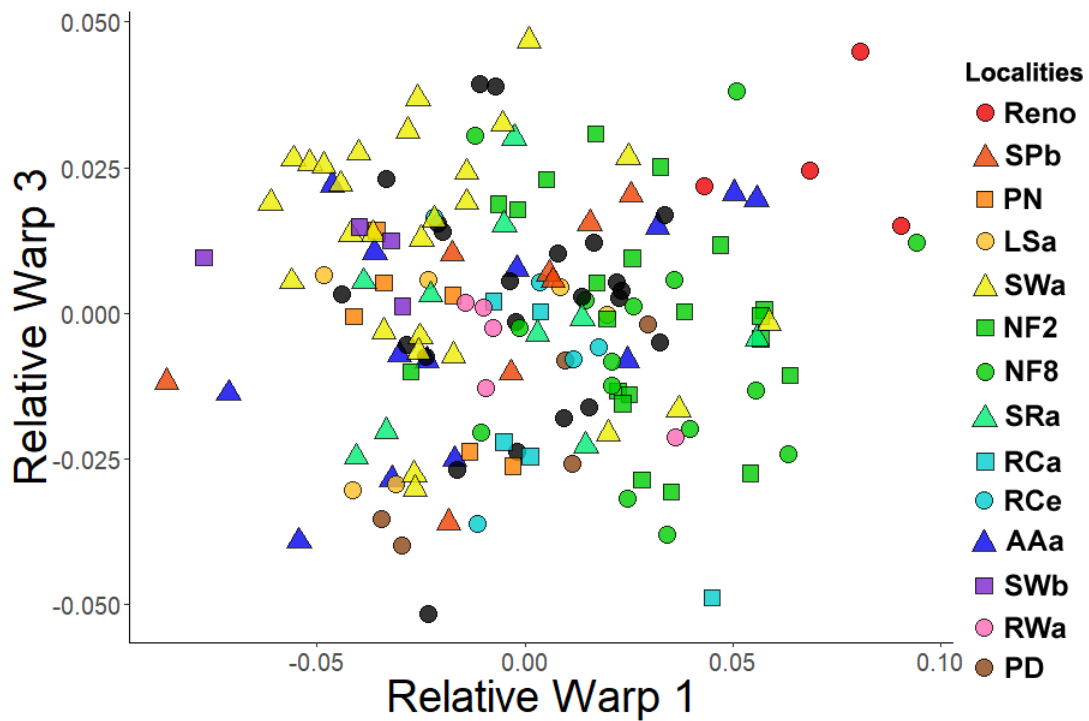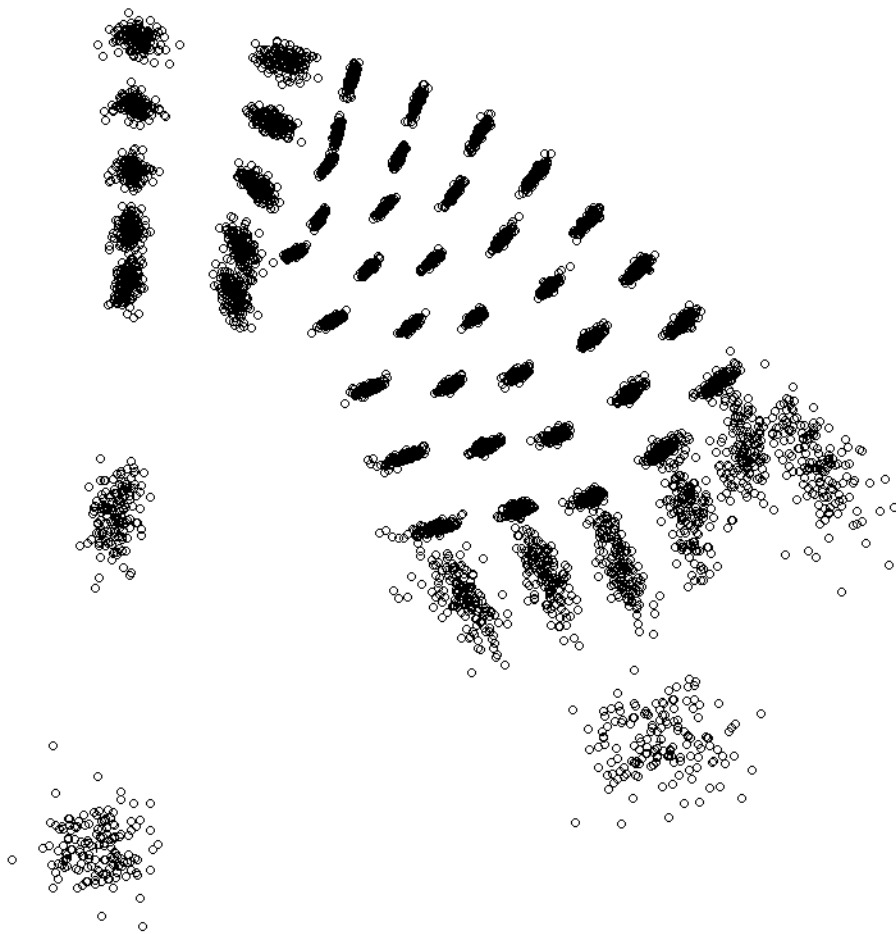
Figure 11. RW1 (32.2% variance explained) versus RW3 (11.0% variance explained). Landmark configuration shown in Fig. 9; reference form is the mean of all 157 configurations in the sample. Color gradient represents relative age with the red locality being the oldest and the purple locality being the youngest. Relative ages of pink and brown localities are unknown. Black circles represent localities with less than four specimens.
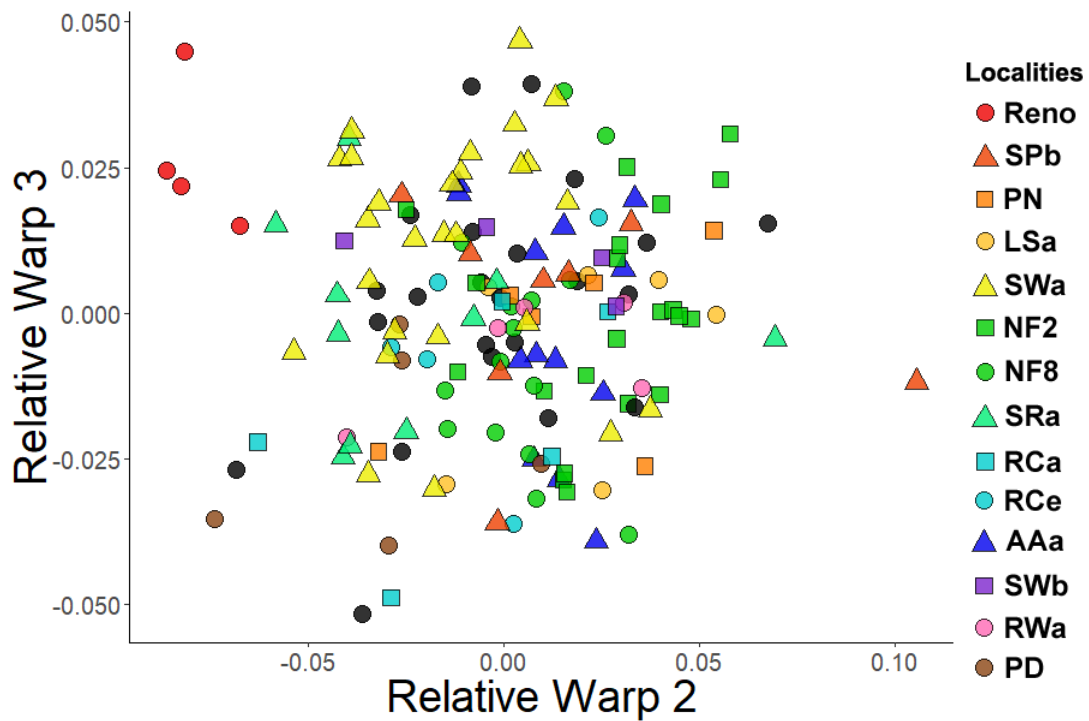
Figure 12. RW2 (27.5% variance explained) versus RW3 (11.0% variance explained). Landmark configuration shown in Fig. 9; reference form is the mean of all 157 configurations in the sample. Color gradient represents relative age with the red locality being the oldest and the purple locality being the youngest. Relative ages of pink and brown localities are unknown. Black circles represent localities with less than four specimens.
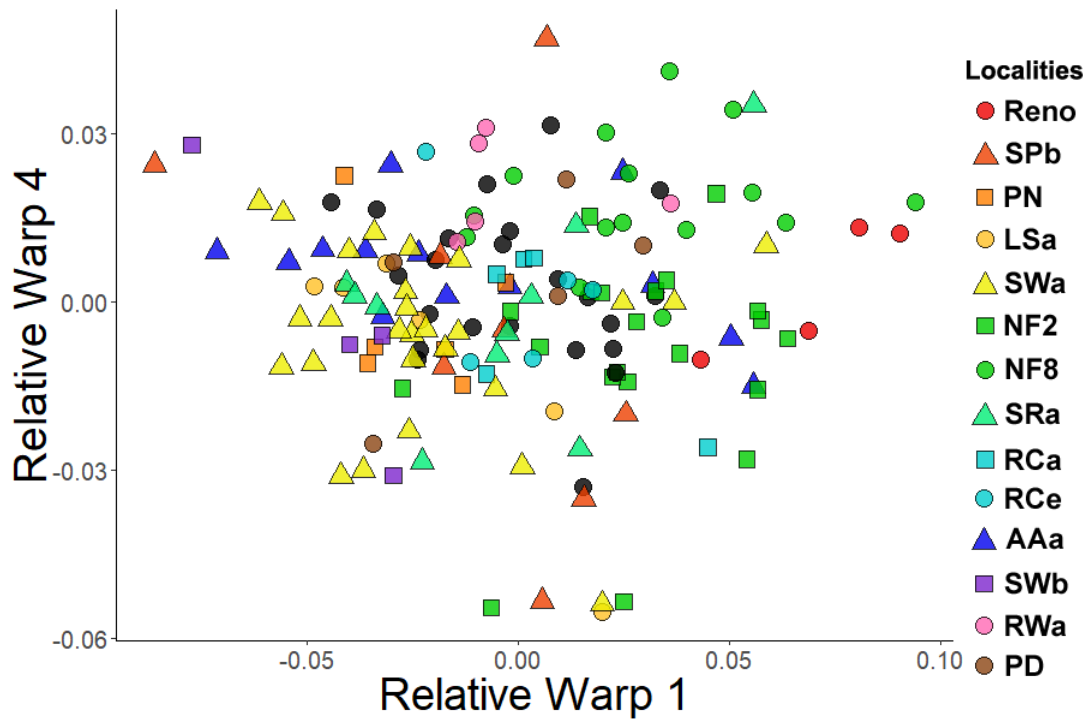
Figure 13. RW1 (32.2% variance explained) versus RW4 (9.1% variance explained). Landmark configuration shown in Fig. 9; reference form is the mean of all 157 configurations in the sample. Color gradient represents relative age with the red locality being the oldest and the purple locality being the youngest. Relative ages of pink and brown localities are unknown. Black circles represent localities with less than four specimens.
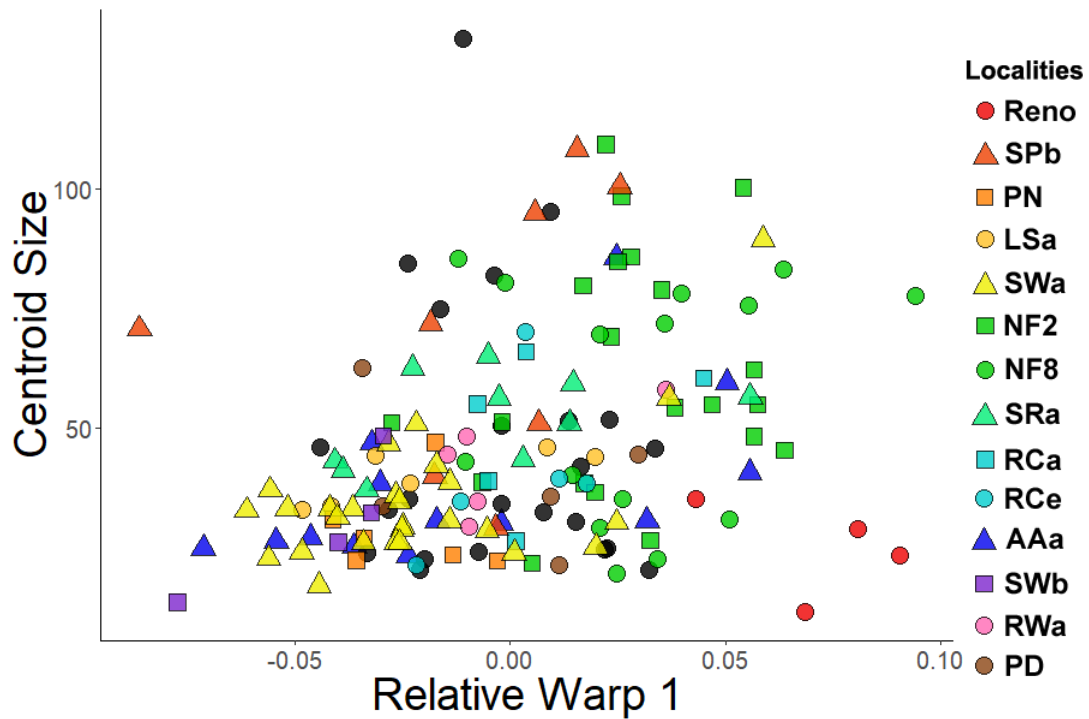
Figure 14. RW1 (32.2% variance explained) versus centroid size. Landmark configuration shown in Fig. 9; reference form is the mean of all 157 configurations in the sample. Color gradient represents relative age with the red locality being the oldest and the purple locality being the youngest. Relative ages of pink and brown localities are unknown. Black circles represent localities with less than four specimens.
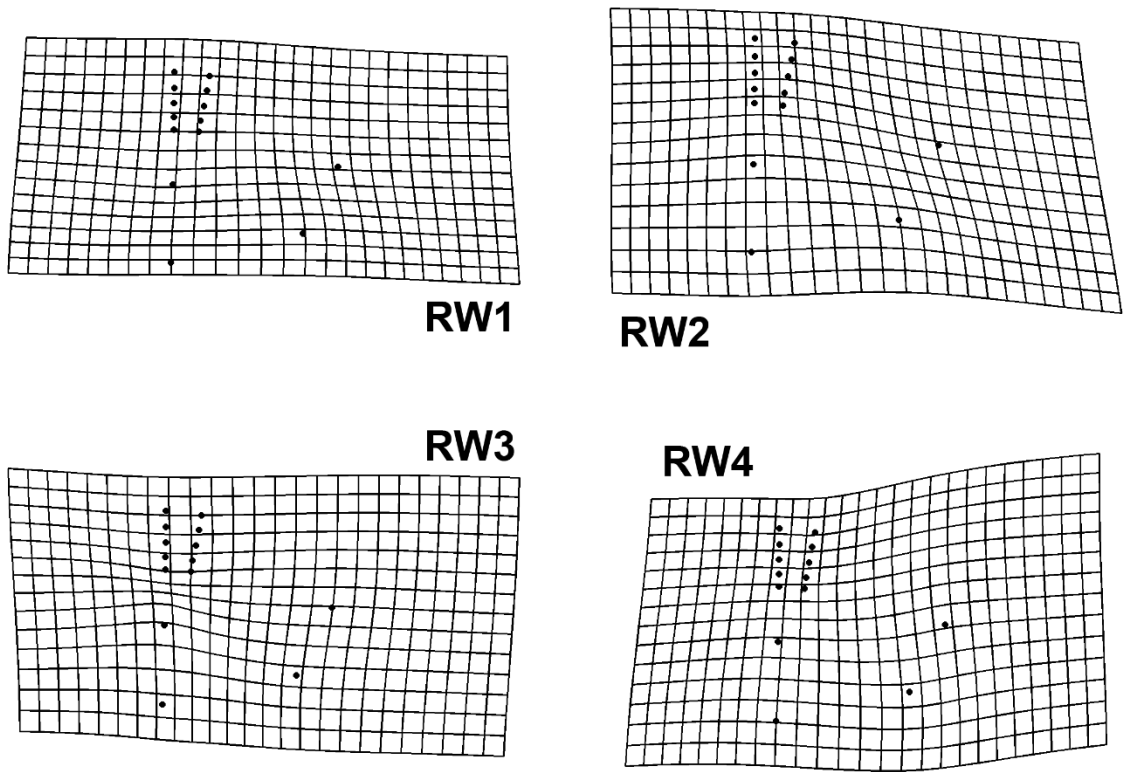
Figure 15. Thin-plate spline deformation grids depicting shape variation along the first four relative warps in a positive direction for 14 landmarks of 157 *Dikelocephalus* specimens (Fig. 9). RW1 summarizes 32.2% of the variation, RW2 summarizes 27.5% of the variation, RW3 summarizes 11.0% of the variation, and RW4 summarizes 9.1% of the variation.
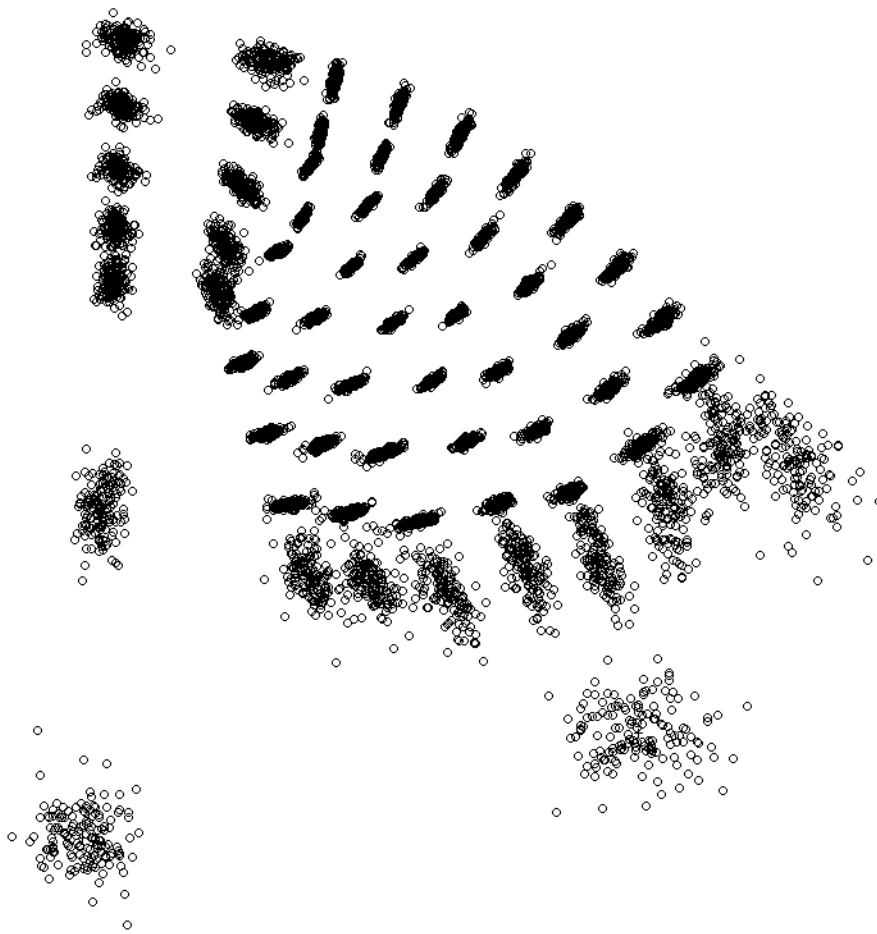
Figure 16. Partial Procrustes superimposition of 21 landmarks and 41 semilandmarks for 152 pygidia specimens of *Dikelocephalus* from multiple localities. Five outliers excluded (compare to Fig. 2).
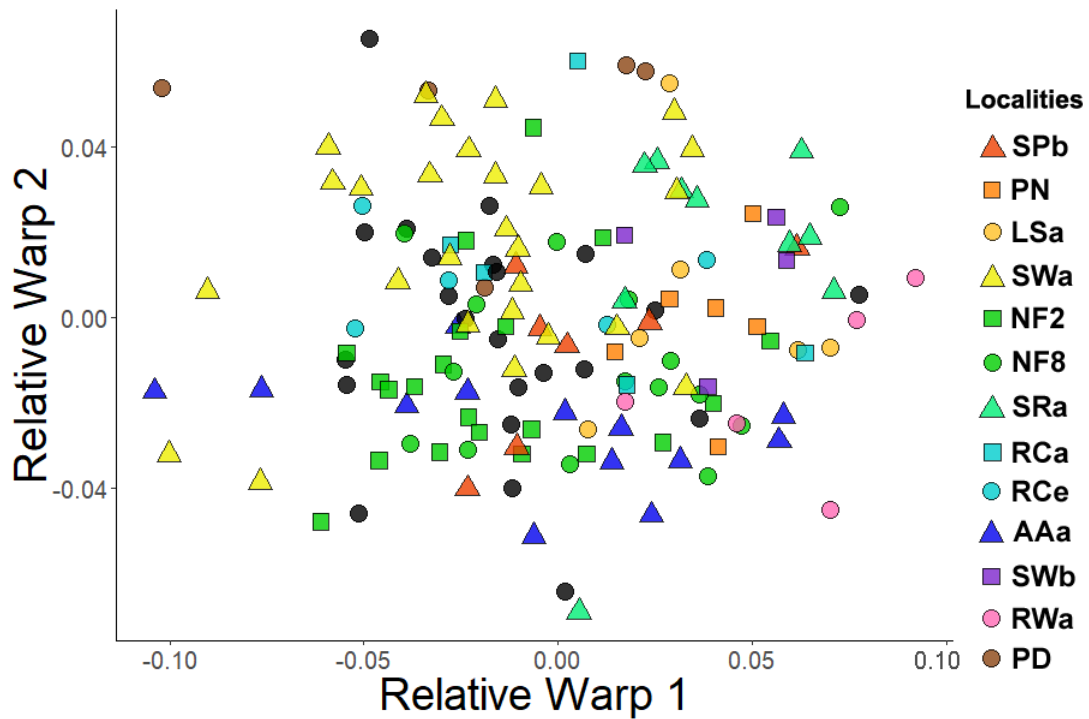
Figure 17. RW1 (32.4% variance explained) versus RW2 (15.2% variance explained). Landmark configuration shown in Fig. 16; reference form is the mean of all 152 configurations in the sample. Color gradient represents relative age with the orange locality being the oldest and the purple locality being the youngest. Relative ages of pink and brown localities are unknown. Black circles represent localities with less than four specimens.
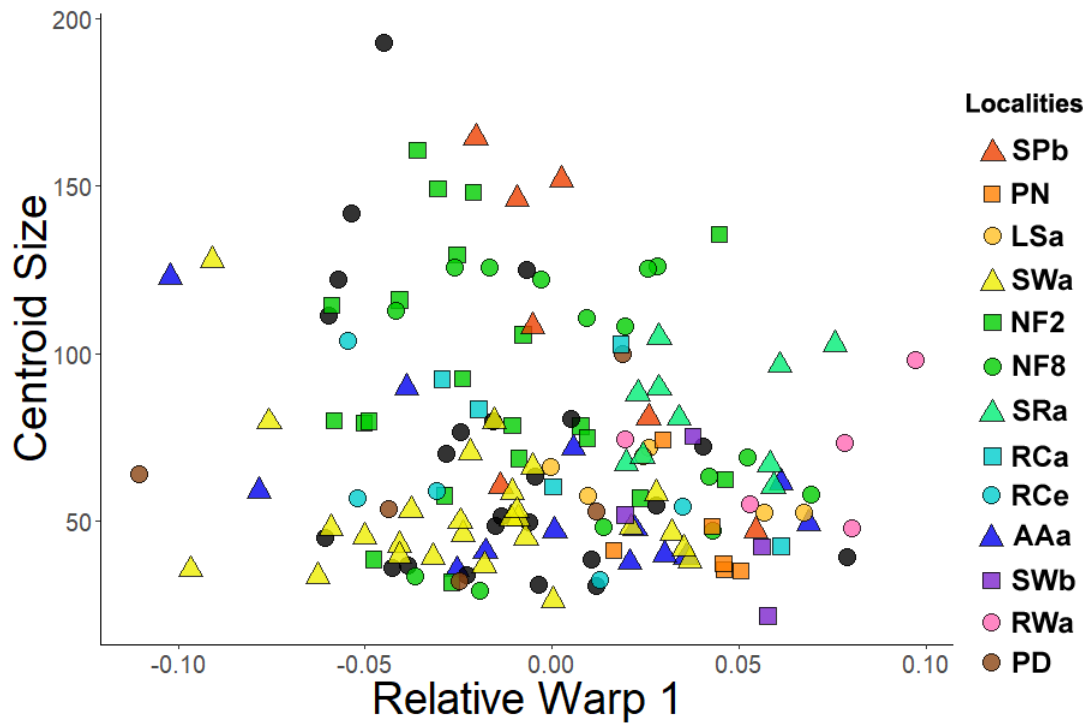
Figure 18. RW1 (32.4% variance explained) versus RW3 (8.3% variance explained). Landmark configuration shown in Fig. 16; reference form is the mean of all 152 configurations in the sample. Color gradient represents relative age with the orange locality being the oldest and the purple locality being the youngest. Relative ages of pink and brown localities are unknown. Black circles represent localities with less than four specimens.

Figure 19. RW2 (15.2% variance explained) versus RW3 (8.3% variance explained). Landmark configuration shown in Fig. 16; reference form is the mean of all 152 configurations in the sample. Color gradient represents relative age with the orange locality being the oldest and the purple locality being the youngest. Relative ages of pink and brown localities are unknown. Black circles represent localities with less than four specimens.

Figure 20. RW1 (32.4% variance explained) versus RW4 (7.8% variance explained). Landmark configuration shown in Fig. 16; reference form is the mean of all 152 configurations in the sample. Color gradient represents relative age with the orange locality being the oldest and the purple locality being the youngest. Relative ages of pink and brown localities are unknown. Black circles represent localities with less than four specimens.

Figure 21. RW1 (32.4% variance explained) versus centroid size. Landmark configuration shown in Fig. 16; reference form is the mean of all 152 configurations in the sample. Color gradient represents relative age with the orange locality being the oldest and the purple locality being the youngest. Relative ages of pink and brown localities are unknown. Black circles represent localities with less than four specimens.

Figure 22. Thin-plate spline deformation grids depicting shape variation along the first four relative warps in a positive direction for 21 landmarks and 41 semilandmarks of 152 *Dikelocephalus* specimens (Fig. 16). RW1 summarizes 32.4% of the variation, RW2 summarizes 15.2% of the variation, RW3 summarizes 8.3% of the variation, and RW4 summarizes 7.8% of the variation.
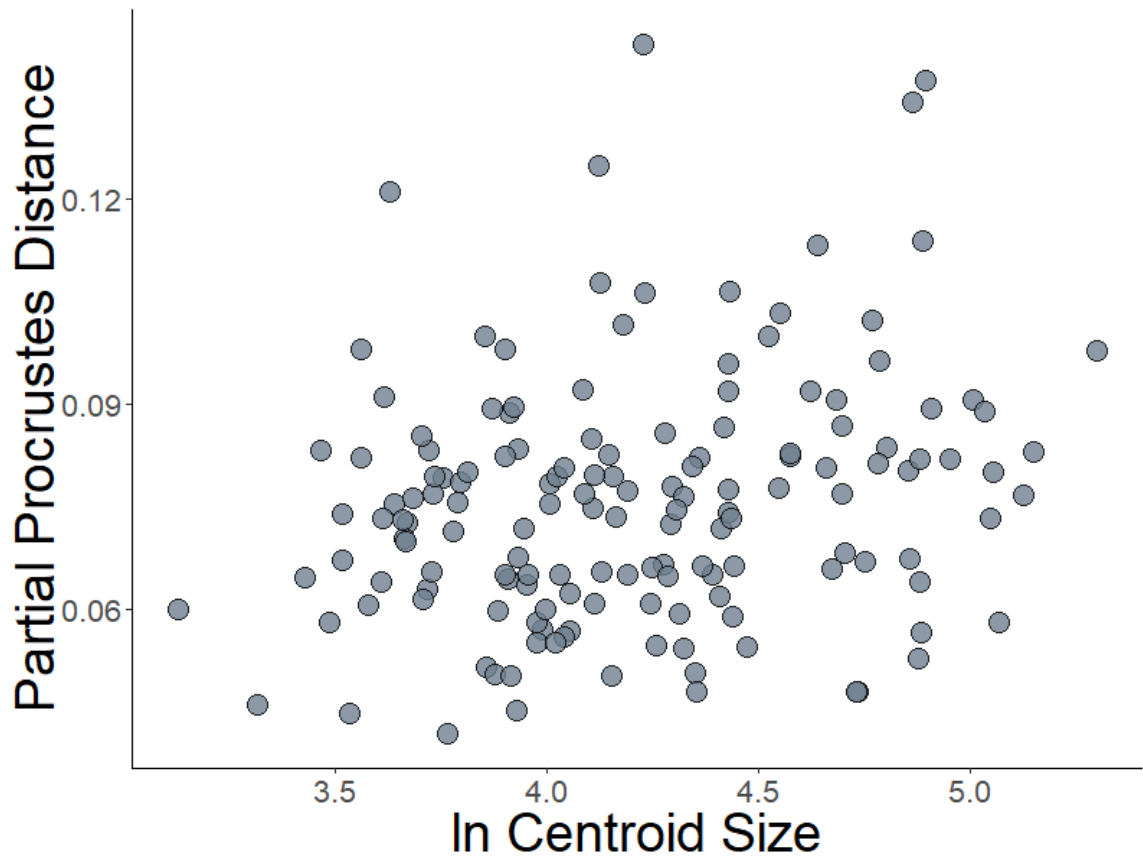
Figure 23. Partial Procrustes distance from the reference form (mean configuration of smallest three specimens) versus logarithm of centroid size (lnCS) for 21 landmarks and 41 semilandmarks of 152 *Dikelocephalus* specimens (Fig. 16). Regression of partial Procrustes distance against lnCS is significant (slope=0.0093, p=0.0021, r=0.2299).
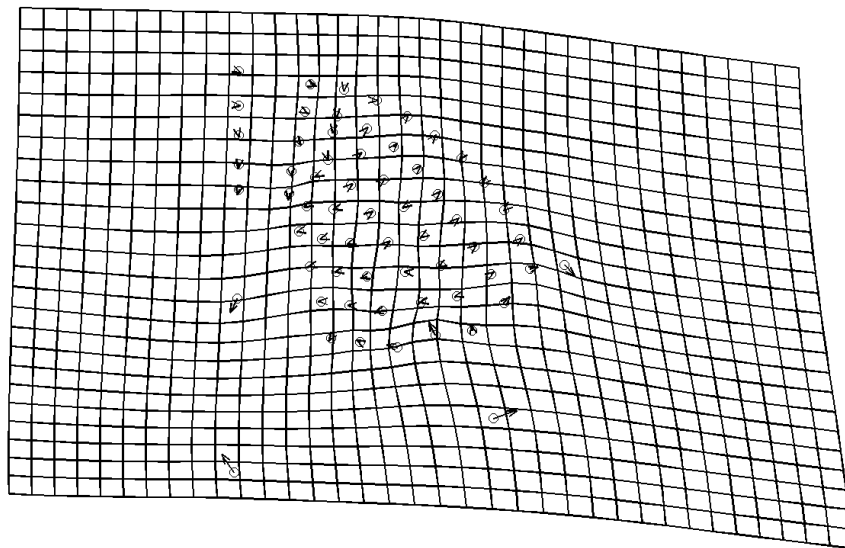
Figure 24. Thin-plate spline deformation grid depicting shape change with growth for 21 landmarks and 41 semilandmarks of 152 *Dikelocephalus* specimens (Fig. 16). Shape change calculated by a multivariate regression of partial warp scores against lnCS and 2.58% of total shape variance (based on summed squared residuals expressed in Procrustes units) is explained by allometry (p=0.001250 from 1600 bootstraps).

Figure 25. Partial Procrustes superimposition of 19 landmarks and 34 semilandmarks for 152 pygidia specimens of *Dikelocephalus* from multiple localities. Landmarks and semilandmarks corresponding to the posteriormost pair of pleural furrows removed (compare to Fig. 16). Five outliers excluded.
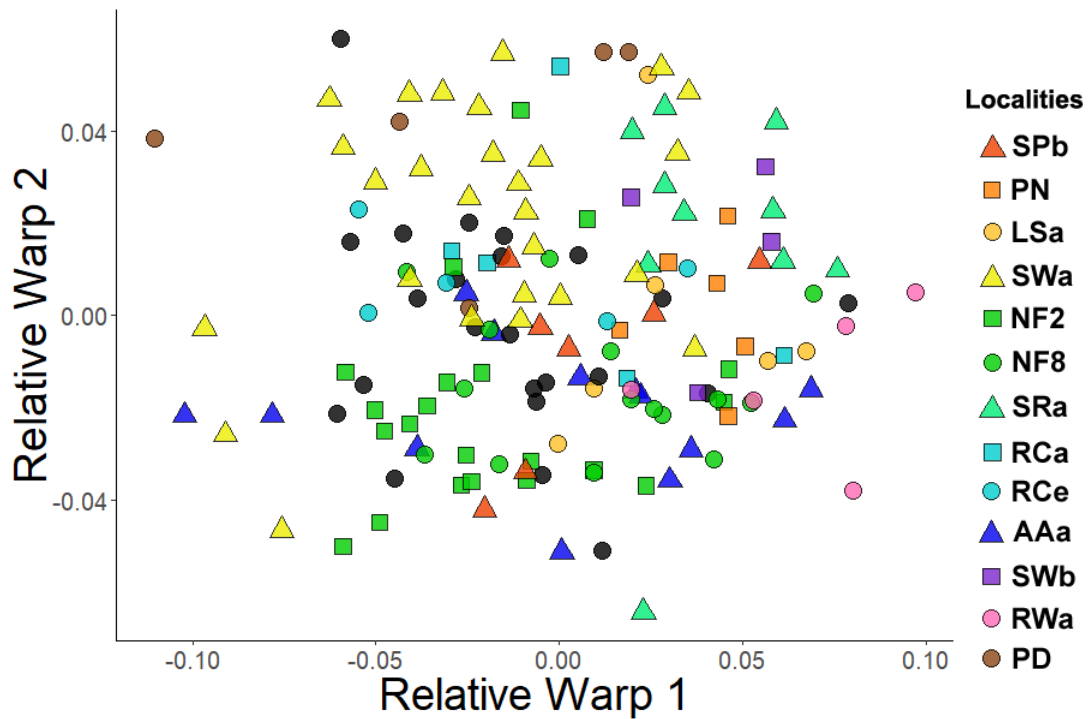
Figure 26. RW1 (35.0% variance explained) versus RW2 (15.5% variance explained). Landmark configuration shown in Fig. 25; reference form is the mean of all 152 configurations in the sample. Color gradient represents relative age with the orange locality being the oldest and the purple locality being the youngest. Relative ages of pink and brown localities are unknown. Black circles represent localities with less than four specimens.
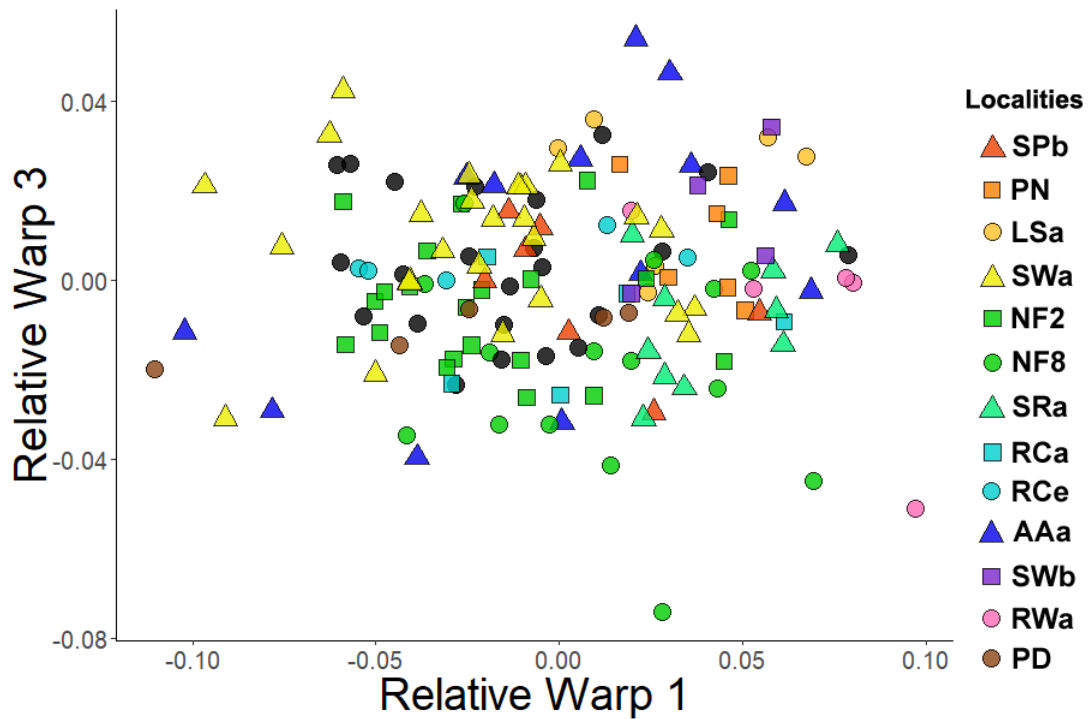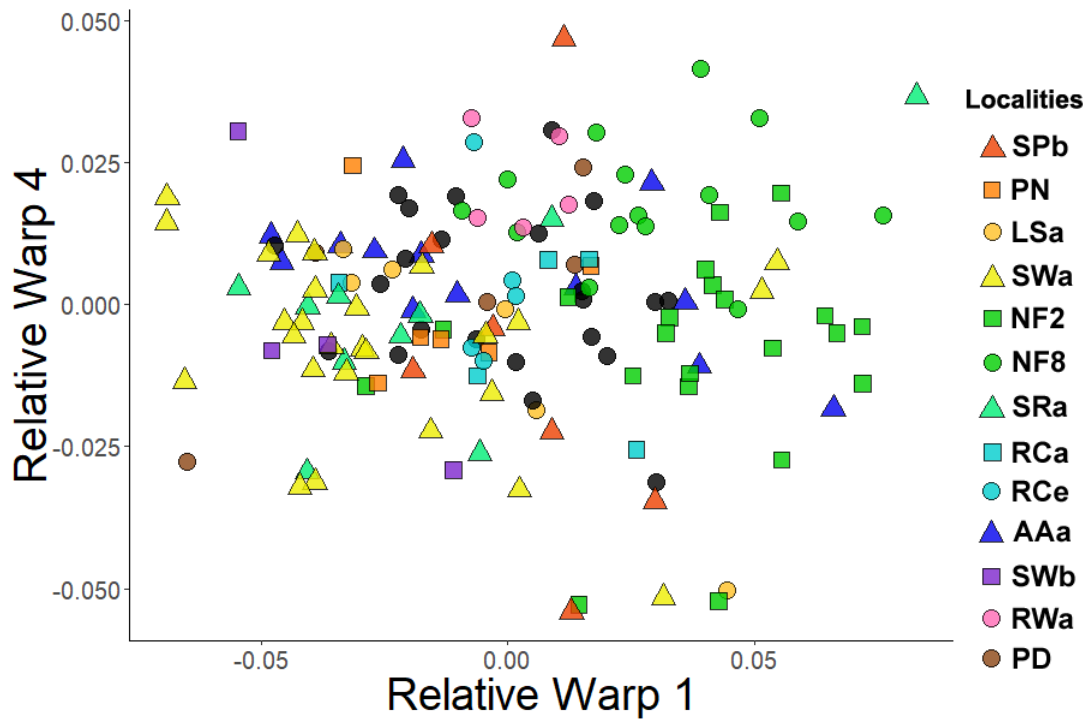
Figure 27. RW1 (35.0% variance explained) versus RW3 (8.4% variance explained). Landmark configuration shown in Fig. 25; reference form is the mean of all 152 configurations in the sample. Color gradient represents relative age with the orange locality being the oldest and the purple locality being the youngest. Relative ages of pink and brown localities are unknown. Black circles represent localities with less than four specimens.
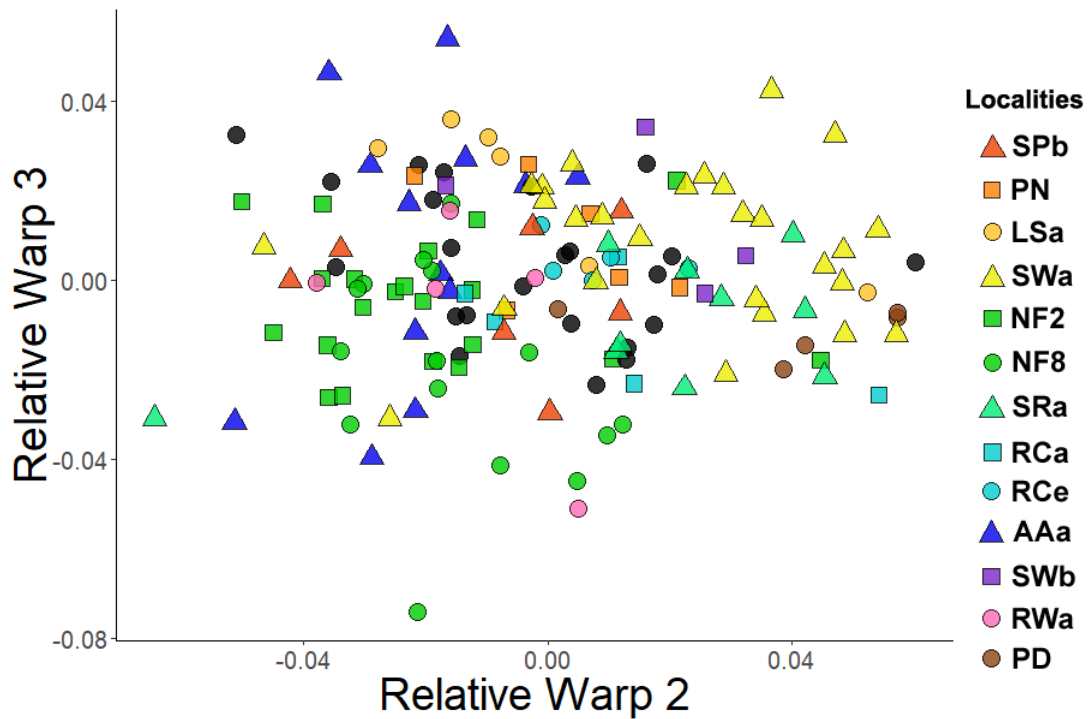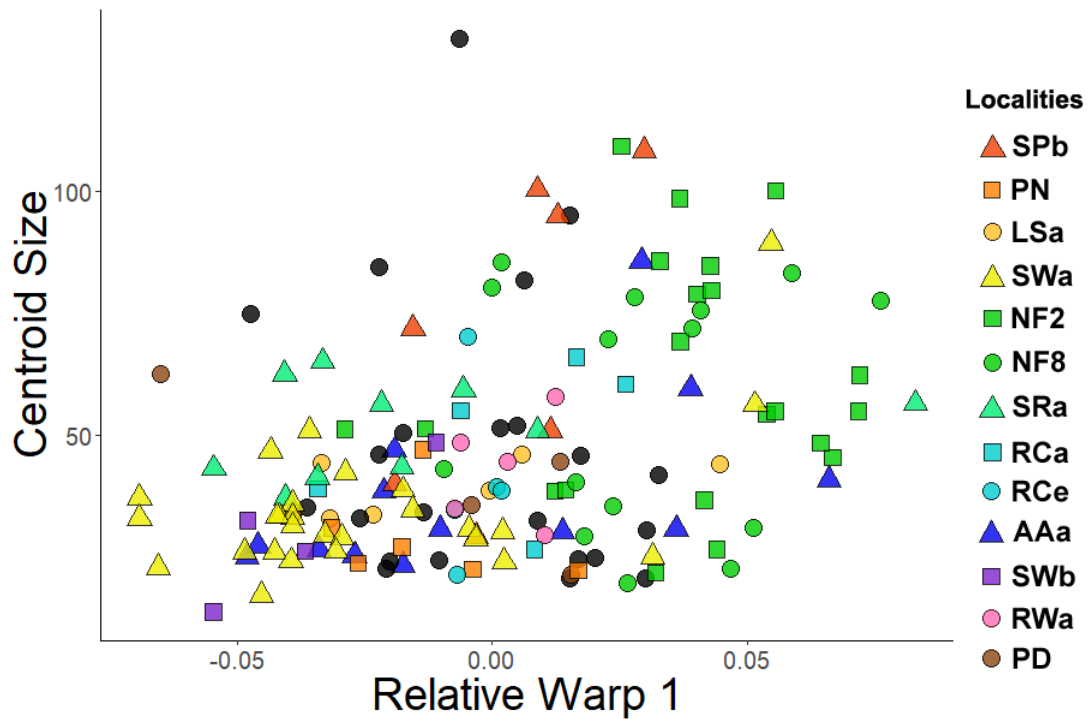
Figure 28. RW2 (15.5% variance explained) versus RW3 (8.4% variance explained). Landmark configuration shown in Fig. 25; reference form is the mean of all 152 configurations in the sample. Color gradient represents relative age with the orange locality being the oldest and the purple locality being the youngest. Relative ages of pink and brown localities are unknown. Black circles represent localities with less than four specimens.
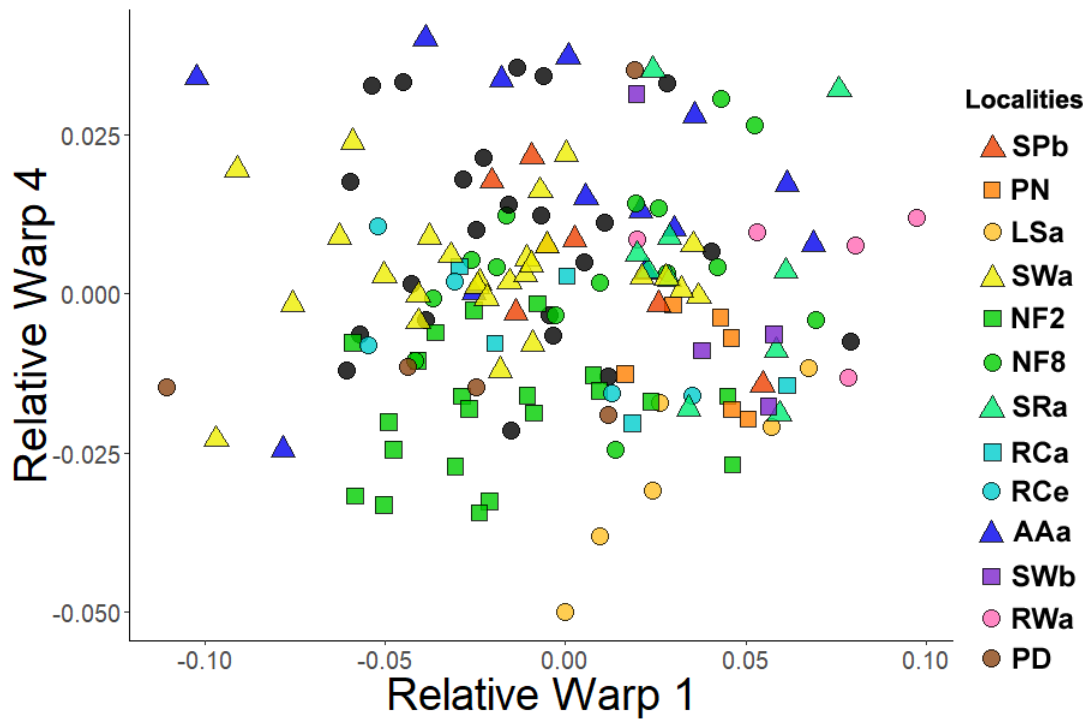
Figure 29. RW1 (35.0% variance explained) versus RW4 (6.5% variance explained). Landmark configuration shown in Fig. 25; reference form is the mean of all 152 configurations in the sample. Color gradient represents relative age with the orange locality being the oldest and the purple locality being the youngest. Relative ages of pink and brown localities are unknown. Black circles represent localities with less than four specimens.

Figure 30. RW1 (35.0% variance explained) versus centroid size. Landmark configuration shown in Fig. 25; reference form is the mean of all 152 configurations in the sample. Color gradient represents relative age with the orange locality being the oldest and the purple locality being the youngest. Relative ages of pink and brown localities are unknown. Black circles represent localities with less than four specimens.
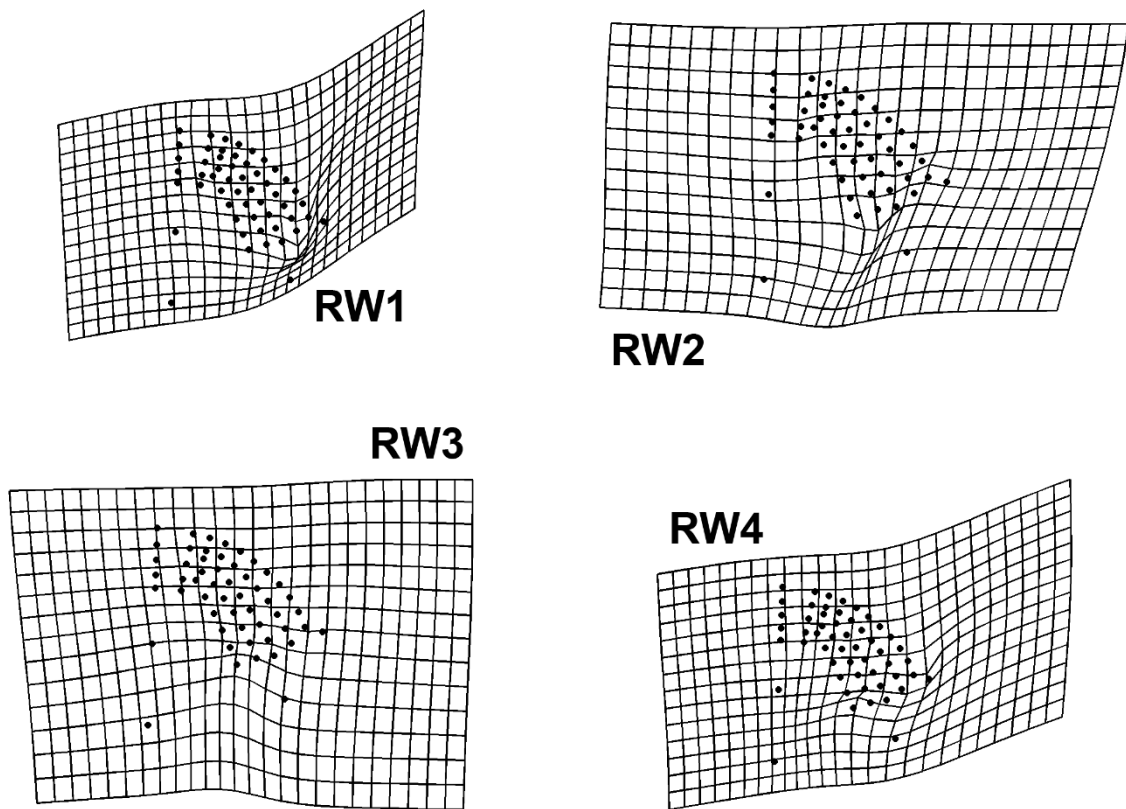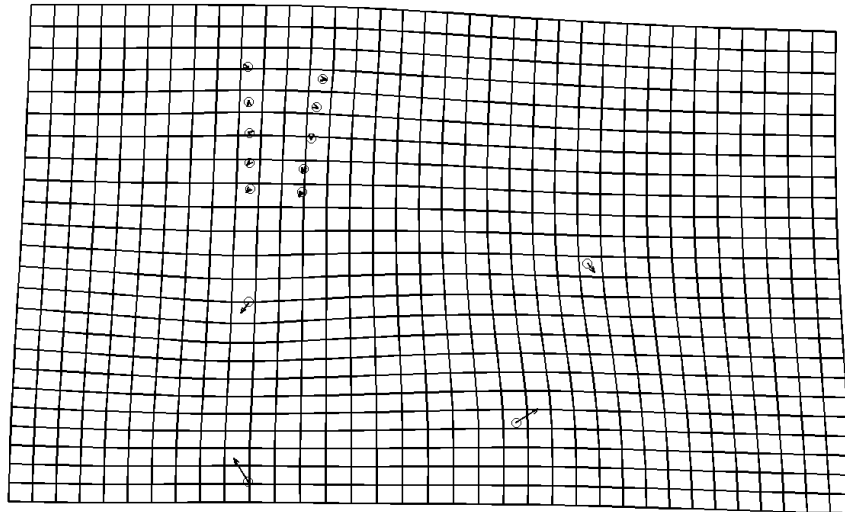
Figure 31. Thin-plate spline deformation grids depicting shape variation along the first four relative warps in a positive direction for 19 landmarks and 34 semilandmarks of 152 *Dikelocephalus* specimens (Fig. 25). RW1 summarizes 35.0% of the variation, RW2 summarizes 15.5% of the variation, RW3 summarizes 8.4% of the variation, and RW4 summarizes 6.5% of the variation.
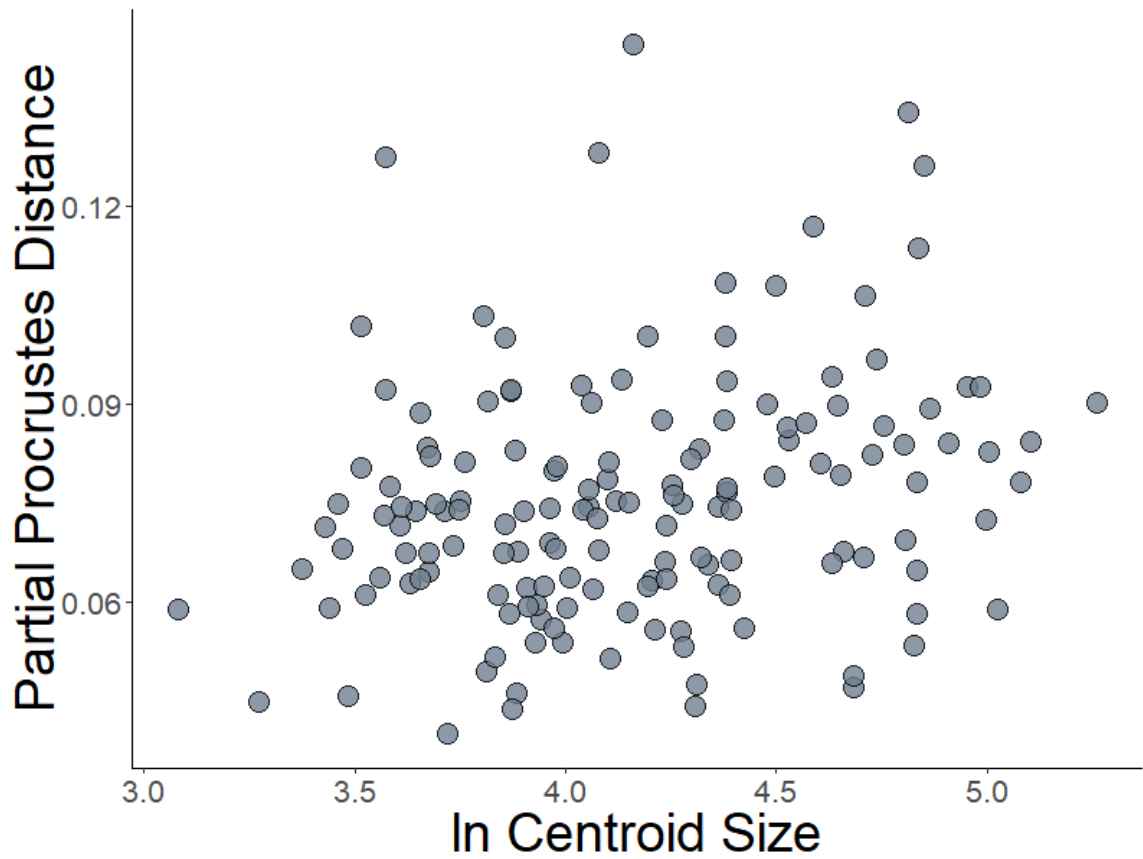
Figure 32. Partial Procrustes distance from the reference form (mean configuration of smallest three specimens) versus logarithm of centroid size (lnCS) for 19 landmarks and 34 semilandmarks of 152 *Dikelocephalus* specimens (Fig. 25). Regression of partial Procrustes distance against lnCS is significant (slope=0.0100, p=0.0011, r=0.2456).
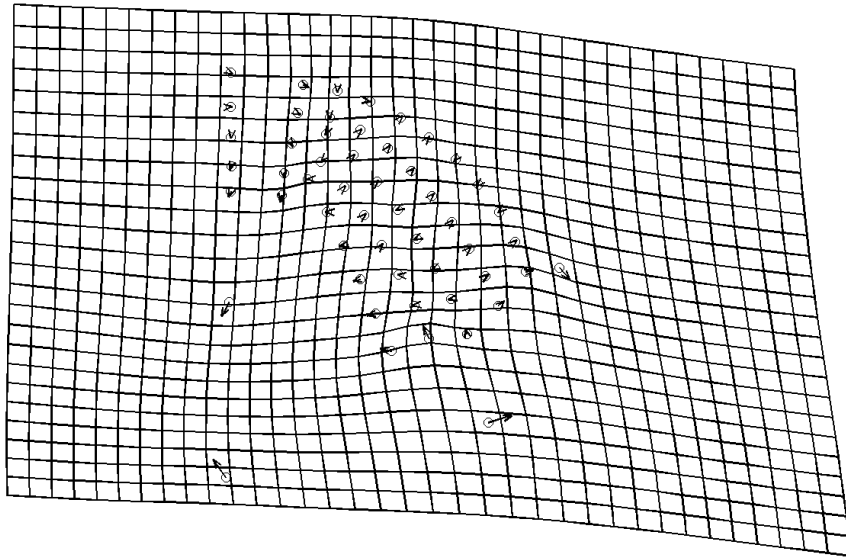
Figure 33. Thin-plate spline deformation grid depicting shape change with

growth for 19 landmarks and 34 semilandmarks of 152 *Dikelocephalus*

specimens (Fig. 25). Shape change calculated by a multivariate regression of

partial warp scores against lnCS and 2.81% of total shape variance (based on

summed squared residuals expressed in Procrustes units) is explained by

allometry (p<0.000625 from 1600 bootstraps).
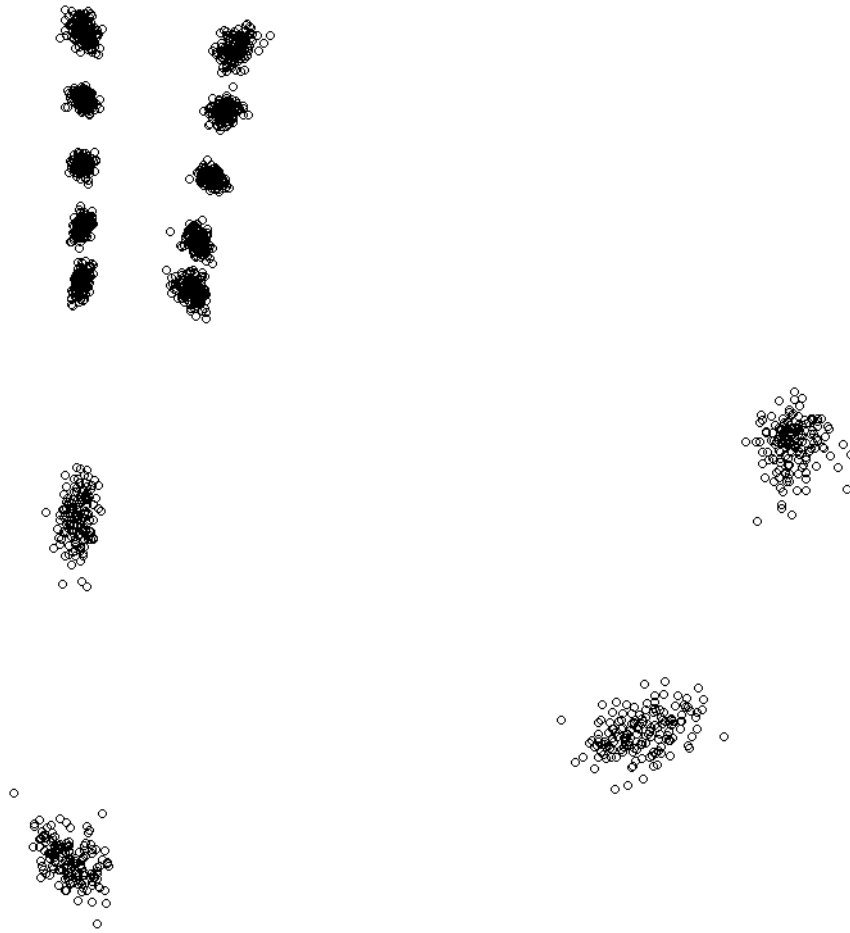
Figure 34. Partial Procrustes superimposition of 14 landmarks for 152 pygidia specimens of *Dikelocephalus* from multiple localities. Landmarks and semilandmarks corresponding to pleural furrows removed (compare to Fig. 16). Five outliers excluded (compare to Fig. 9).
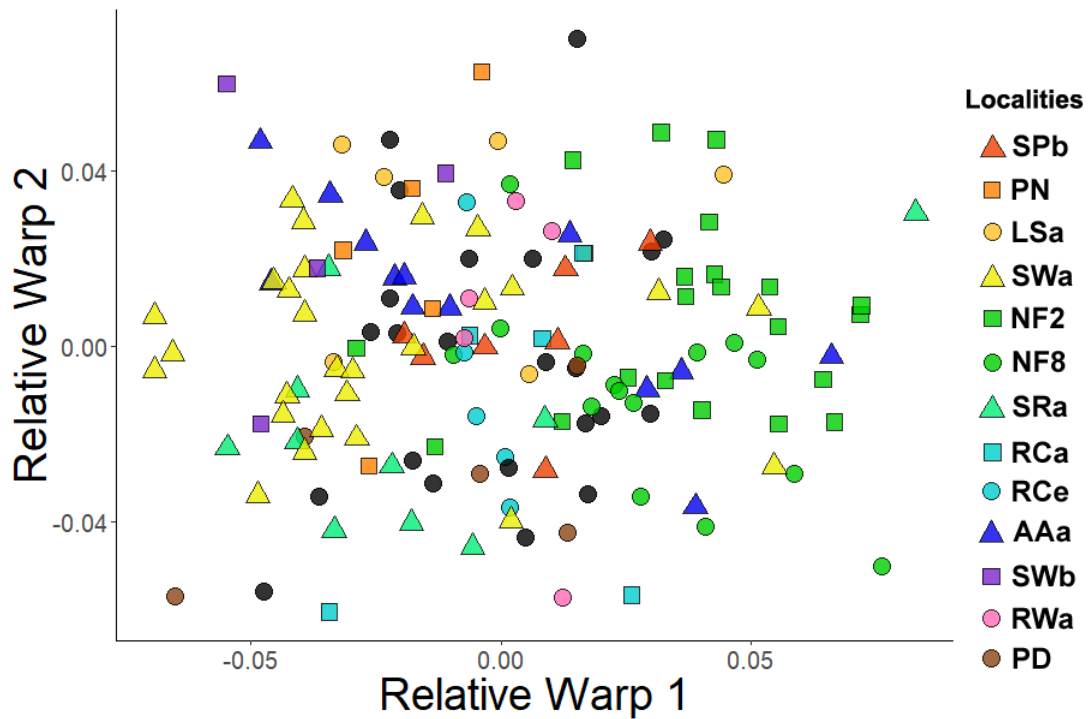
Figure 35. RW1 (35.4% variance explained) versus RW2 (22.1% variance explained). Landmark configuration shown in Fig. 34; reference form is the mean of all 152 configurations in the sample. Color gradient represents relative age with the orange locality being the oldest and the purple locality being the youngest. Relative ages of pink and brown localities are unknown. Black circles represent localities with less than four specimens.
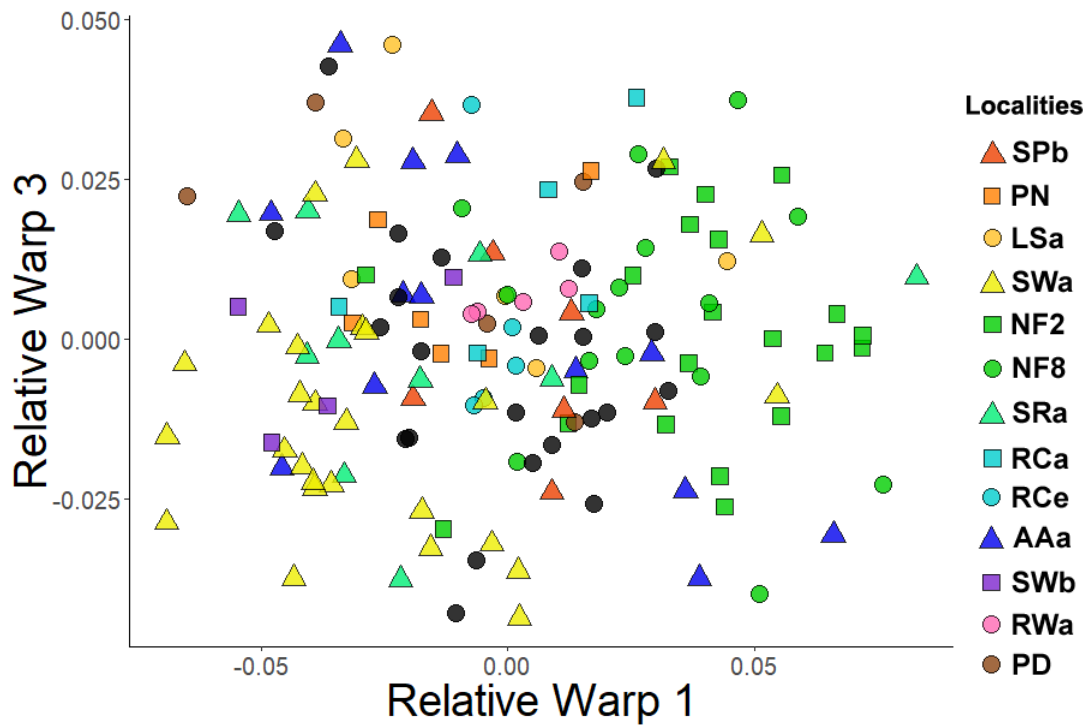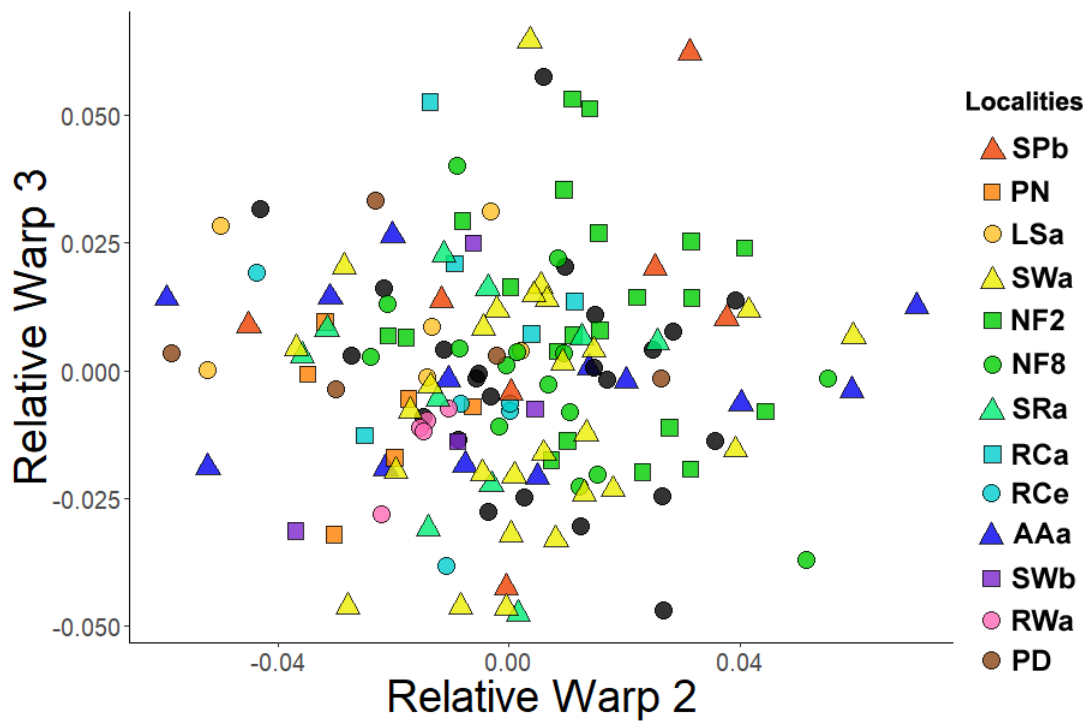
Figure 36. RW1 (35.4% variance explained) versus RW3 (11.7% variance explained). Landmark configuration shown in Fig. 34; reference form is the mean of all 152 configurations in the sample. Color gradient represents relative age with the orange locality being the oldest and the purple locality being the youngest. Relative ages of pink and brown localities are unknown. Black circles represent localities with less than four specimens.
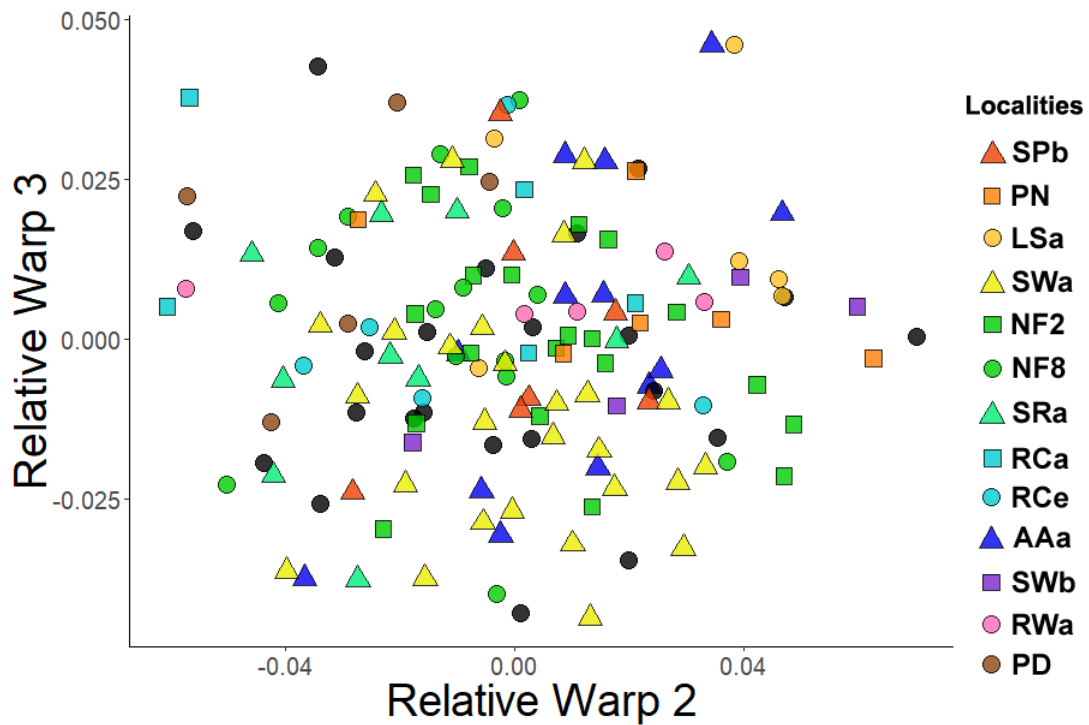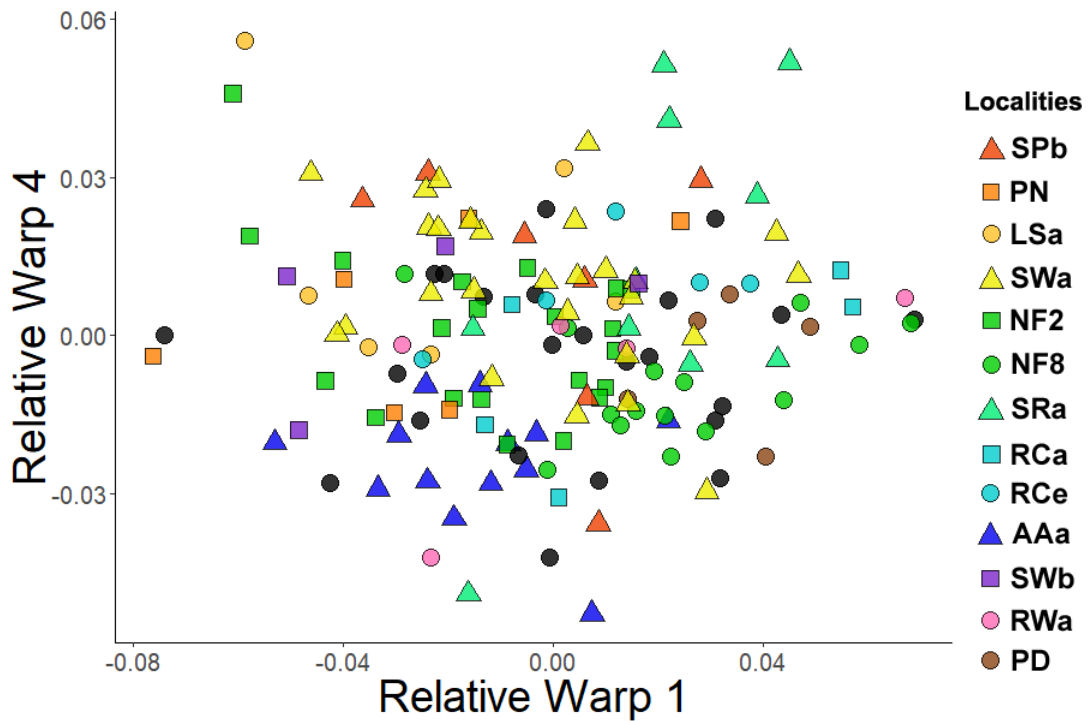
Figure 37. RW2 (22.1% variance explained) versus RW3 (11.7% variance explained). Landmark configuration shown in Fig. 34; reference form is the mean of all 152 configurations in the sample. Color gradient represents relative age with the orange locality being the oldest and the purple locality being the youngest. Relative ages of pink and brown localities are unknown. Black circles represent localities with less than four specimens.

Figure 38. RW1 (35.4% variance explained) versus RW4 (10.4% variance explained). Landmark configuration shown in Fig. 34; reference form is the mean of all 152 configurations in the sample. Color gradient represents relative age with the orange locality being the oldest and the purple locality being the youngest. Relative ages of pink and brown localities are unknown. Black circles represent localities with less than four specimens.
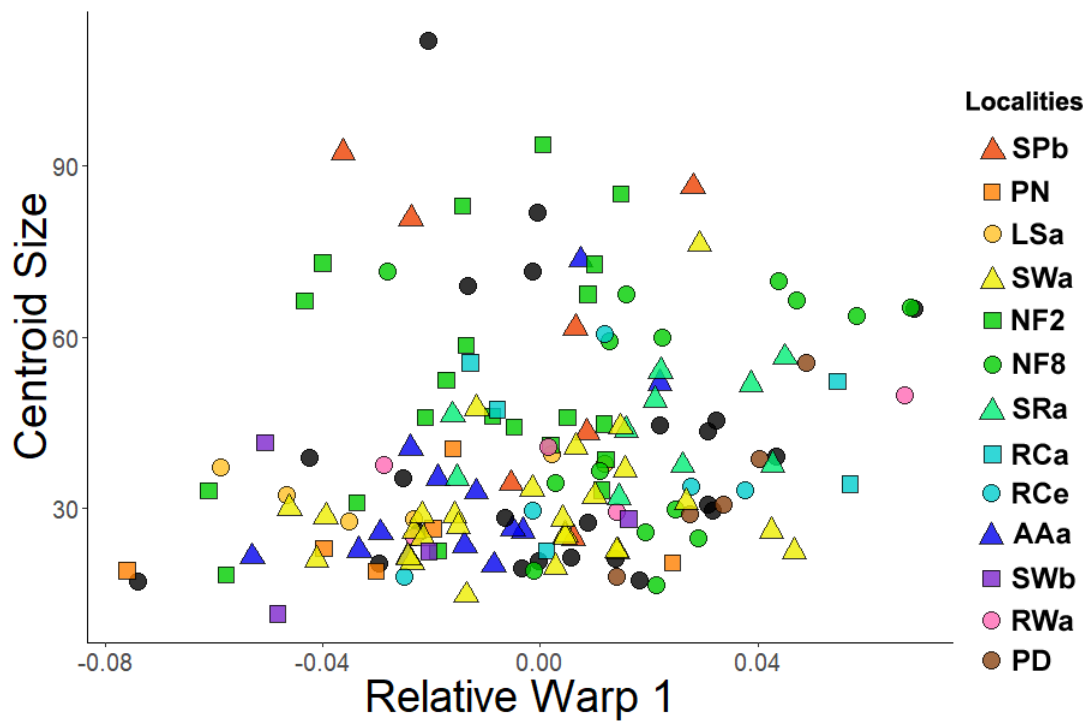
Figure 39. RW1 (35.4% variance explained) versus centroid size. Landmark configuration shown in Fig. 34; reference form is the mean of all 152 configurations in the sample. Color gradient represents relative age with the orange locality being the oldest and the purple locality being the youngest. Relative ages of pink and brown localities are unknown. Black circles represent localities with less than four specimens.
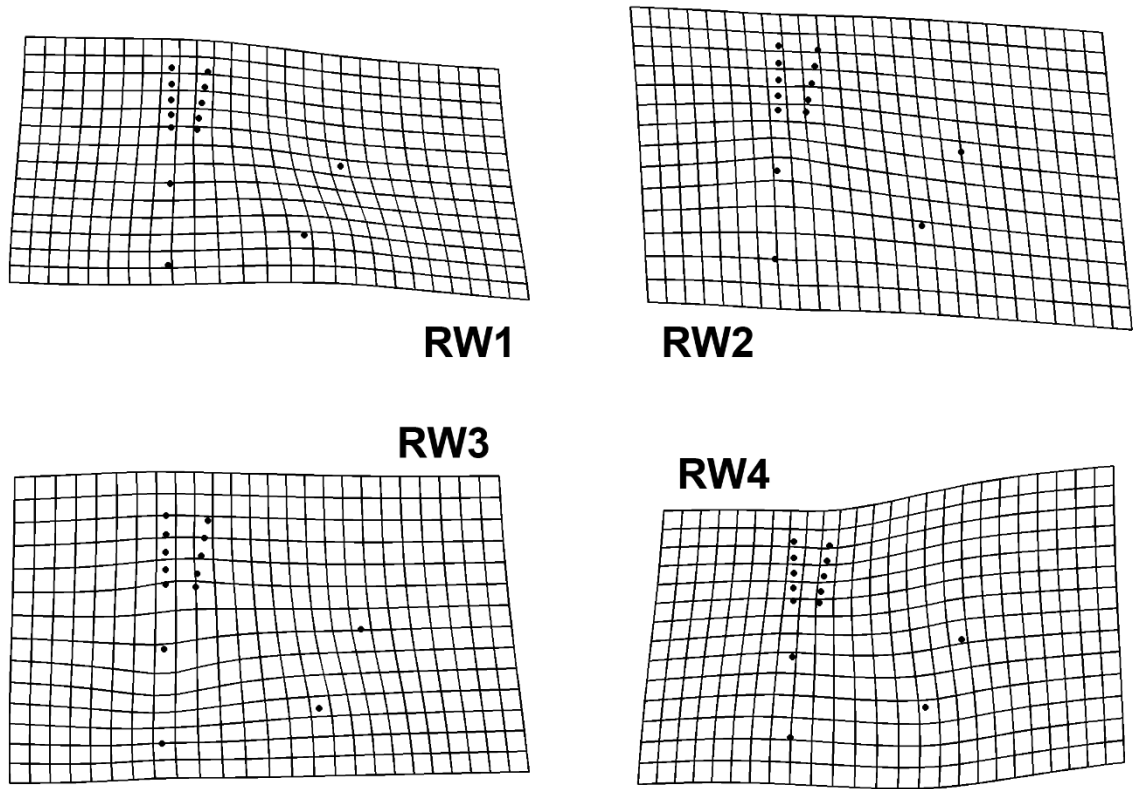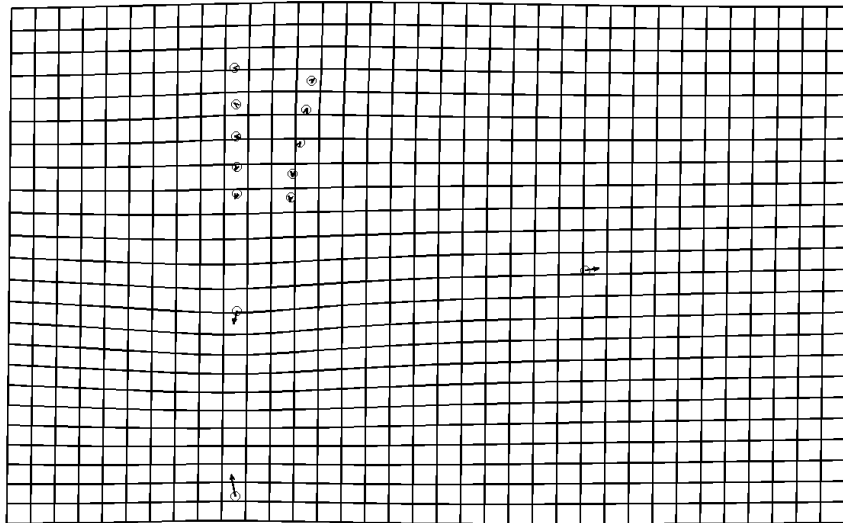
Figure 40. Thin-plate spline deformation grids depicting shape variation along the first four relative warps in a positive direction for 14 landmarks of 152 *Dikelocephalus* specimens (Fig. 34). RW1 summarizes 35.4% of the variation, RW2 summarizes 22.1% of the variation, RW3 summarizes 11.7% of the variation, and RW4 summarizes 10.4% of the variation.
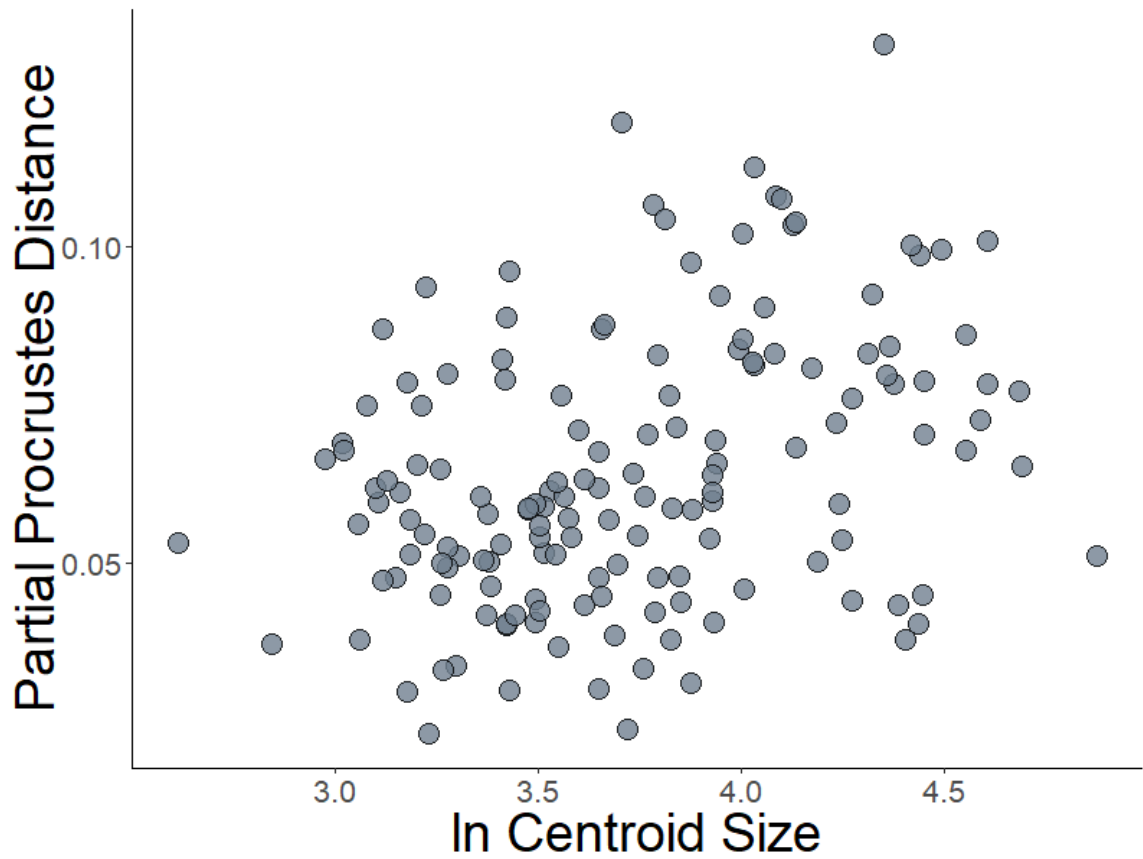
Figure 41. Partial Procrustes distance from the reference form (mean configuration of smallest three specimens) versus logarithm of centroid size (lnCS) for 14 landmarks of 152 *Dikelocephalus* specimens (Fig. 34). Regression of partial Procrustes distance against lnCS is significant (slope=0.0165, p<0.0001, r=0.3533).

Figure 42. Thin-plate spline deformation grid depicting shape change with
growth for 14 landmarks of 152 *Dikelocephalus* specimens (Fig. 34). Shape
change calculated by a multivariate regression of partial warp scores against
lnCS and 6.59% of total shape variance (based on summed squared residuals
expressed in Procrustes units) is explained by allometry (p<0.000625 from 1600
bootstraps).
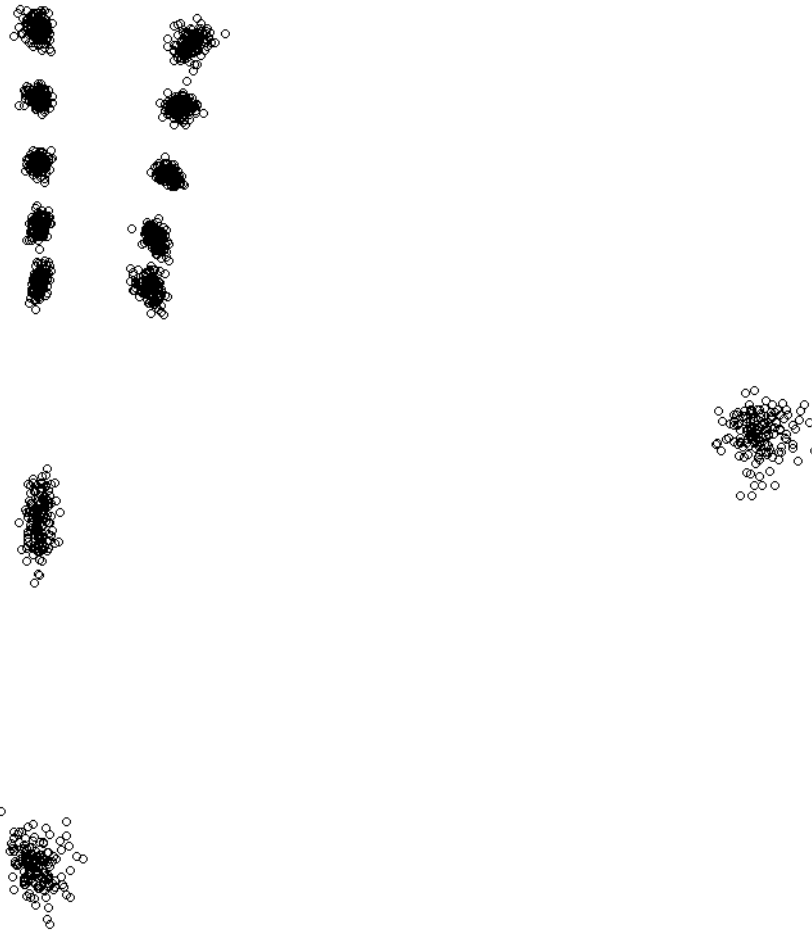
Figure 43. Partial Procrustes superimposition of 13 landmarks for 152 pygidia

specimens of *Dikelocephalus* from multiple localities. The landmark

corresponding to the base of the posterolateral spine removed (compare to Fig

34). Five outliers excluded.
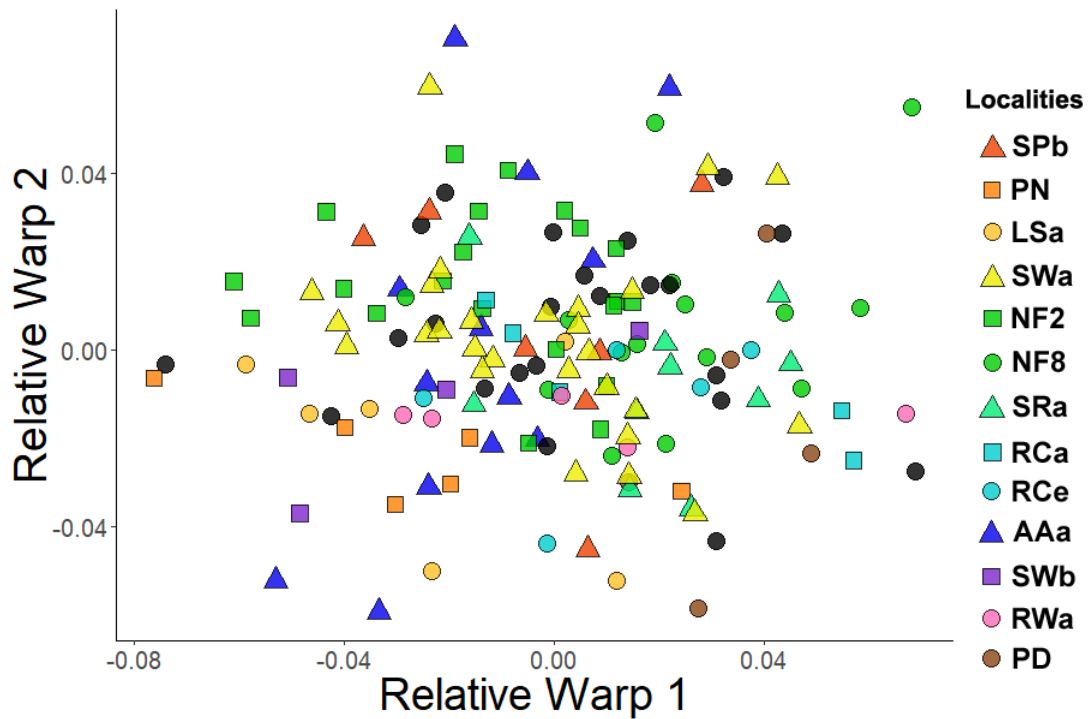
Figure 44. RW1 (31.9% variance explained) versus RW2 (21.9% variance explained). Landmark configuration shown in Fig. 43; reference form is the mean of all 152 configurations in the sample. Color gradient represents relative age with the orange locality being the oldest and the purple locality being the youngest. Relative ages of pink and brown localities are unknown. Black circles represent localities with less than four specimens.
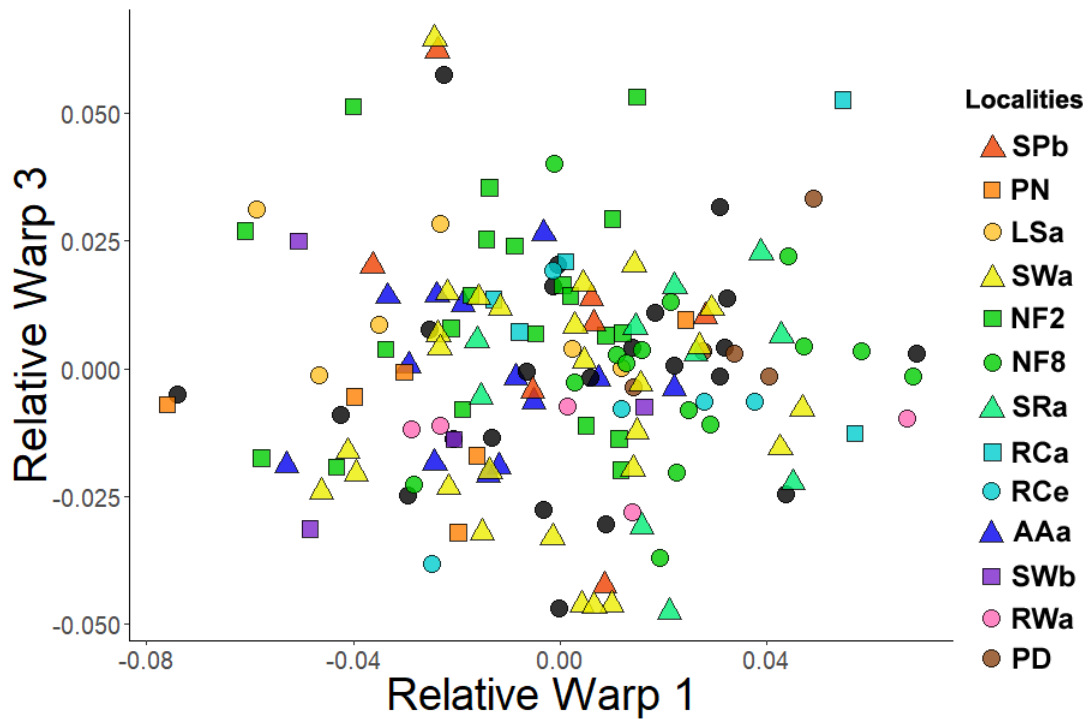
Figure 45. RW1 (31.9% variance explained) versus RW3 (17.7% variance explained). Landmark configuration shown in Fig. 43; reference form is the mean of all 152 configurations in the sample. Color gradient represents relative age with the orange locality being the oldest and the purple locality being the youngest. Relative ages of pink and brown localities are unknown. Black circles represent localities with less than four specimens.

Figure 46. RW2 (21.9% variance explained) versus RW3 (17.7% variance explained). Landmark configuration shown in Fig. 43; reference form is the mean of all 152 configurations in the sample. Color gradient represents relative age with the orange locality being the oldest and the purple locality being the youngest. Relative ages of pink and brown localities are unknown. Black circles represent localities with less than four specimens.

Figure 47. RW1 (31.9% variance explained) versus RW4 (14.4% variance explained). Landmark configuration shown in Fig. 43; reference form is the mean of all 152 configurations in the sample. Color gradient represents relative age with the orange locality being the oldest and the purple locality being the youngest. Relative ages of pink and brown localities are unknown. Black circles represent localities with less than four specimens.

Figure 48. RW1 (31.9% variance explained) versus centroid size. Landmark

configuration shown in Fig. 43; reference form is the mean of all 152

configurations in the sample. Color gradient represents relative age with the

orange locality being the oldest and the purple locality being the youngest.

Relative ages of pink and brown localities are unknown. Black circles represent

localities with less than four specimens.
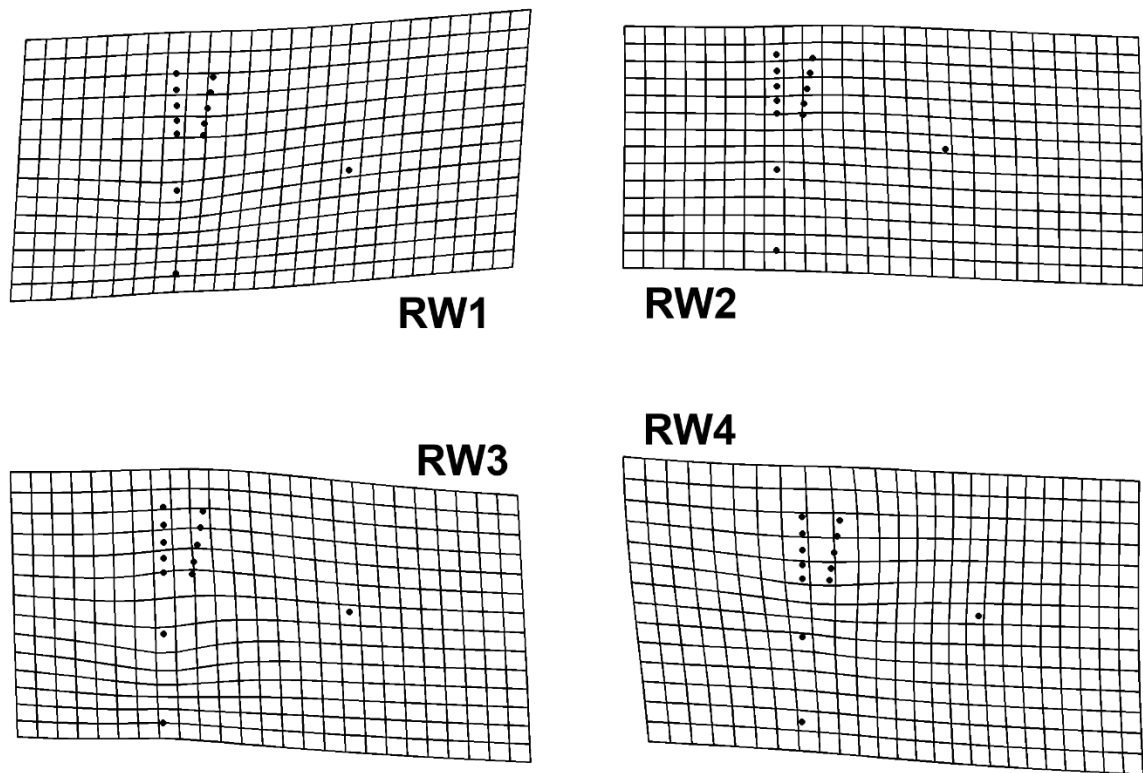
Figure 49. Thin-plate spline deformation grids depicting shape variation along the first four relative warps in a positive direction for 13 landmarks of 152 *Dikelocephalus* specimens (Fig. 43). RW1 summarizes 31.9% of the variation, RW2 summarizes 21.9% of the variation, RW3 summarizes 17.7% of the variation, and RW4 summarizes 14.4% of the variation.
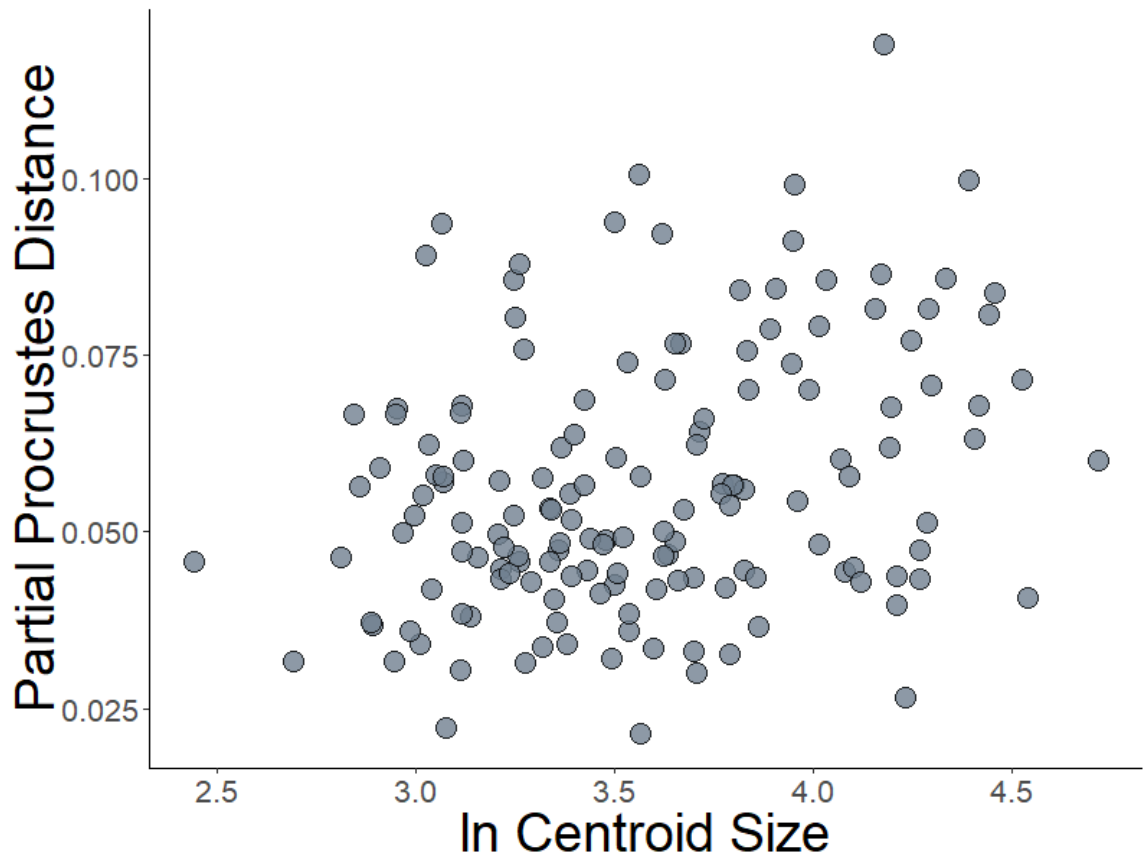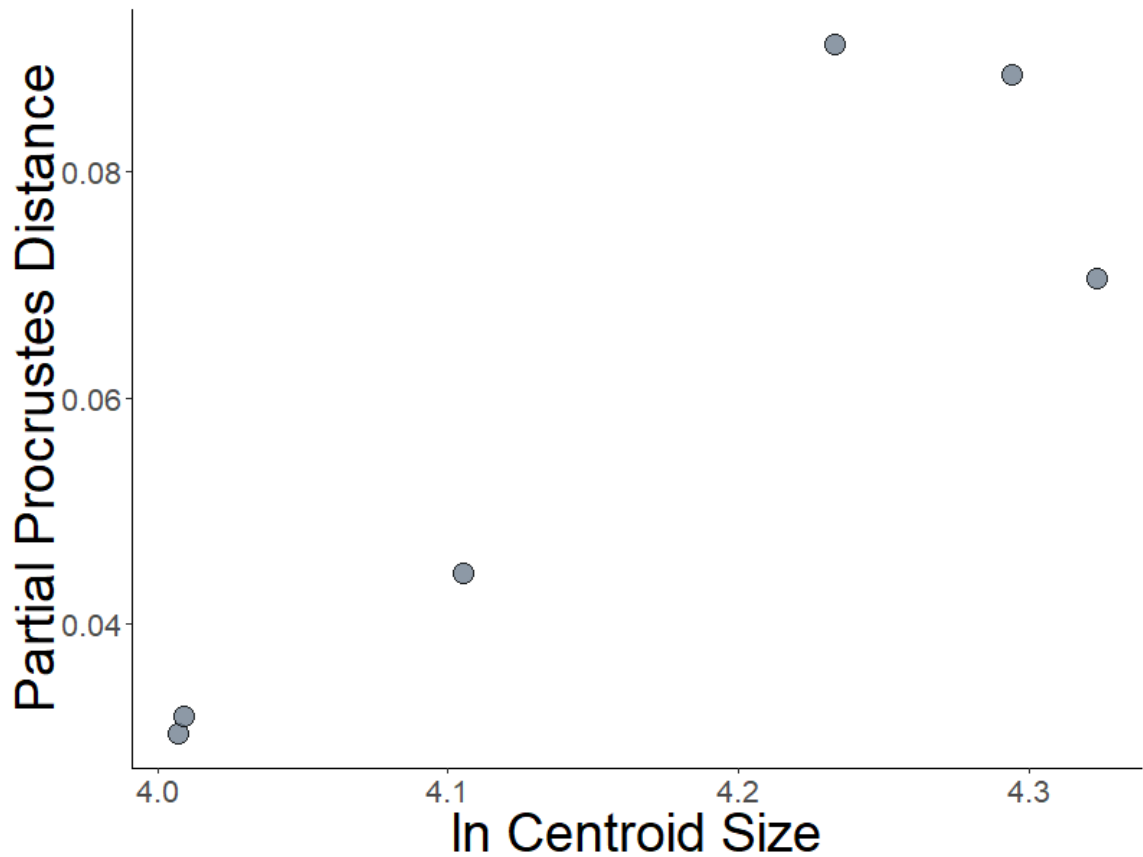
Figure 50. Partial Procrustes distance from the reference form (mean configuration of smallest three specimens) versus logarithm of centroid size (lnCS) for 13 landmarks of 152 *Dikelocephalus* specimens (Fig. 43). Regression of partial Procrustes distance against lnCS is significant (slope=0.0119, $p<0.0001$, r=0.2967).
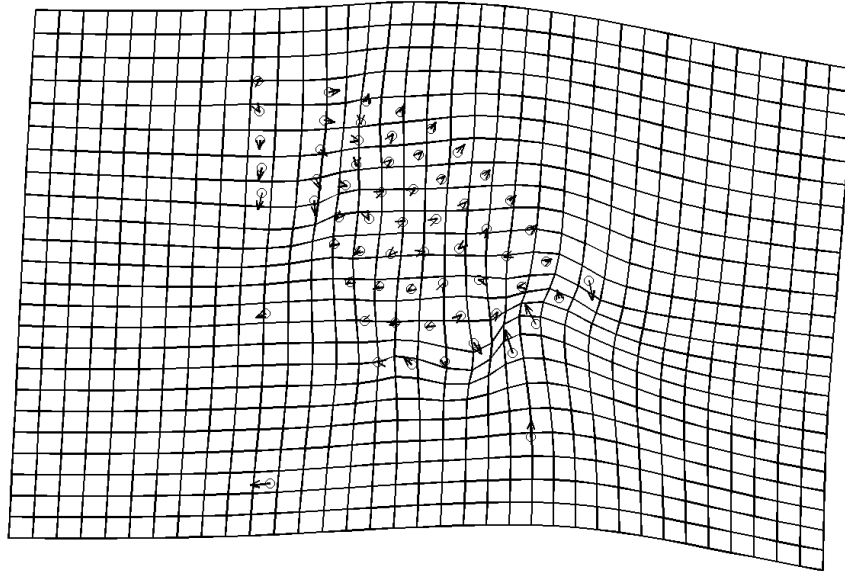
Figure 51. Thin-plate spline deformation grid depicting shape change with growth for 13 landmarks of 152 *Dikelocephalus* specimens (Fig. 43). Shape change calculated by a multivariate regression of partial warp scores against lnCS and 5.30% of total shape variance (based on summed squared residuals expressed in Procrustes units) is explained by allometry (p<0.000625 from 1600 bootstraps).
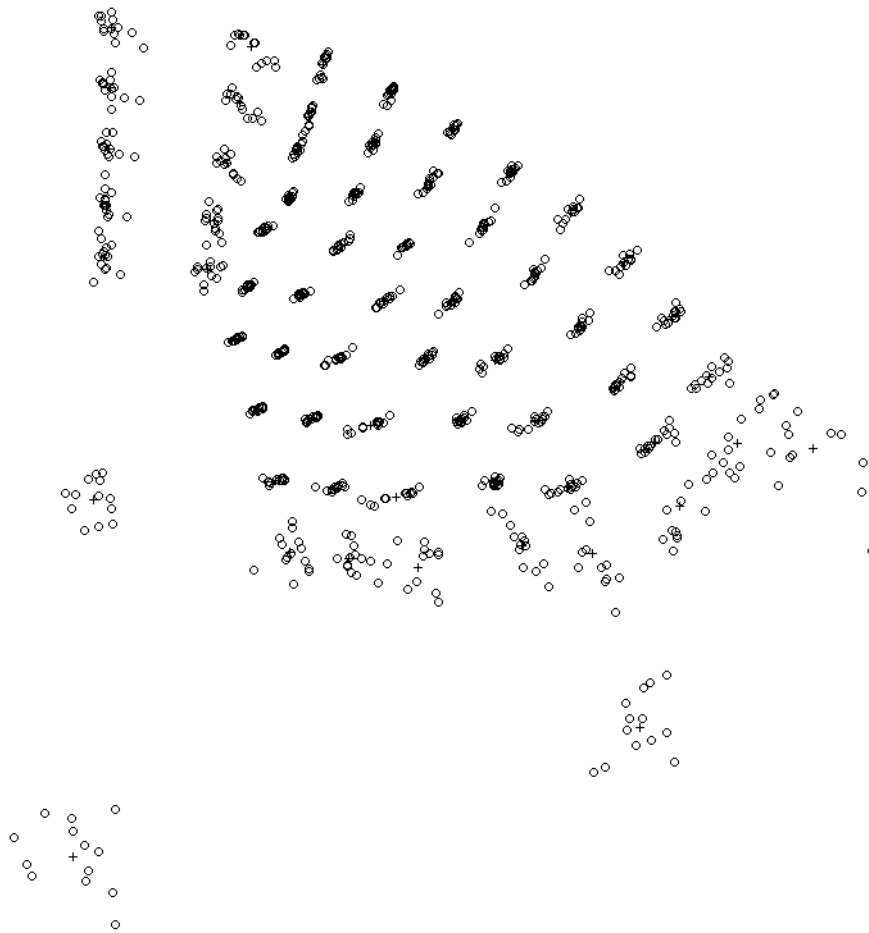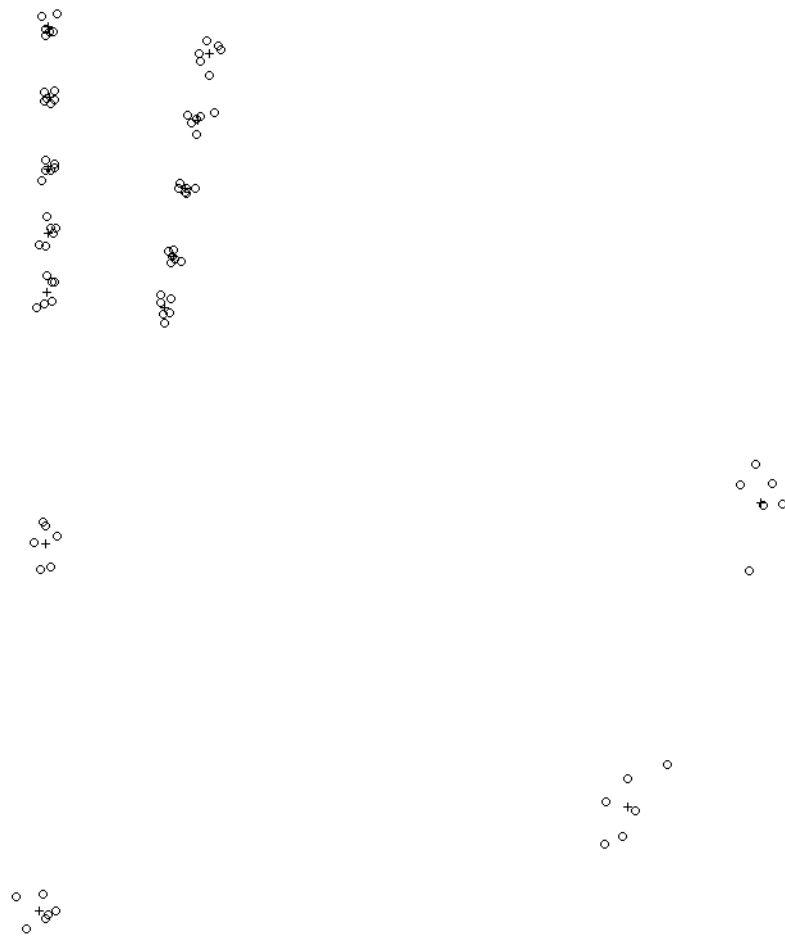
Figure 52. Partial Procrustes superimposition of 21 landmarks and 41 semilandmarks for 13 pygidia specimens of *Dikelocephalus* from Arcadia Bed 18 (AAa).
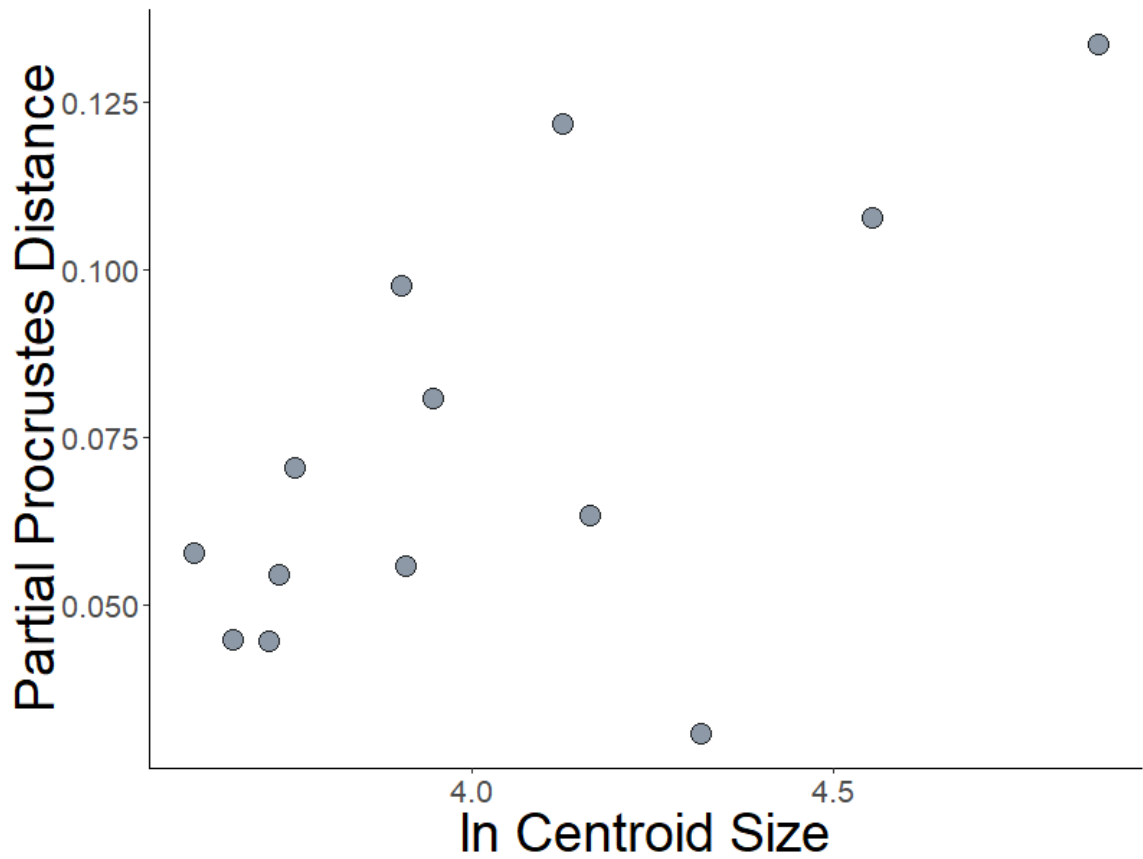
Figure 53. Partial Procrustes distance from the reference form (mean configuration of smallest three specimens) versus logarithm of centroid size (lnCS) for 21 landmarks and 41 semilandmarks of 13 specimens of *Dikelocephalus* from Arcadia Bed 18 (AAa) (Fig. 52). Regression of partial Procrustes distance against lnCS is significant (slope=0.0537, p=0.0099, r=0.6274).
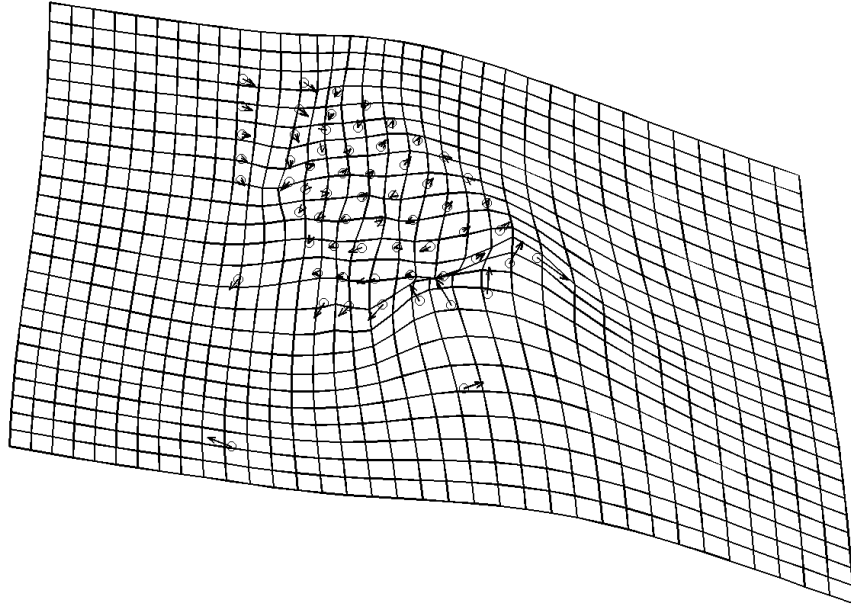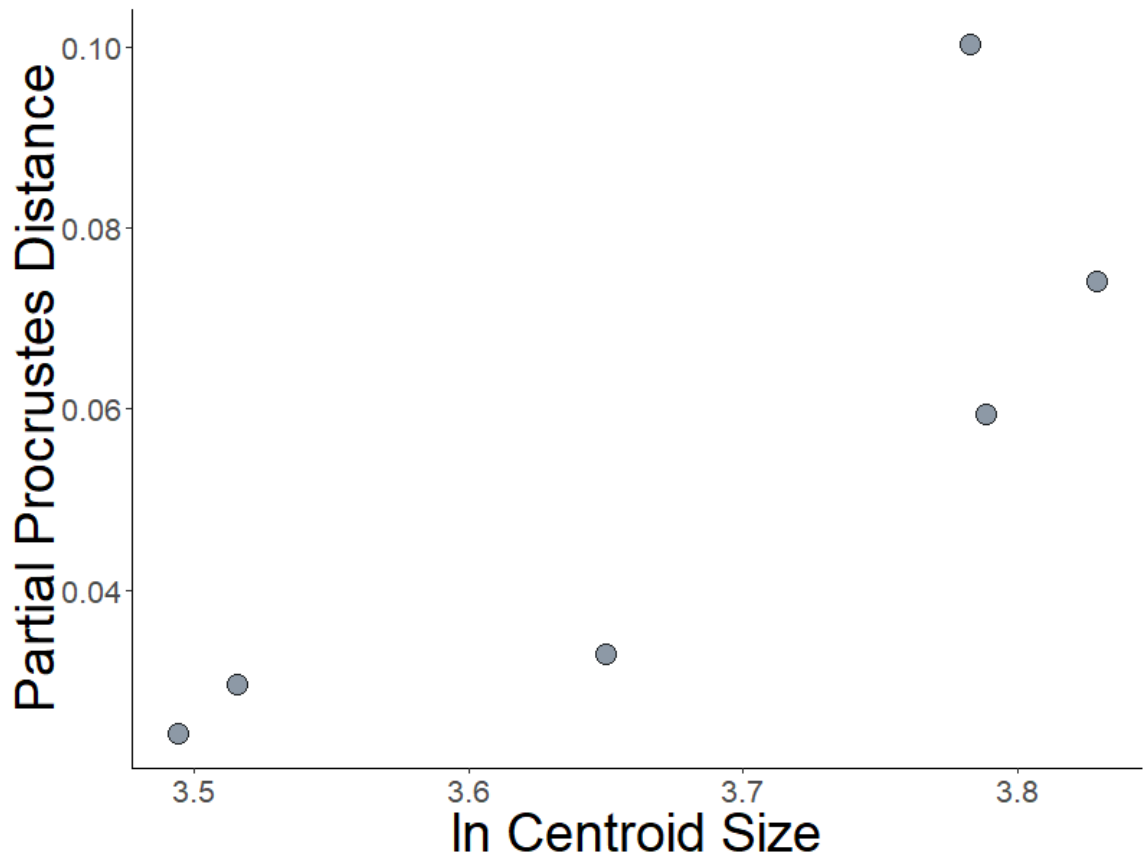
Figure 54. Thin-plate spline deformation grid depicting shape change with growth for 21 landmarks and 41 semilandmarks of 13 specimens of *Dikelocephalus* from Arcadia Bed 18 (AAa) (Fig. 52). Shape change calculated by a multivariate regression of partial warp scores against lnCS and 21.56% of total shape variance (based on summed squared residuals expressed in Procrustes units) is explained by allometry (p=0.0294 from 1600 bootstraps).

Figure 55. Partial Procrustes superimposition of 14 landmarks for 13 pygidia specimens of *Dikelocephalus* from Arcadia Bed 18 (AAa). Landmarks and semilandmarks corresponding to pleural furrows removed (compare to Fig. 52).
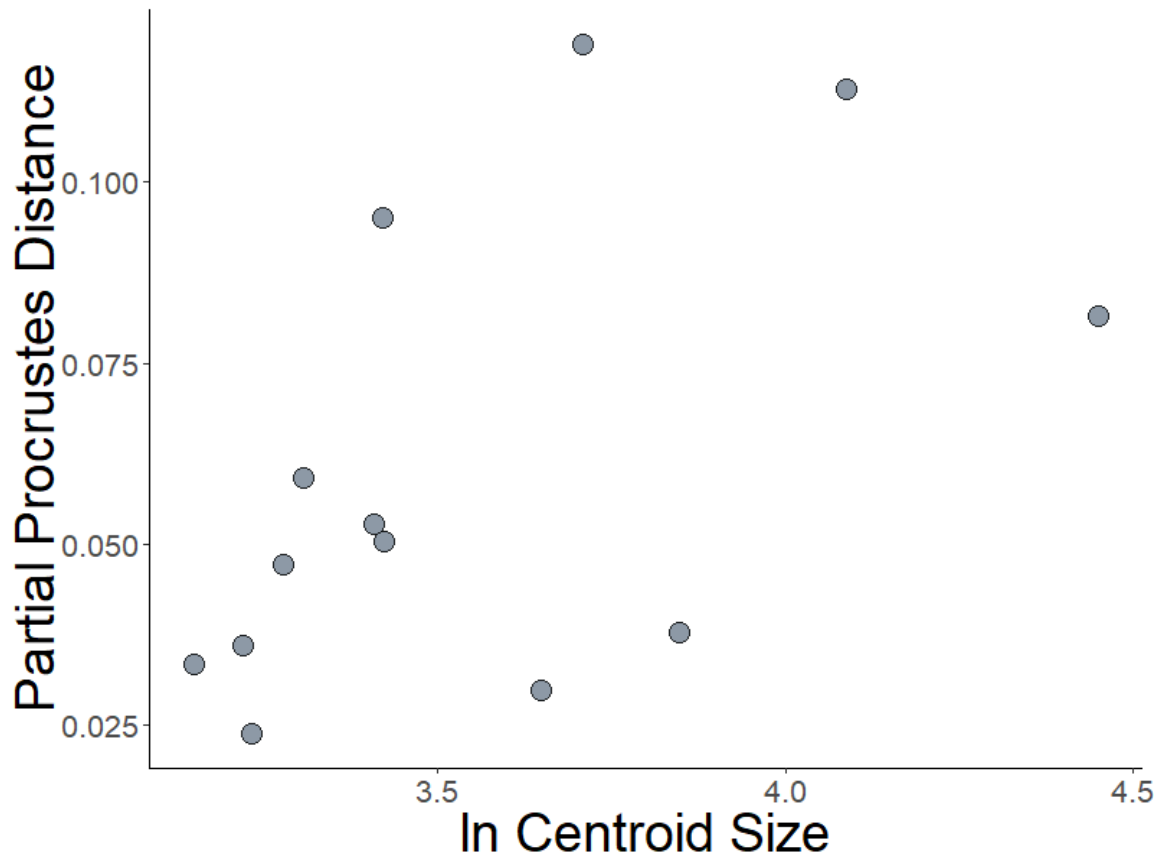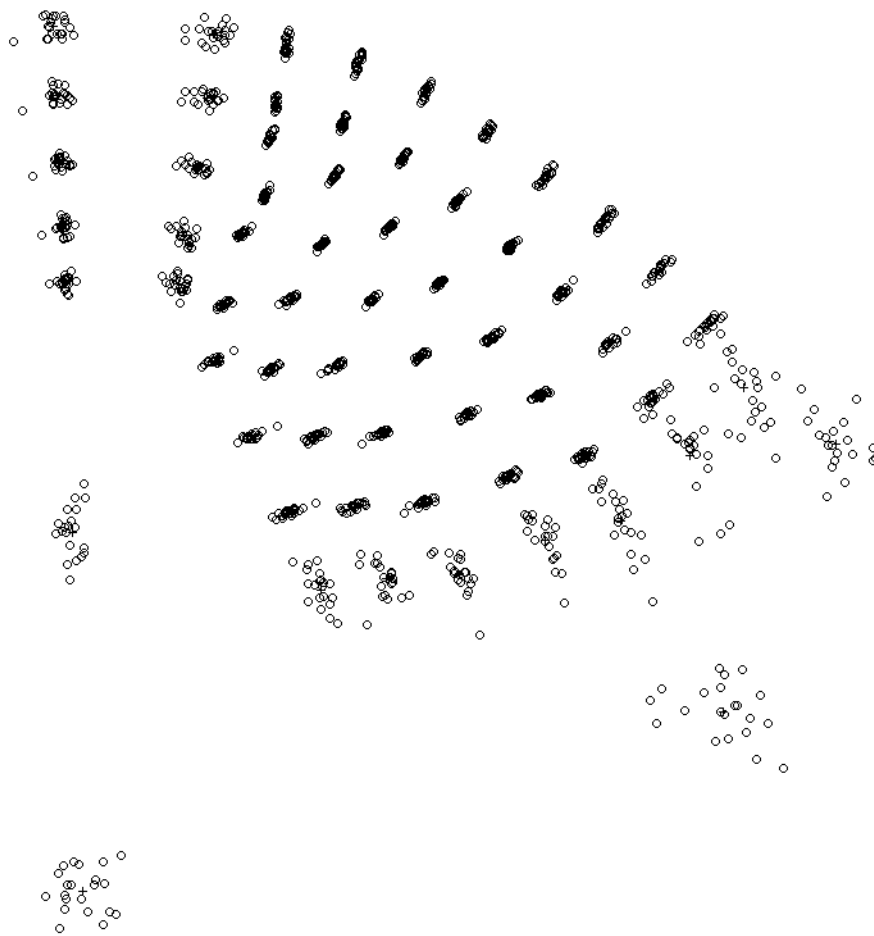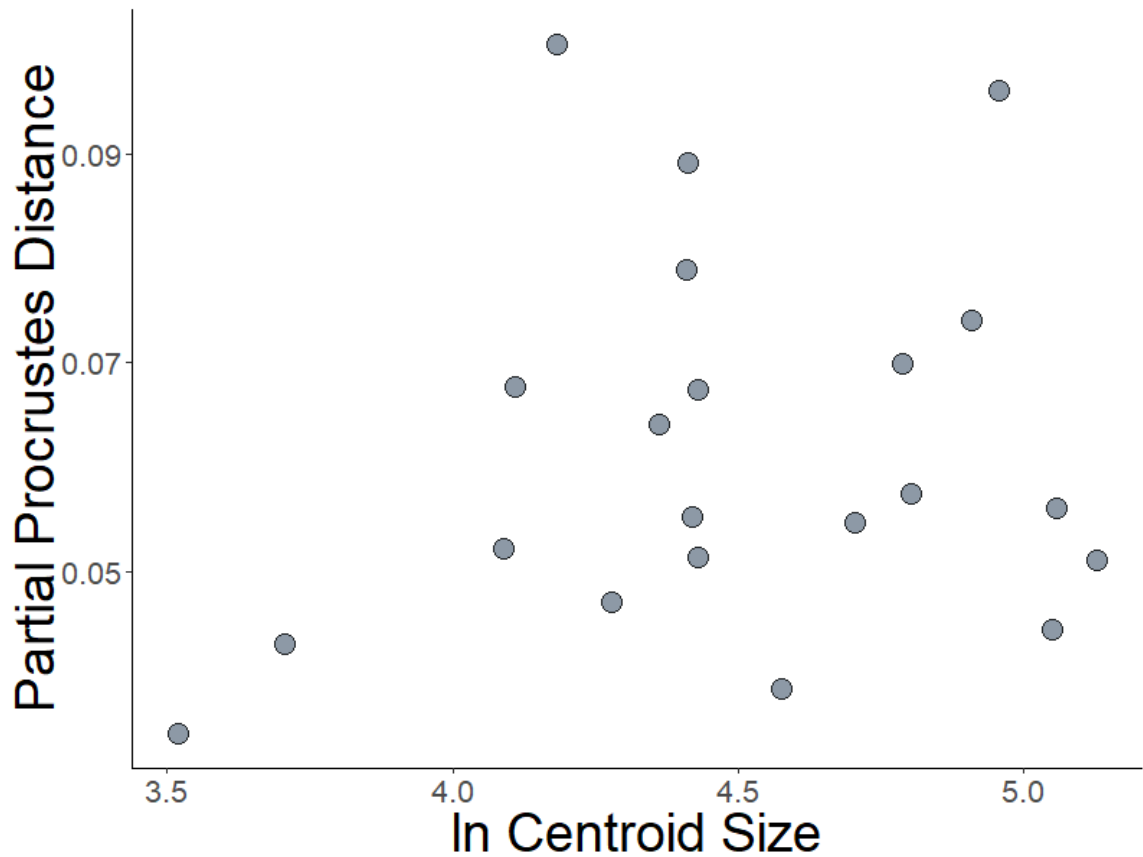
Figure 56. Partial Procrustes distance from the reference form (mean configuration of smallest three specimens) versus logarithm of centroid size (lnCS) for 14 landmarks of 13 specimens of *Dikelocephalus* from Arcadia Bed 18 (AAa) (Fig. 55). Regression of partial Procrustes distance against lnCS is significant (slope=0.0445, p=0.0293, r=0.5356).
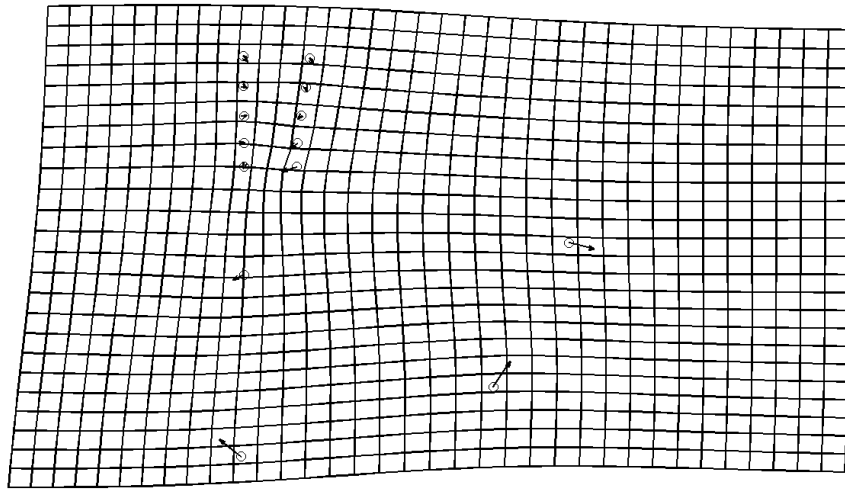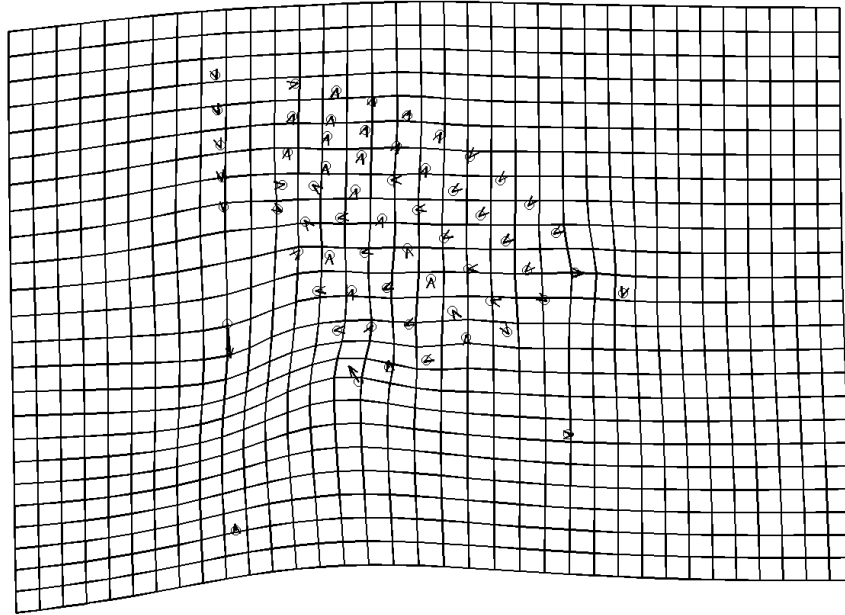
Figure 57. Thin-plate spline deformation grid depicting shape change with growth for 14 landmarks of 13 specimens of *Dikelocephalus* from Arcadia Bed 18 (AAa) (Fig. 55). Shape change calculated by a multivariate regression of partial warp scores against lnCS and 24.96% of total shape variance (based on summed squared residuals expressed in Procrustes units) is explained by allometry (p=0.0263 from 1600 bootstraps).
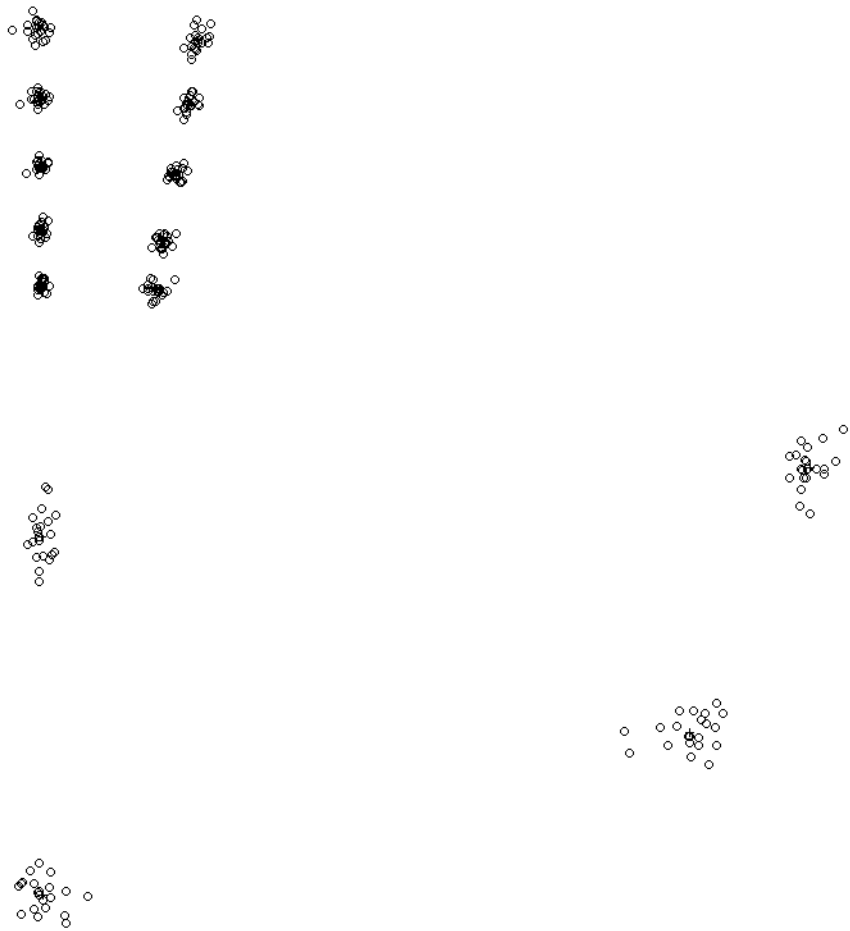
Figure 58. Partial Procrustes superimposition of 21 landmarks and 41 semilandmarks for 6 pygidia specimens of *Dikelocephalus* from Lansing (LSa).
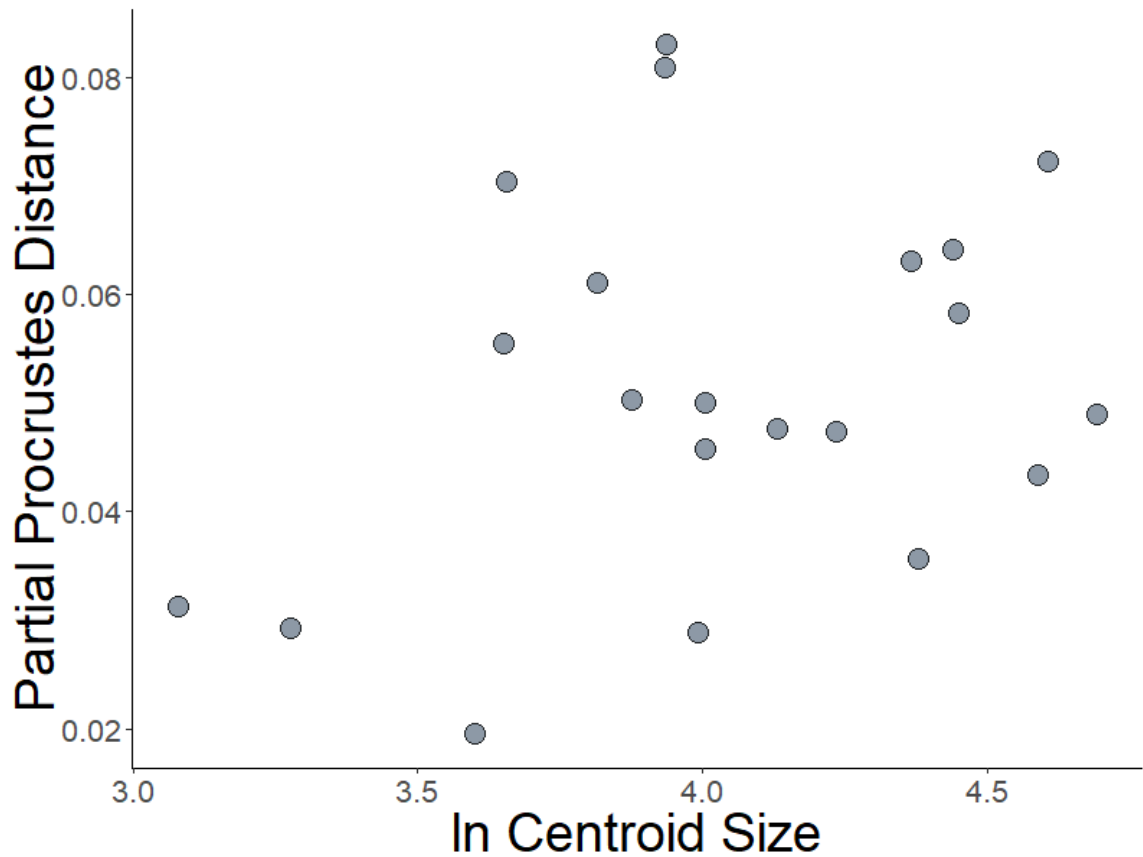
Figure 59. Partial Procrustes distance from the reference form (mean configuration of smallest three specimens) versus logarithm of centroid size (lnCS) for 21 landmarks and 41 semilandmarks of 6 specimens of *Dikelocephalus* from Lansing (LSa) (Fig. 58). Regression of partial Procrustes distance against lnCS is significant (slope=0.1762, p=0.0056, r=0.8985).
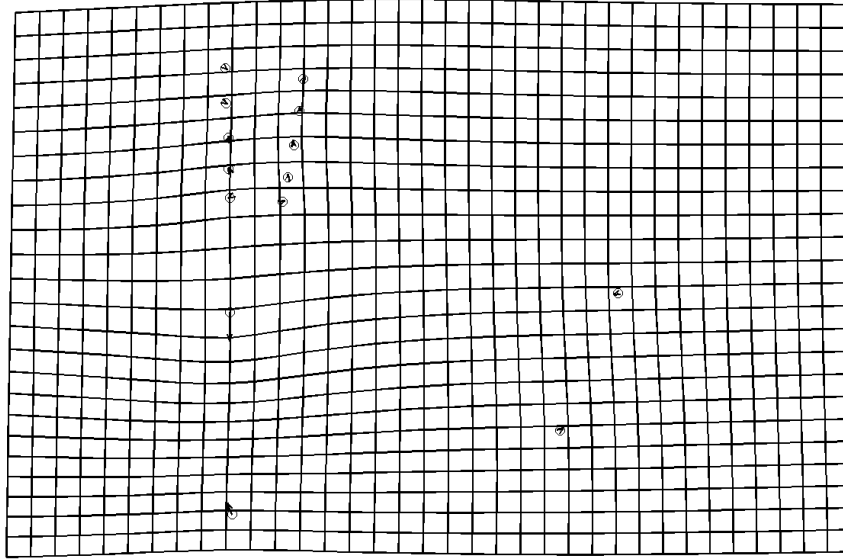
Figure 60. Thin-plate spline deformation grid depicting shape change with growth for 21 landmarks and 41 semilandmarks of 6 specimens of *Dikelocephalus* from Lansing (LSa) (Fig. 58). Shape change calculated by a multivariate regression of partial warp scores against lnCS and 26.06% of shape variance (based on summed squared residuals expressed in Procrustes units) explained by allometry is not significant at a 95% confidence interval (p=0.1875 from 1600 bootstraps).

Figure 61. Partial Procrustes superimposition of 14 landmarks for 6 pygidia

specimens of *Dikelocephalus* from Lansing (LSa). Landmarks and

semilandmarks corresponding to pleural furrows removed (compare to Fig. 58).

Figure 62. Partial Procrustes distance from the reference form (mean configuration of smallest three specimens) versus logarithm of centroid size (lnCS) for 14 landmarks of 6 specimens of *Dikelocephalus* from Lansing (LSa) (Fig. 61). Regression of partial Procrustes distance against lnCS is significant (slope=0.1735, p=0.0163, r=0.8437).
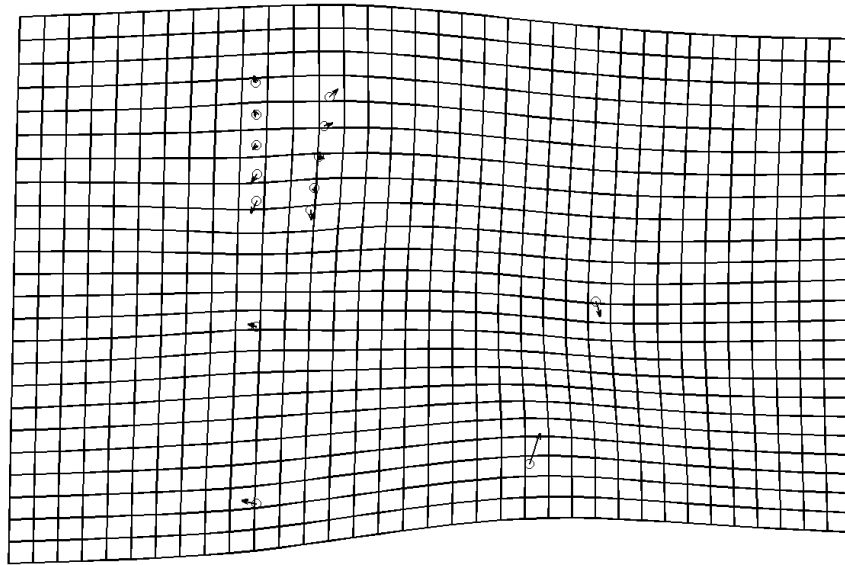
Figure 63. Thin-plate spline deformation grid depicting shape change with
growth for 14 landmarks of 6 specimens of *Dikelocephalus* from Lansing (LSa)
(Fig. 61). Shape change calculated by a multivariate regression of partial warp
scores against lnCS and 37.15% of shape variance (based on summed squared
residuals expressed in Procrustes units) explained by allometry is not significant
at a 95% confidence interval (p=0.0963 from 1600 bootstraps).

Figure 64. Partial Procrustes superimposition of 21 landmarks and 41

semilandmarks for 21 pygidia specimens of *Dikelocephalus* from North Freedom
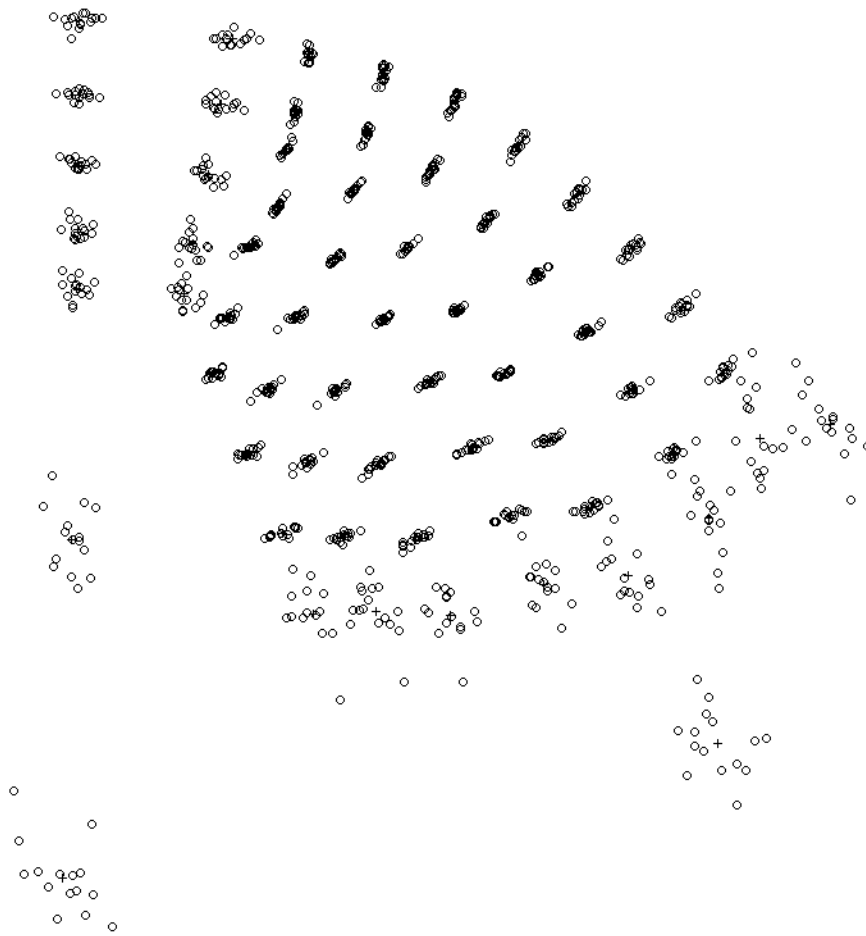
Bed 2 (NF2).

Figure 65. Partial Procrustes distance from the reference form (mean

configuration of smallest three specimens) versus logarithm of centroid size

(lnCS) for 21 landmarks and 41 semilandmarks of 21 specimens of

Dikelocephalus from North Freedom Bed 2 (NF2) (Fig. 64). Regression of partial

Procrustes distance against lnCS is not significant at a 95% confidence interval
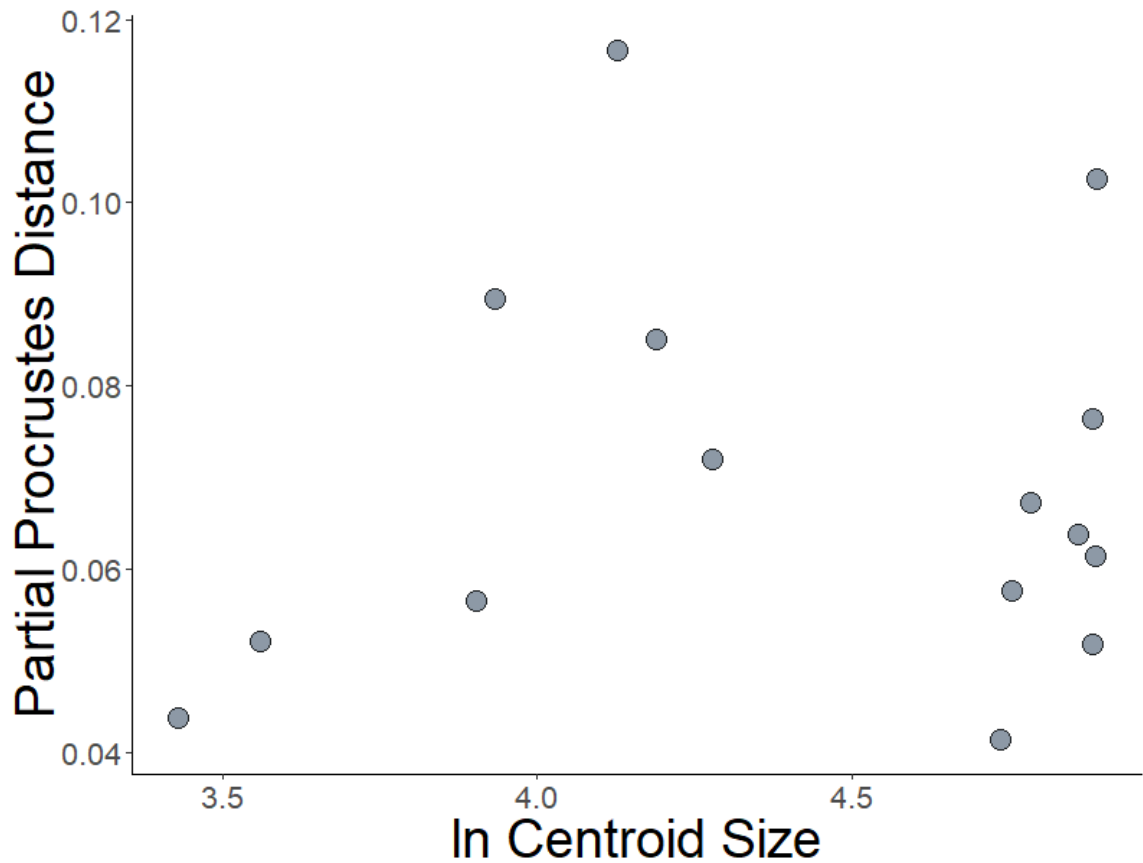
(slope=0.0080, p=0.2066, r=0.1905).

Figure 66. Thin-plate spline deformation grid depicting shape change with growth for 21 landmarks and 41 semilandmarks of 21 specimens of *Dikelocephalus* from North Freedom Bed 2 (NF2) (Fig. 64). Shape change calculated by a multivariate regression of partial warp scores against lnCS and 3.94% of shape variance (based on summed squared residuals expressed in Procrustes units) explained by allometry is not significant at a 95% confidence interval (p=0.6119 from 1600 bootstraps).
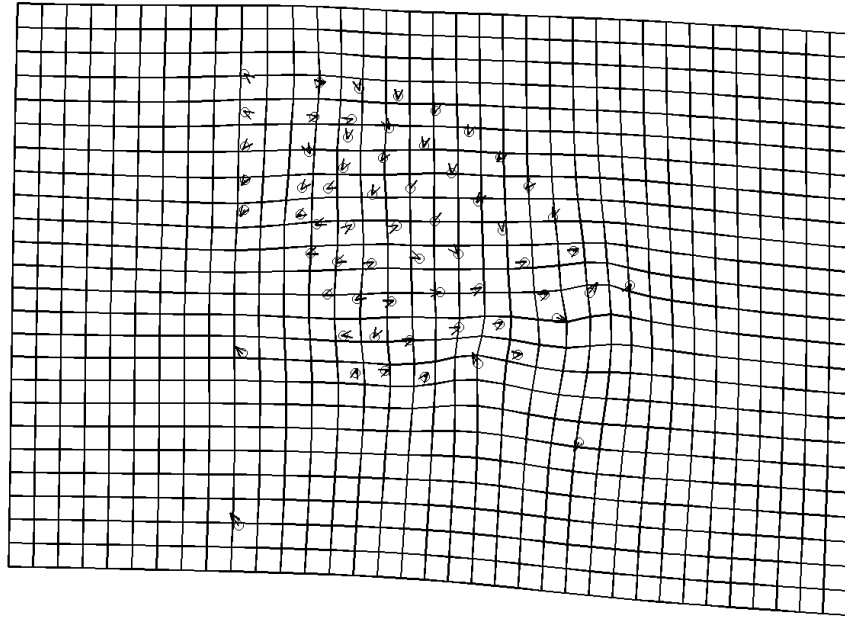
Figure 67. Partial Procrustes superimposition of 14 landmarks for 21 pygidia specimens of *Dikelocephalus* from North Freedom Bed 2 (NF2). Landmarks and semilandmarks corresponding to pleural furrows removed (compare to Fig. 64).
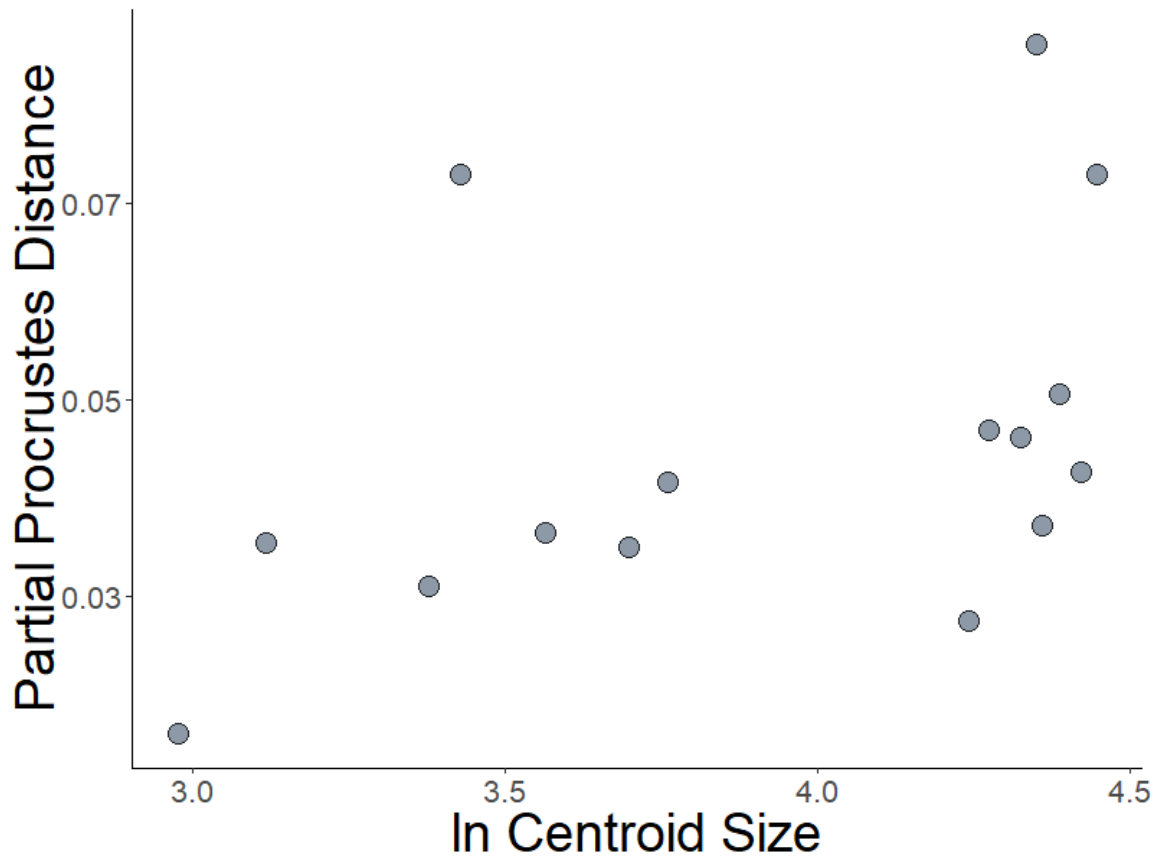
Figure 68. Partial Procrustes distance from the reference form (mean configuration of smallest three specimens) versus logarithm of centroid size (lnCS) for 14 landmarks of 21 specimens of *Dikelocephalus* from North Freedom Bed 2 (NF2) (Fig. 67). Regression of partial Procrustes distance against lnCS is not significant at a 95% confidence interval (slope=0.0122, p=0.0901, r=0.3058).
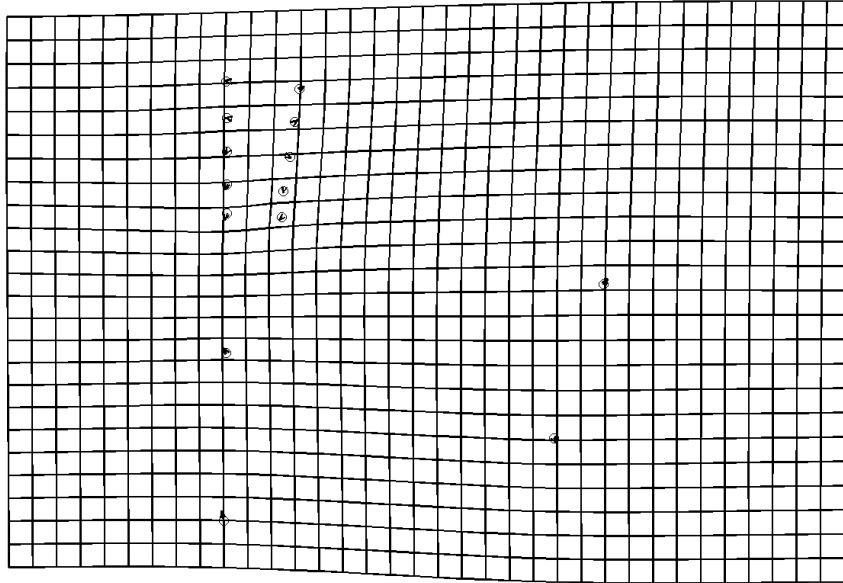
Figure 69. Thin-plate spline deformation grid depicting shape change with

growth for 14 landmarks of 21 specimens of *Dikelocephalus* from North Freedom

Bed 2 (NF2) (Fig. 67). Shape change calculated by a multivariate regression of

partial warp scores against lnCS and 8.49% of shape variance (based on

summed squared residuals expressed in Procrustes units) explained by allometry

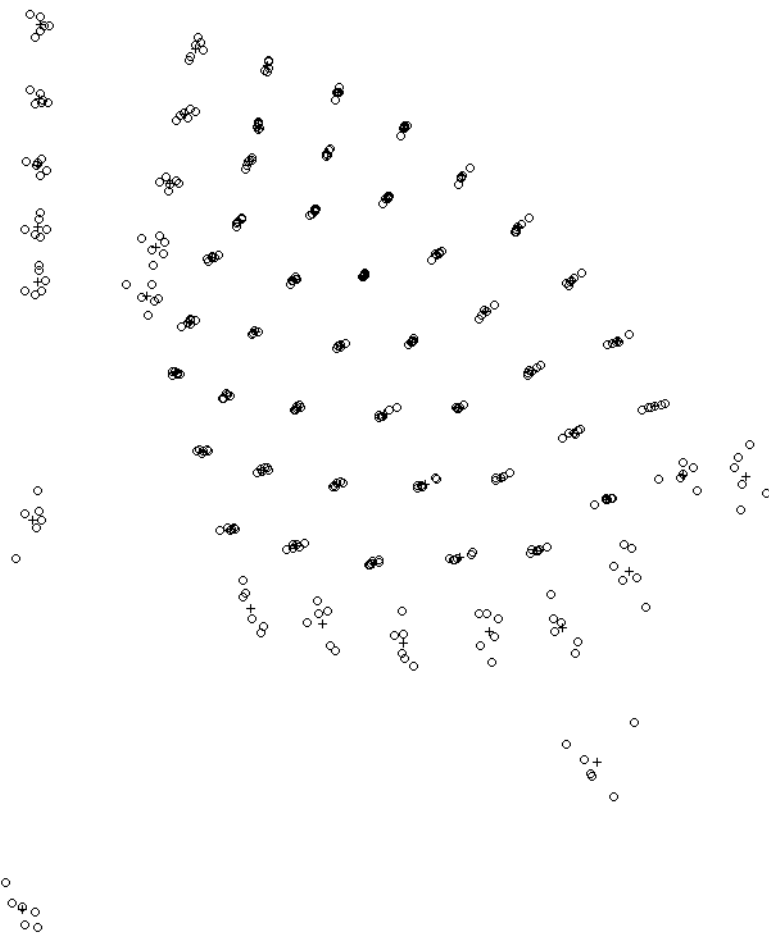is not significant at a 95% confidence interval (p=0.1063 from 1600 bootstraps).

Figure 70. Partial Procrustes superimposition of 21 landmarks and 41 semilandmarks for 15 pygidia specimens of *Dikelocephalus* from North Freedom Bed 8 (NF8).
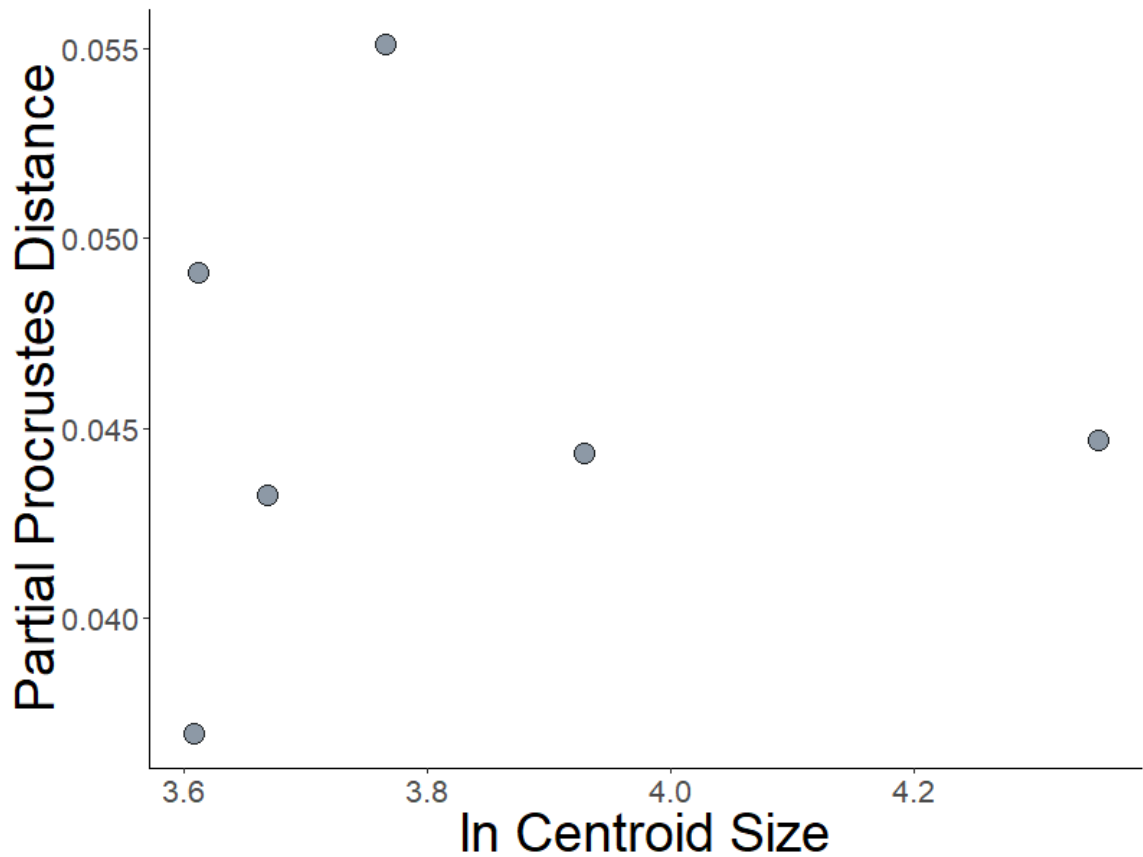
Figure 71. Partial Procrustes distance from the reference form (mean configuration of smallest three specimens) versus logarithm of centroid size (lnCS) for 21 landmarks and 41 semilandmarks of 15 specimens of *Dikelocephalus* from North Freedom Bed 8 (NF8) (Fig. 70). Regression of partial Procrustes distance against lnCS is not significant at a 95% confidence interval (slope=0.0027, p=0.4107, r=0.0651).

Figure 72. Thin-plate spline deformation grid depicting shape change with

growth for 21 landmarks and 41 semilandmarks of 15 specimens of

Dikelocephalus from North Freedom Bed 8 (NF8) (Fig. 70). Shape change

calculated by a multivariate regression of partial warp scores against lnCS and

3.62% of shape variance (based on summed squared residuals expressed in

Procrustes units) explained by allometry is not significant at a 95% confidence
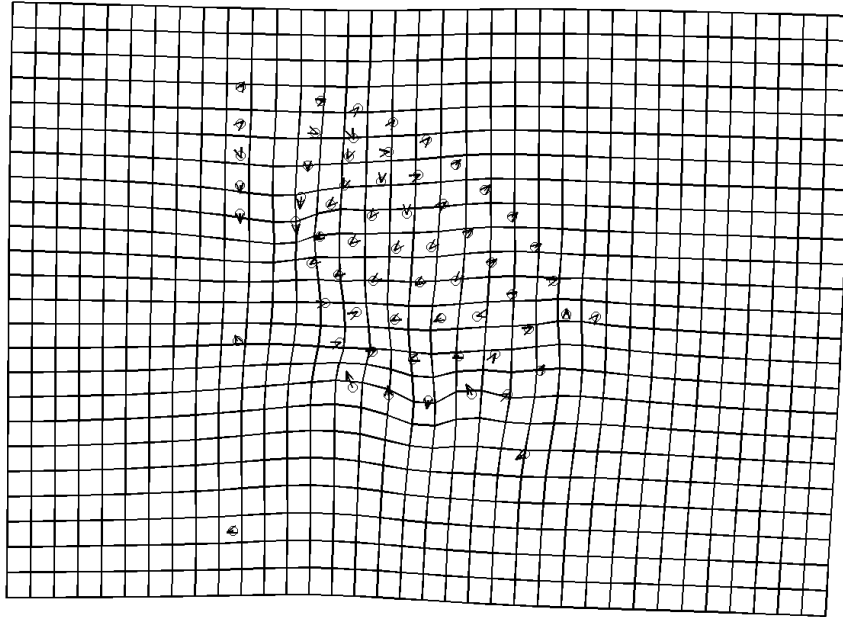
interval (p=0.8950 from 1600 bootstraps).

Figure 73. Partial Procrustes superimposition of 14 landmarks for 15 pygidia specimens of *Dikelocephalus* from North Freedom Bed 8 (NF8). Landmarks and semilandmarks corresponding to pleural furrows removed (compare to Fig. 70).
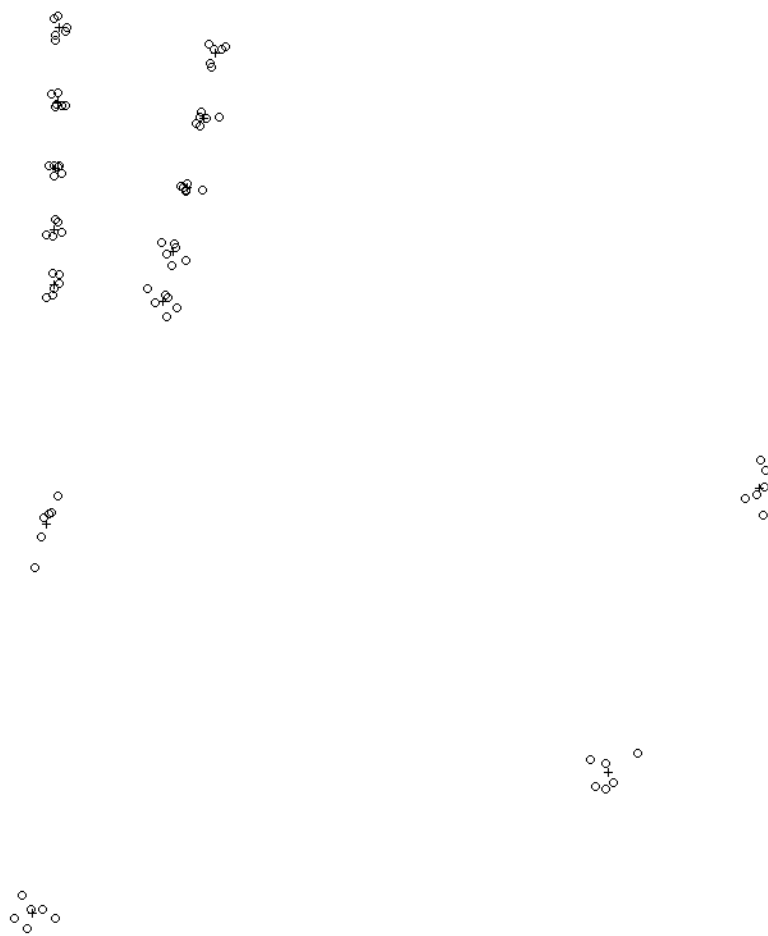
Figure 74. Partial Procrustes distance from the reference form (mean configuration of smallest three specimens) versus logarithm of centroid size (lnCS) for 14 landmarks of 15 specimens of *Dikelocephalus* from North Freedom Bed 8 (NF8) (Fig. 73). Regression of partial Procrustes distance against lnCS is not significant at a 95% confidence interval (slope=0.0160, p=0.0500, r=0.4421).
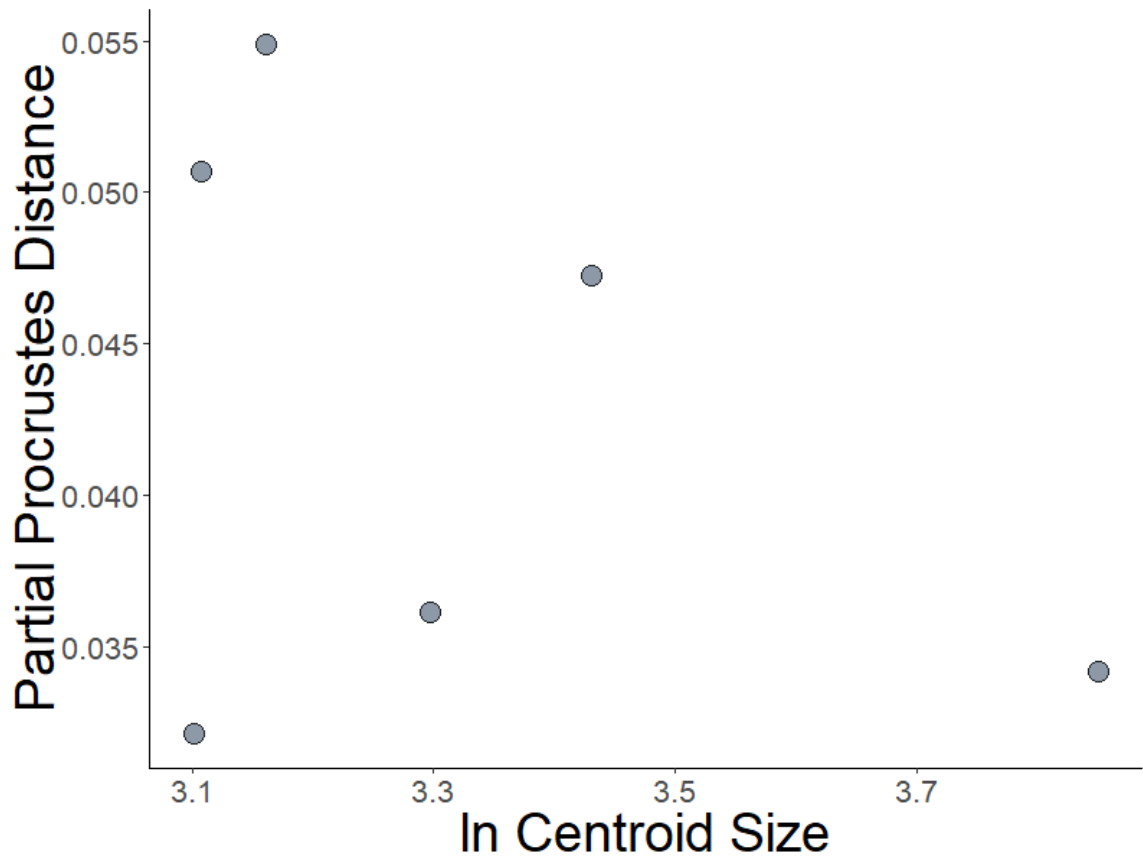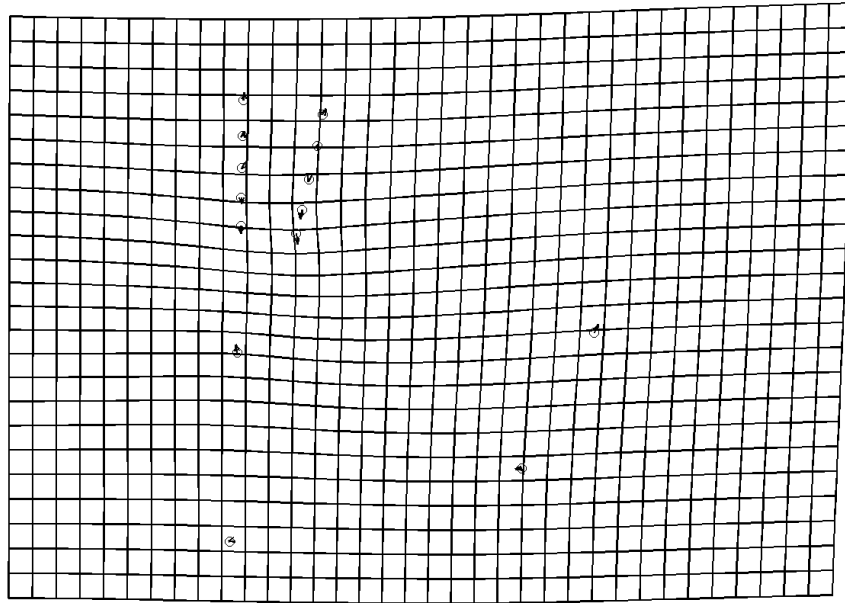
Figure 75. Thin-plate spline deformation grid depicting shape change with growth for 14 landmarks of 15 specimens of *Dikelocephalus* from North Freedom Bed 8 (NF8) (Fig. 73). Shape change calculated by a multivariate regression of partial warp scores against lnCS and 5.57% of shape variance (based on summed squared residuals expressed in Procrustes units) explained by allometry is not significant at a 95% confidence interval (p=0.5531 from 1600 bootstraps).
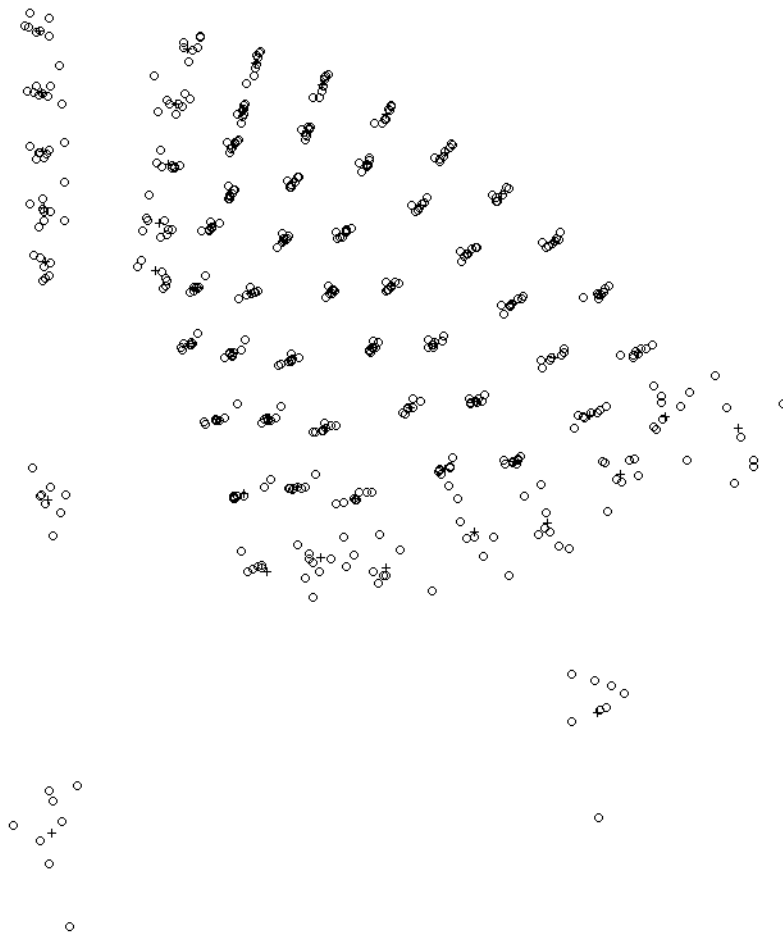
Figure 76. Partial Procrustes superimposition of 21 landmarks and 41

semilandmarks for 6 pygidia specimens of *Dikelocephalus* from Plain (PN).

Figure 77. Partial Procrustes distance from the reference form (mean configuration of smallest three specimens) versus logarithm of centroid size (lnCS) for 21 landmarks and 41 semilandmarks of 6 specimens of *Dikelocephalus* from Plain (PN) (Fig. 76). Regression of partial Procrustes distance against lnCS is not significant at a 95% confidence interval (slope=0.0007, p=0.4759, r=0.0349).

Figure 78. Thin-plate spline deformation grid depicting shape change with growth for 21 landmarks and 41 semilandmarks of 6 specimens of *Dikelocephalus* from Plain (PN) (Fig. 76). Shape change calculated by a multivariate regression of partial warp scores against lnCS and 13.51% of shape variance (based on summed squared residuals expressed in Procrustes units) explained by allometry is not significant at a 95% confidence interval (p=0.8706 from 1600 bootstraps).

Figure 79. Partial Procrustes superimposition of 14 landmarks for 6 pygidia specimens of *Dikelocephalus* from Plain (PN). Landmarks and semilandmarks corresponding to pleural furrows removed (compare to Fig. 76).
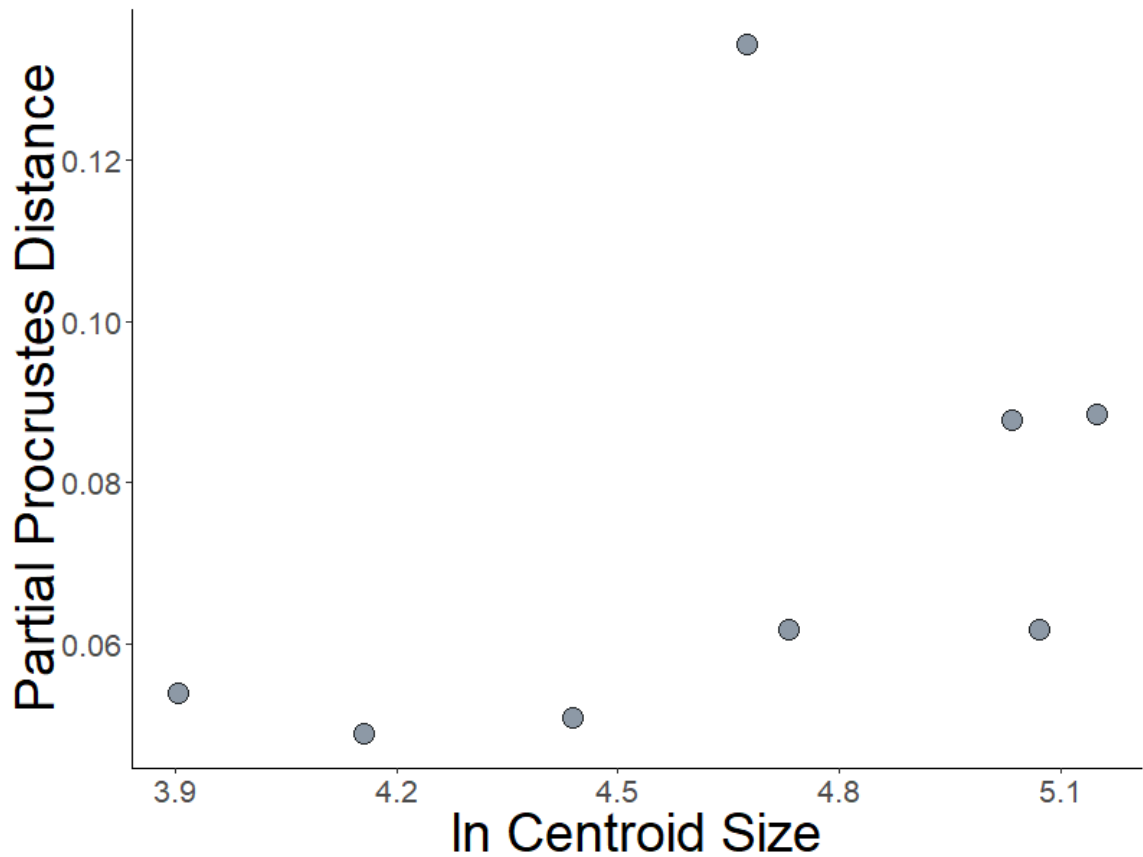
Figure 80. Partial Procrustes distance from the reference form (mean configuration of smallest three specimens) versus logarithm of centroid size (lnCS) for 14 landmarks of 6 specimens of *Dikelocephalus* from Plain (PN) (Fig. 79). Regression of partial Procrustes distance against lnCS is not significant at a 95% confidence interval (slope=-0.0126, p=0.7538, r=-0.3768).
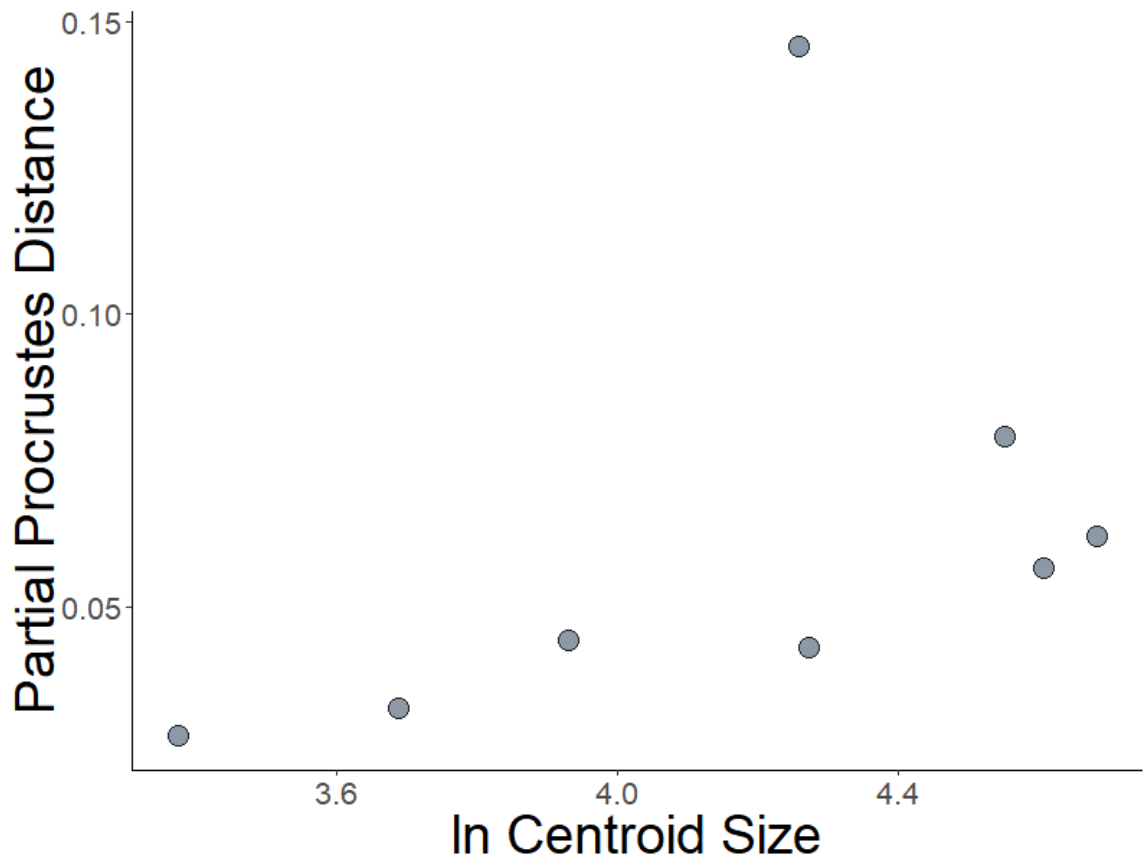
Figure 81. Thin-plate spline deformation grid depicting shape change with

growth for 14 landmarks of 6 specimens of *Dikelocephalus* from Plain (PN) (Fig.

79). Shape change calculated by a multivariate regression of partial warp scores

against lnCS and 11.36% of shape variance (based on summed squared

residuals expressed in Procrustes units) explained by allometry is not significant

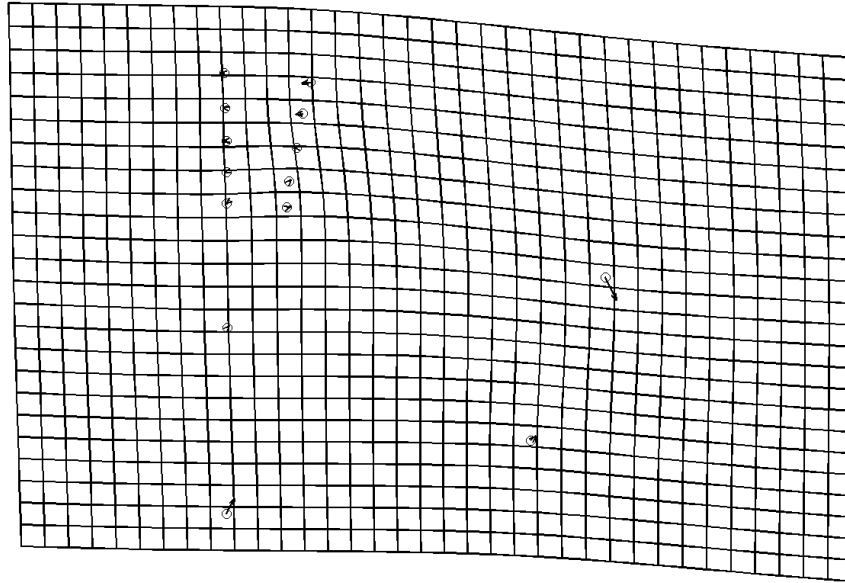at a 95% confidence interval (p=0.7775 from 1600 bootstraps).

Figure 82. Partial Procrustes superimposition of 21 landmarks and 41 semilandmarks for 8 pygidia specimens of *Dikelocephalus* from Prairie du Sac (SPb).

Figure 83. Partial Procrustes distance from the reference form (mean configuration of smallest three specimens) versus logarithm of centroid size (lnCS) for 21 landmarks and 41 semilandmarks of 8 specimens of *Dikelocephalus* from Prairie du Sac (SPb) (Fig. 82). Regression of partial Procrustes distance against lnCS is not significant at a 95% confidence interval (slope=0.0282, p=0.1472, r=0.4373).
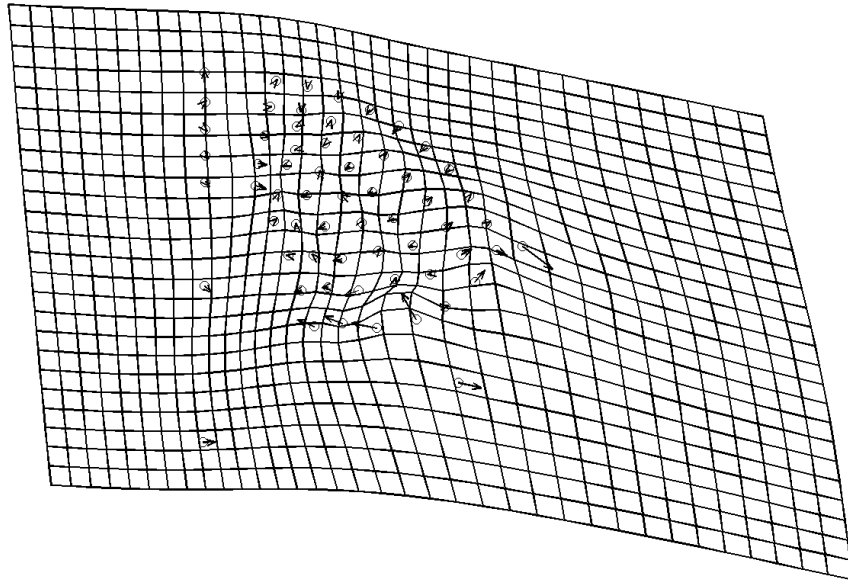
Figure 84. Thin-plate spline deformation grid depicting shape change with growth for 21 landmarks and 41 semilandmarks of 8 specimens of *Dikelocephalus* from Prairie du Sac (SPb) (Fig. 82). Shape change calculated by a multivariate regression of partial warp scores against lnCS and 19.94% of shape variance (based on summed squared residuals expressed in Procrustes units) explained by allometry is not significant at a 95% confidence interval (p=0.1594 from 1600 bootstraps).

Figure 85. Partial Procrustes superimposition of 14 landmarks for 8 pygidia

specimens of *Dikelocephalus* from Prairie du Sac (SPb). Landmarks and

semilandmarks corresponding to pleural furrows removed (compare to Fig. 82).
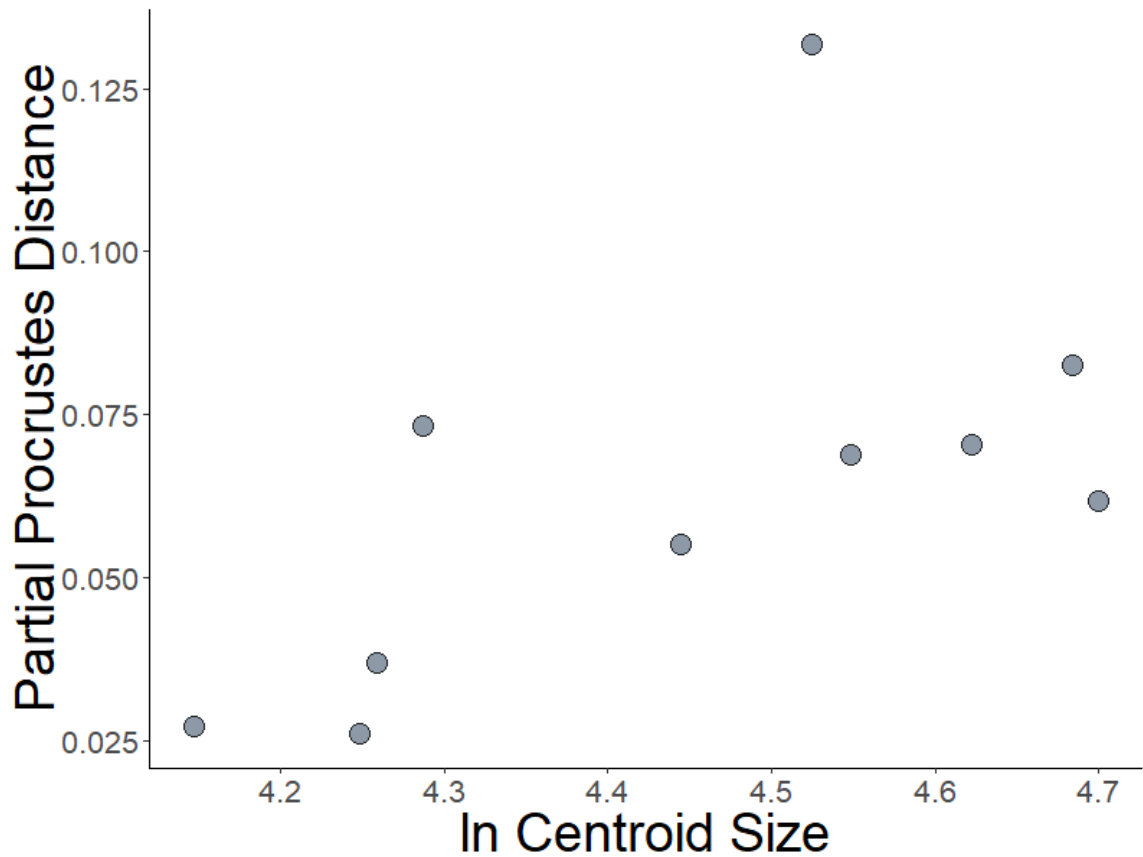
Figure 86. Partial Procrustes distance from the reference form (mean configuration of smallest three specimens) versus logarithm of centroid size (lnCS) for 14 landmarks of 8 specimens of *Dikelocephalus* from Prairie du Sac (SPb) (Fig. 85). Regression of partial Procrustes distance against lnCS is not significant at a 95% confidence interval (slope=0.0358, p=0.1437, r=0.4431).

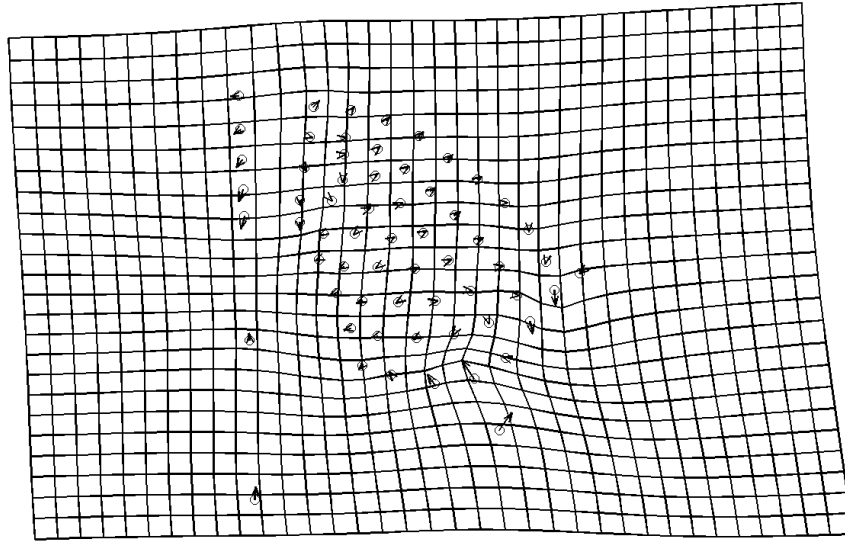**Figure 87.** Thin-plate spline deformation grid depicting shape change with growth for 14 landmarks of 8 specimens of *Dikelocephalus* from Prairie du Sac (SPb) (Fig. 85). Shape change calculated by a multivariate regression of partial warp scores against lnCS and 7.50% of shape variance (based on summed squared residuals expressed in Procrustes units) explained by allometry is not significant at a 95% confidence interval (p=0.7625 from 1600 bootstraps).

Figure 88. Partial Procrustes superimposition of 21 landmarks and 41 semilandmarks for 10 pygidia specimens of *Dikelocephalus* from Spring Green (SRa).
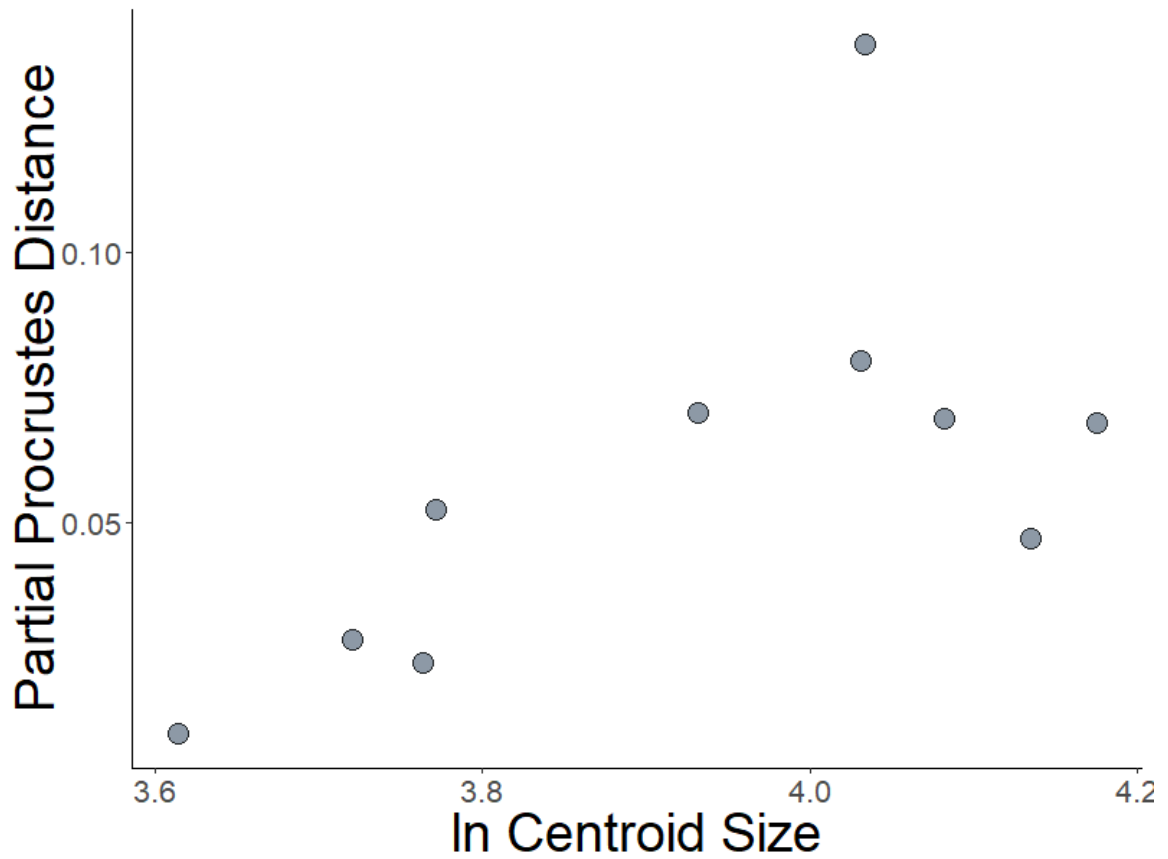
Figure 89. Partial Procrustes distance from the reference form (mean configuration of smallest three specimens) versus logarithm of centroid size (lnCS) for 21 landmarks and 41 semilandmarks of 10 specimens of *Dikelocephalus* from Spring Green (SRa) (Fig. 88). Regression of partial Procrustes distance against lnCS is significant (slope=0.0922, p=0.0363, r=0.5905).
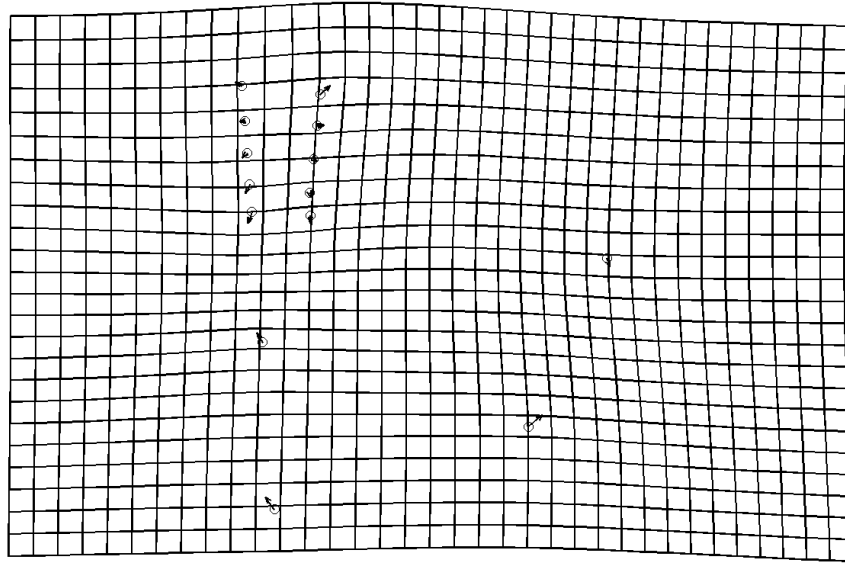
Figure 90. Thin-plate spline deformation grid depicting shape change with growth for 21 landmarks and 41 semilandmarks of 10 specimens of *Dikelocephalus* from Spring Green (SRa) (Fig. 88). Shape change calculated by a multivariate regression of partial warp scores against lnCS and 11.70% of shape variance (based on summed squared residuals expressed in Procrustes units) explained by allometry is not significant at a 95% confidence interval (p=0.4031 from 1600 bootstraps).

Figure 91. Partial Procrustes superimposition of 14 landmarks for 10 pygidia

specimens of *Dikelocephalus* from Spring Green (SRa). Landmarks and

semilandmarks corresponding to pleural furrows removed (compare to Fig. 88).
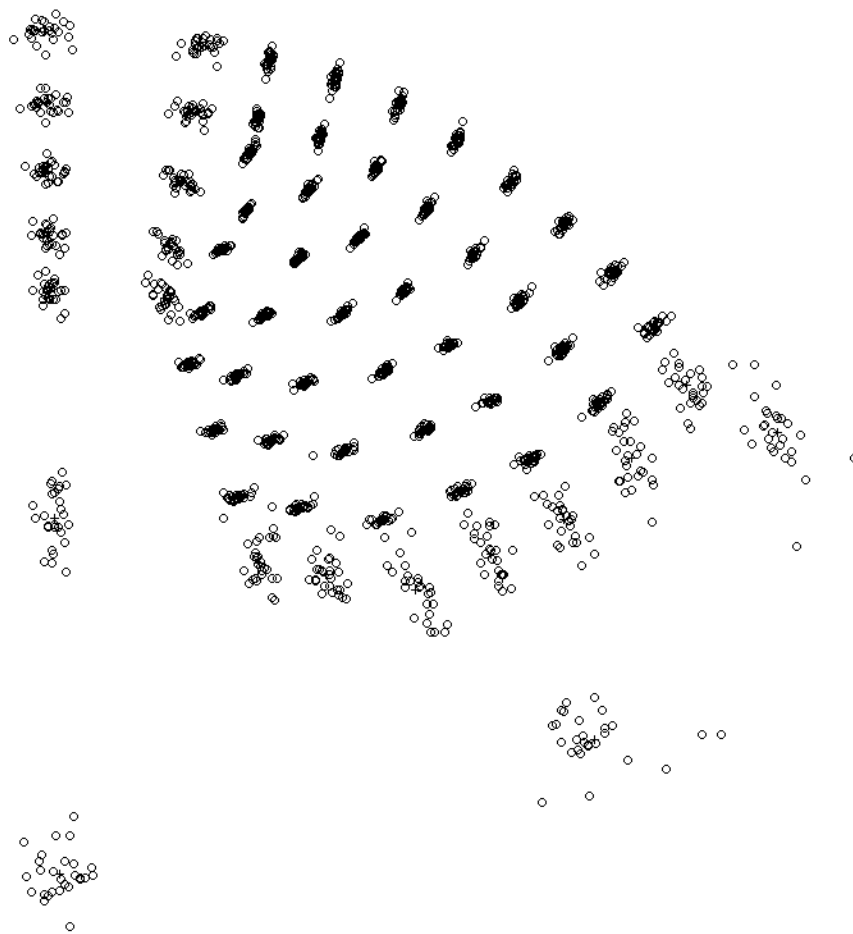
Figure 92. Partial Procrustes distance from the reference form (mean configuration of smallest three specimens) versus logarithm of centroid size (lnCS) for 14 landmarks of 10 specimens of *Dikelocephalus* from Spring Green (SRa) (Fig. 91). Regression of partial Procrustes distance against lnCS is significant (slope=0.1170, p=0.0237, r=0.6347).
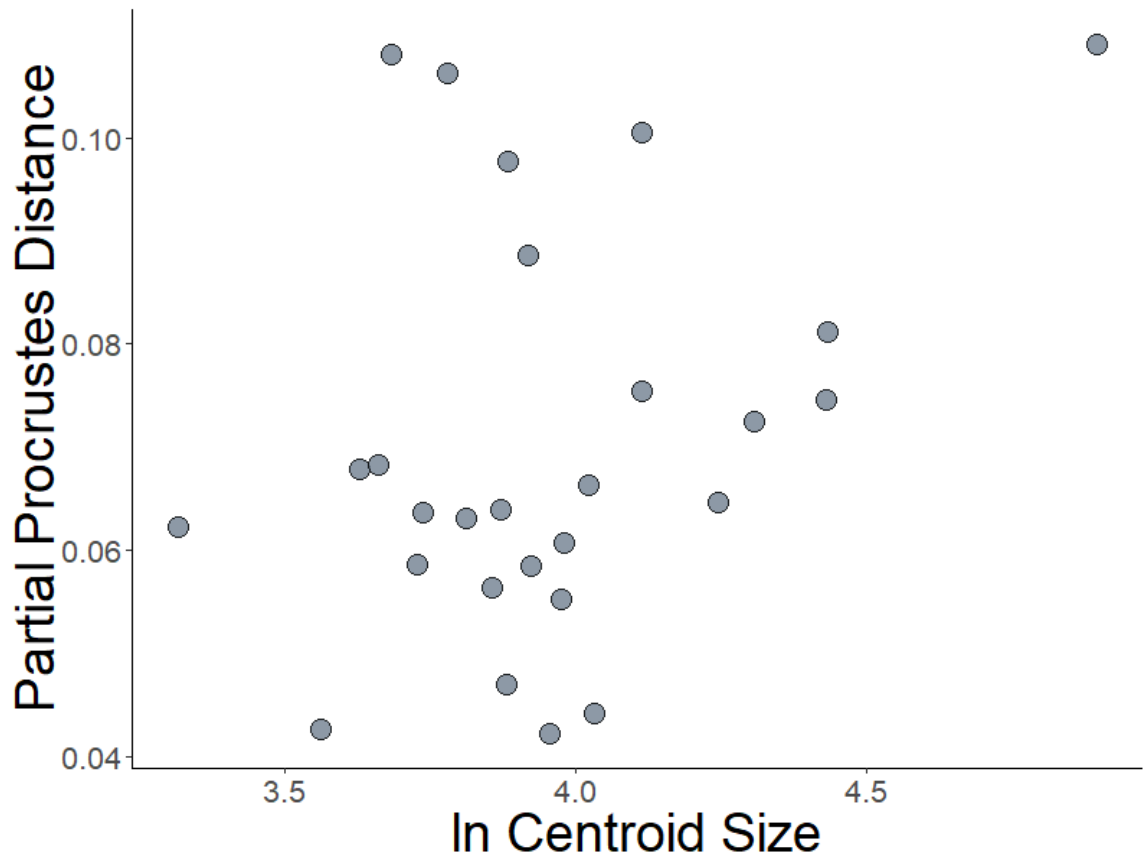
Figure 93. Thin-plate spline deformation grid depicting shape change with growth for 14 landmarks of 10 specimens of *Dikelocephalus* from Spring Green (SRa) (Fig. 91). Shape change calculated by a multivariate regression of partial warp scores against lnCS and 13.02% of shape variance (based on summed squared residuals expressed in Procrustes units) explained by allometry is not significant at a 95% confidence interval (p=0.3400 from 1600 bootstraps).
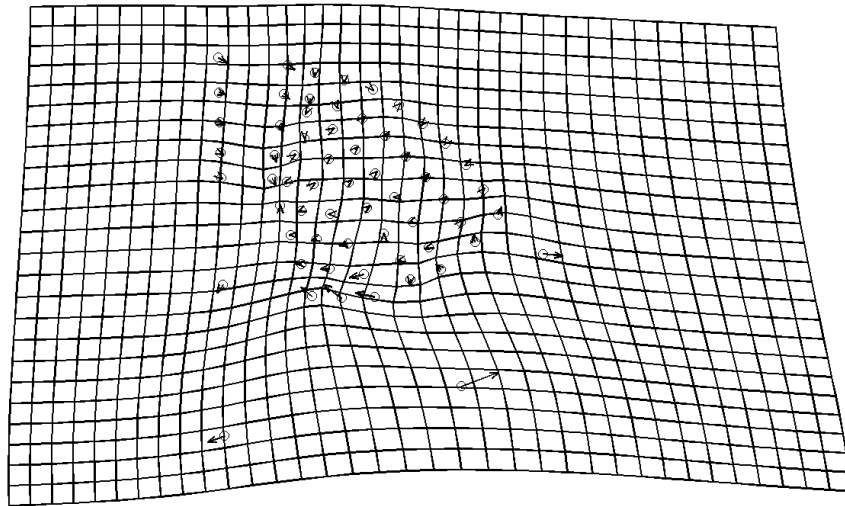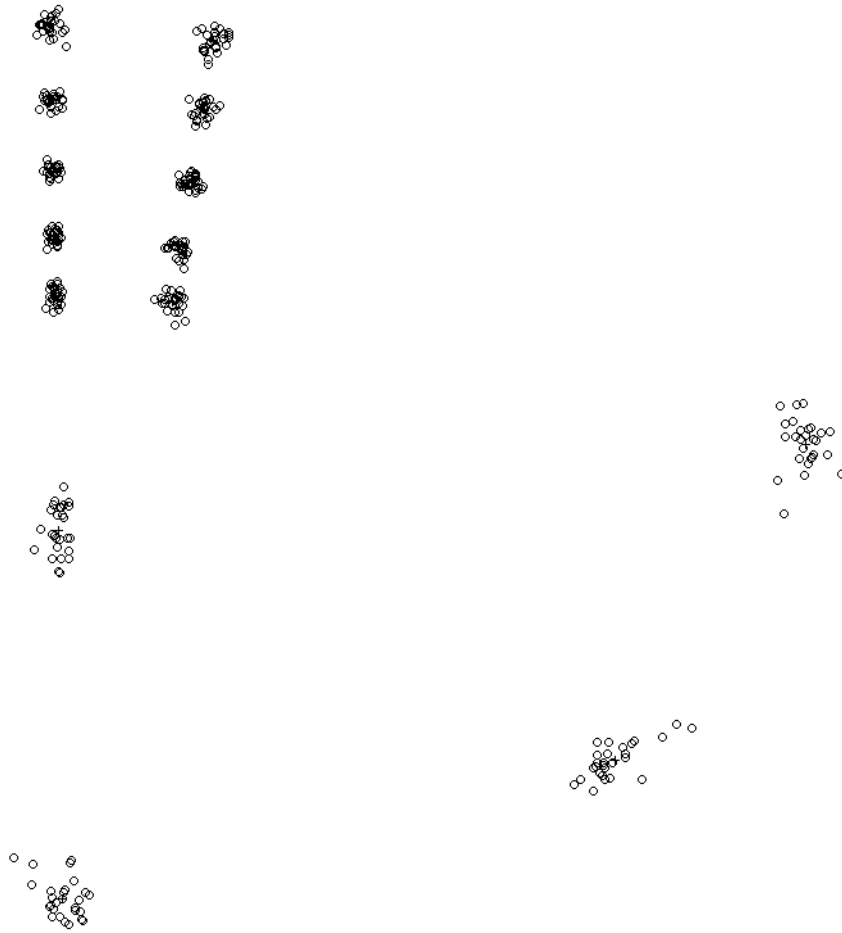
Figure 94. Partial Procrustes superimposition of 21 landmarks and 41 semilandmarks for 27 pygidia specimens of *Dikelocephalus* from Stillwater, Fairy Glen (SWa).
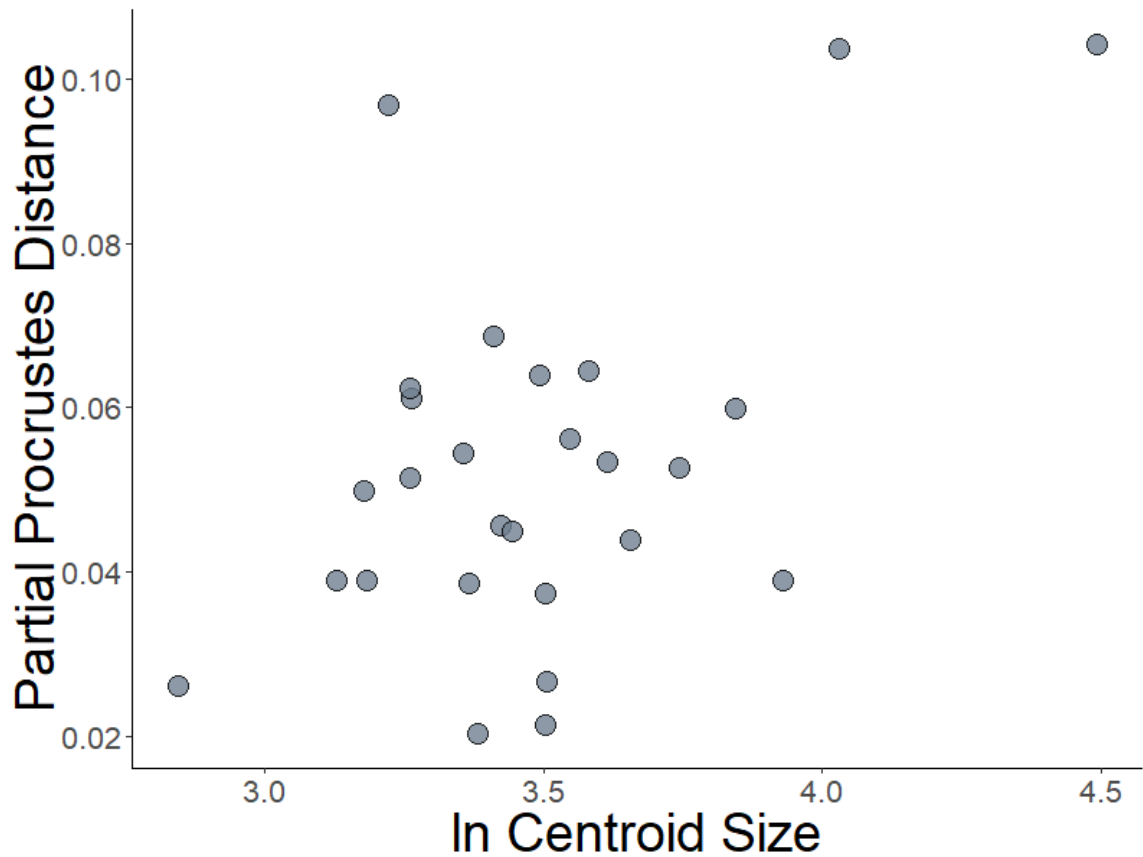
Figure 95. Partial Procrustes distance from the reference form (mean configuration of smallest three specimens) versus logarithm of centroid size (lnCS) for 21 landmarks and 41 semilandmarks of 27 specimens of *Dikelocephalus* from Stillwater, Fairy Glen (SWa) (Fig. 94). Regression of partial Procrustes distance against lnCS is not significant at a 95% confidence interval (slope=0.0202, p=0.0501, r=0.3236).
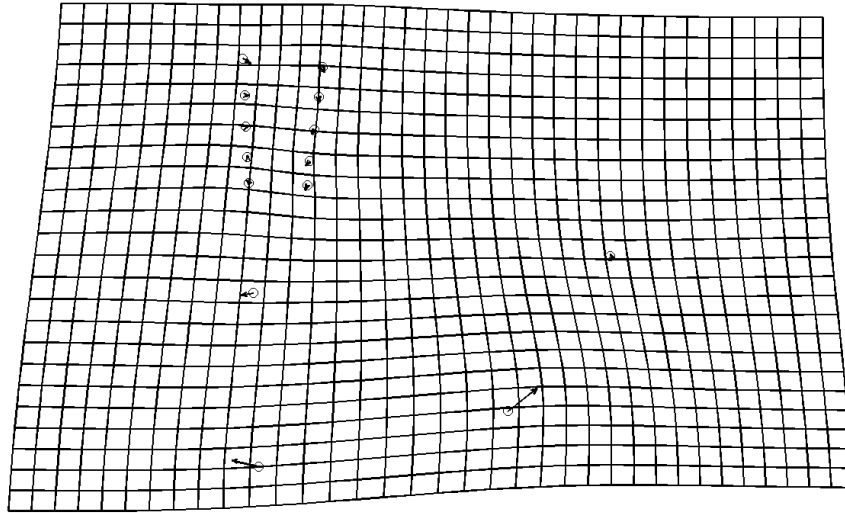
Figure 96. Thin-plate spline deformation grid depicting shape change with growth for 21 landmarks and 41 semilandmarks of 27 specimens of *Dikelocephalus* from Stillwater, Fairy Glen (SWa) (Fig. 94). Shape change calculated by a multivariate regression of partial warp scores against lnCS and 7.13% of shape variance (based on summed squared residuals expressed in Procrustes units) explained by allometry is not significant at a 95% confidence interval (p=0.1038 from 1600 bootstraps).

Figure 97. Partial Procrustes superimposition of 14 landmarks for 27 pygidia specimens of *Dikelocephalus* from Stillwater, Fairy Glen (SWa). Landmarks and semilandmarks corresponding to pleural furrows removed (compare to Fig. 94).

Figure 98. Partial Procrustes distance from the reference form (mean configuration of smallest three specimens) versus logarithm of centroid size (lnCS) for 14 landmarks of 27 specimens of *Dikelocephalus* from Stillwater, Fairy Glen (SWa) (Fig. 97). Regression of partial Procrustes distance against lnCS is significant (slope=0.0329, p=0.0046, r=0.4872).

Figure 99. Thin-plate spline deformation grid depicting shape change with growth for 14 landmarks of 27 specimens of *Dikelocephalus* from Stillwater, Fairy Glen (SWa) (Fig. 97). Shape change calculated by a multivariate regression of partial warp scores against lnCS and 10.54% of total shape variance (based on summed squared residuals expressed in Procrustes units) is explained by allometry (p=0.0256 from 1600 bootstraps).